TECHNICAL REPORT 87-28

Crosshole Investigations – Results from Seismic Borehole Tomography

Jörgen Pihl
Monica Hammarström
Sven Ivansson
Per Morén

December 1986

National Defence Research Institute, Sweden

Nagra
Nationale
Genossenschaft
für die Lagerung
radioaktiver Abfälle

Cédra
Société coopérative
nationale
pour l'entreposage
de déchets radioactifs

Cisra
Società cooperativa
nazionale
per l'immagazzinamento
di scorie radioattive

TECHNICAL REPORT 87-28

Crosshole Investigations – Results from Seismic Borehole Tomography

Jörgen Pihl
Monica Hammarström
Sven Ivansson
Per Morén

December 1986

National Defence Research Institute, Sweden

Parkstrasse 23 5401 Baden/Schweiz Telephon 056/20 55 11

Der vorliegende Bericht betrifft eine Studie, die für das Stripa-Projekt ausgeführt wurde. Die Autoren haben ihre eigenen Ansichten und Schlussfolgerungen dargestellt.Diese müssen nicht unbedingt mit denjenigen des Auftraggebers übereinstimmen.

Le présent rapport a été préparé pour le projet de Stripa. Les opinions et conclusions présentées sont celles des auteurs et ne correspondent pas nécessairement à ceux du client.

This report concerns a study which was conducted for the Stripa Project. The conclusions and viewpoints presented in the report are those of the authors and do not necessarily coincide with those of the client.

Das Stripa-Projekt ist ein Projekt der Nuklearagentur der OECD. Unter internationaler Beteiligung werden von 1980-86 Forschungsarbeiten in einem unterirdischen Felslabor in Schweden durchgeführt. Diese sollen die Kenntnisse auf folgenden Gebieten erweitern:
- hydrogeologische und geochemische Messungen in Bohrlöchern
- Ausbreitung des Grundwassers und Transport von Radionukliden durch Klüfte im Gestein
- Verhalten von Materialien, welche zur Verfüllung und Versiegelung von Endlagern eingesetzt werden sollen
- Methoden zur zerstörungsfreien Ortung von Störzonen im Fels

Seitens der Schweiz beteiligt sich die Nagra an diesen Untersuchungen. Die technischen Berichte aus dem Stripa-Projekt erscheinen gleichzeitig in der NTB-Serie der Nagra.

The Stripa Project is organised as an autonomous project of the Nuclear Energy Agency of the OECD. In the period from 1980-86, an international cooperative programme of investigations is being carried out in an underground rock laboratory in Sweden. The aim of the work is to improve our knowledge in the following areas:
- hydrogeological and geochemical measurement methods in boreholes
- flow of groundwater and transport of radionuclides in fissured rock
- behaviour of backfilling and sealing materials in a real geological environment
- non-destructive methods for location of disturbed zones in the rock

Switzerland is represented in the Stripa Project by Nagra and the Stripa Project technical reports appear in the Nagra NTB series.

Le projet Stripa est un projet autonome de l'Agence de l'OCDE pour l'Energie Nucléaire. Il s'agit d'un programme de recherche avec participation internationale, qui sera réalisé entre 1980 et 1986 dans un laboratoire souterrain, en Suède. Le but de ces travaux est d'améliorer et d'étendre les connaissances dans les domaines suivants:
- mesures hydrogéologiques et géochimiques dans les puits de forage
- chimie des eaux souterraines à grande profondeur
- écoulement des eaux souterraines et transport des radionucléides dans les roches fracturées
- comportement des matériaux de colmatage et de scellement des dépôt finals
- méthodes de localisation non destructive des zones de perturbation de la roche

La Suisse est représentée dans le projet Stripa par la Cédra. Les rapports techniques du projet Stripa sont publiés dans la série des rapports techniques de la Cédra (NTB).

ABSTRACT

A system for seismic crosshole measurements has been designed, built and tested. The system can be used both for small-scale (ie 10 - 200 m) and large-scale (ie 200 - 1000 m) operations.

The design includes both borehole receivers, amplifiers and recording system. The receivers can be used down to 700 m depth in slim boreholes.

Much work has gone into the development of analysis methods. Tomographic algorithms have been developed for the analysis of seismic data. The development includes basic theory as well as numerical methods.

Special care has been taken to minimize systematic errors. Many data quality checks have been made.

Field tests have been carried out at the large-scale test site at Gideå and at the small-scale test site at Stripa.

In the large-scale test, some zones of fractured rock were found. In addition, there appears to be a relatively large area of rock without any major anomalous features.

It appears that problems ascociated with large-scale crosshole seismics are still substantial. Further work is needed to solve the problems with ray-bending and anisotropy.

In the small-scale test the measurements could be carried out with high precision. Several zones with different properties are visible in the tomograms.

It is our opinion that the technique for small-scale crosshole seismics is now developed to a level where it can be utilized as a useful tool for rock-quality assessment.

RESUME

On a conçu, élaboré et testé un système permettant d'effectuer des mesures sismiques entre puits. Ce système peut être utilisé tant pour des opérations à petite échelle (par ex. 10 à 200 m) qu'à grande échelle (par ex. 200 à 1000 m).

Le système conçu comprend à la fois des capteurs et des amplificateurs placés dans le forage, ainsi qu'une installation d'enregistrement. Les capteurs peuvent être utilisés jusqu'à une profondeur de 700 m, à l'intérieur de forages très étroits.

Le développement des méthodes d'analyses a requis beaucoup de travail. Des algorithmes tomographiques ont été mis au point pour analyser les données sismiques. Ce développement concerne la théorie de base et les méthodes numériques.

On s'est particulièrement attaché à minimiser les erreurs systématiques. On a procédé à de nombreux controles de qualité des données.

Des tests in situ ont été réalisés à grande échelle sur le site de Gideå et à petite échelle sur le site de Stripa.

L'essai à grande échelle a révélé quelques zones de roches diaclasées. De plus, il semble y avoir une région relativement étendue de roches exemptées de perturbations majeures.

Les problèmes liés à la sismique entre puits à grande échelle semblent encore importants. De nombreux problèmes de sismique réfraction et d'anisotropie restent à résoudre.

Dans l'essai à plus petite échelle, les mesures ont pu être réalisées avec une grande précision. Plusieurs zones aux propriétés différentes sont mises en évidence par les tomogrammes.

Nous pensons que la technique de sismique entre puits à petite échelle a maintenant atteint un niveau lui permettant d'etre utilisée comme un instrument utile en vue de l'évaluation de la qualité de la roche.

ZUSAMMENFASSUNG

Ein System für die seismische Durchstrahlung zwischen Bohrungen (Cross-hole) wurde entwickelt, aufgebaut und getestet. Das System kann sowohl für kleinräumige (d.h. 10 bis 200 m) wie auch grossräumige (d.h. 200 bis 1000 m) Felduntersuchungen verwendet werden.

Der Aufbau enthält zwei Komponenten - Bohrlochempfänger mit Verstärkern und das Registriersystem. Die Empfänger können in Bohrlöchern bis zu einer Tiefe von 700 m benutzt werden.

In die Entwicklung der Auswertungsmethoden wurde viel Zeit investiert. Tomographische Algorithmen wurden für die Analyse von seismischen Daten entwickelt. Diese enthalten sowohl prinzipiell theoretische Aspekte als auch numerische Methoden.

Es wurden besondere Vorkehrungen zur Vermeidung systematischer Fehler getroffen. Daten-Qualitätskontrollen wurden häufig durchgeführt.

Feldversuche wurden im grossräumigen Testfeld Gideå und im kleinräumigen Feld Stripa durchgeführt.

In Gideå wurden einige Zonen mit geklüftetem Fels ermittelt; ansonsten scheint der grössere Teil des Gebirges keine besondere Anomalien aufzuweisen.

Bei der grossräumigen seismischen Durchstrahlung treten immer noch substantielle Probleme auf. Weitere Entwicklungsarbeiten sind erforderlich um die Einflüsse der Strahlenbrechung und der Anisotropie in Griff zu bekommen.

Die Messungen im kleinräumigen Feld konnten mit hoher Genauigkeit ausgeführt werden. Einige Zonen mit unterschiedlichen Eigenschaften wurden in den Tomogrammen wieder erkannt.

Nach unserer Meinung ist die Technik für kleinräumige seismische Durchstrahlungen nun soweit entwickelt, dass sie ein nützliches Instrument für die Qualitätsabschätzung des Gebirges darstellt

TABLE OF CONTENTS

SUMMARY

The objective of the work which is presented in this report was to develop measurement and analysis techniques for the detection and characterization of fracture zones. The aim was to find accurate methods to determine the location, extent, thickness and physical properties of anomalous zones by using the seismic crosshole technique.

Crosshole measurement techniques are quite new to the geophysical society. There are few reports in the literature before 1980. At the start of the Stripa II Project very little was known about the problems of applying crosshole techniques at large distances. Furthermore, the underlying theories had not been developed. It was thus uncertain if a tomographic analysis of crosshole data could give a usable result at all.

For seismic crosshole measurements, as developed in the Stripa Phase II project, the experimental setup can be as depicted in Figure 1-1 (page 3). Two or more boreholes are drilled in the area of interest. Seismic sources are placed in one borehole and receivers in the other holes and on the surface. Rays can be sent through the whole area by varying the depths of the sources and the borehole receivers.

From the recorded signals parameters such as traveltimes (time-of-flight), amplitudes and frequencies are determined. Mainly the traveltimes are used in the seismic tomography analysis. The result is a map of slowness (reciprocal velocity) of the area under study. This map is then interpreted and compared to geological models.

The development of new measurement techniques made construction of new equipment necessary. In the present project, seismic sources, receivers, as well as data-recording systems have been designed and constructed. The integrated system is capable of detecting seismic signals up to 8 kHz in frequency. It can be used at distances from ten metres up to a kilometre. The borehole receiving units can be used down to a depth of 700 m.

The data-recording system has 128 channels. The total sampling rate is 150000 samples per second. All analysis can, if needed, be made on the field-computer system.

The theories of tomographic analysis have been extensively developed during the project. Theoretical proofs of uniqueness have been found, showing that with

ideal data-sets the crosshole method can indeed provide an unambiguous picture of the area under study.

The tomographic analysis is very intensive computationally unless special care is taken. A substantial part of the work during the project has been the development of fast numerical algorithms. A twenty-fold increase in the rate of convergence has been obtained. With the new computer programs it is now possible to analyse a large data-set in half an hour on a mini-computer.

In the Stripa Phase II Project several field tests have been made. Two test sites have been used; the large-scale test site at Gideå, and the small-scale test site at Stripa.

The results from the tests show that the equipment is reliable and versatile in field work. It is sensitive enough to record at large distances and has also the high frequency response and timing accuracy needed for recordings at short distances.

For the small-scale tests in particular, the tomographic analysis has provided detailed and encouraging images. Comparison with results from measurements with other geophysical methods have shown good agreement.

Several checks on the data quality have been made to ensure that no systematic errors are present. This is particularly important when the contrasts are small, as is the case for the Stripa measurements.

1 INTRODUCTION

This report is a review of the seismic programme which was carried out by FOA in the Stripa Phase II project "Crosshole techniques for the detection and characterization of fracture zones." The programme include the following items

- Design and development of equipment for seismic borehole measurements (source, receivers and data collection system)
- Field tests at the Gideå site for large-scale measurements and at the Stripa site for small-scale measurements
- Development of tomographic analysis and interpretation techniques

1.1 BACKGROUND

During recent years there has been a demand for new or improved methods to measure the in situ physical properties of rock.

Development is going on in various areas, such as

- Mineral exploration
- Monitoring of water reservoirs
- Guidance for tunnel constructions
- Landslide warning systems
- Site selection for radioactive waste disposal

All these areas are of great importance to society. Therefore much research has been conducted in order to find accurate methods for rock investigation.

Until recently most geophysical borehole investigation techniques have only given information on the area very close to a borehole. There is clearly a need for methods which can give information on the properties between the holes, i.e. a kind of 'X-ray' image. The crosshole method is a new technique to measure the

properties of an area of ground between two or more boreholes. Today several such techniques are under development. In the crosshole part of the Stripa Phase II project three different techniques are being developed: georadar, water hydraulics and seismics. All these methods aim at finding the physical properties of the area between (and around) the boreholes.

This report deals with the seismic research of the crosshole programme in the Stripa project which has been carried out by FOA.

1.2 CROSSHOLE SEISMICS

In the seismic crosshole technique seismic waves are used to investigate the properties of ground rock. Seismic p-waves are sensitive to a number of physical parameters such as

- Density
- Porosity
- Water content
- Crack size and orientation

Besides, seismic waves have a deep penetration in rock. They are therefore very suitable for use as an instrument to determine the quality of ground rock at sites of very different sizes.

The use of seismic waves for crosshole measurements makes it possible to interpret the data using the tomographic method.

The main parameter used is the speed of propagation for the seismic waves. It is determined by the formula

$$V = \left(\frac{\lambda + 2\mu}{\rho}\right)^{\frac{1}{2}}$$

V - Seismic p-velocity
λ - Lamé's modulus
μ - Shear modulus
ρ - Density

In fractured rock the shear modulus is significantly less than in competent rock. Lamés modulus and the density are affected to a less extent. Thus the seismic p-velocity can be used as a measure of rock quality.

1.3 THE TOMOGRAPHY METHOD

The crosshole technique makes it possible to interpret the data using the tomography method. The word tomography originates from the Greek words "tomos" (a cut or a slice) and "grapho" (to draw lines, paint). One could say that the method of making pictures with tomography is to construct an image by combining several elements of information or slices. As this is best handled by a computer, the term "Computerized Tomography", or CT, is often used.

Compare another modern process, holography (from Greek "holos", whole), where the whole picture is constructed from one integrated element of data.

Tomographic analysis was introduced in medicine in 1973. An X-ray scanner was coupled to a computer and the signals were analysed using the CT method. The result was a clear image of the interior of the human organ under study.

Very soon after the first results with X-ray CT other types of radiation were used. Examples are:

- Gamma rays
- Electron beams
- Magnetic fields
- Ultra-sound
- Radio-frequency and microwave fields
- Seismic waves

A comprehensive overview of CT is given in Proc. IEEE March 1983 (20).

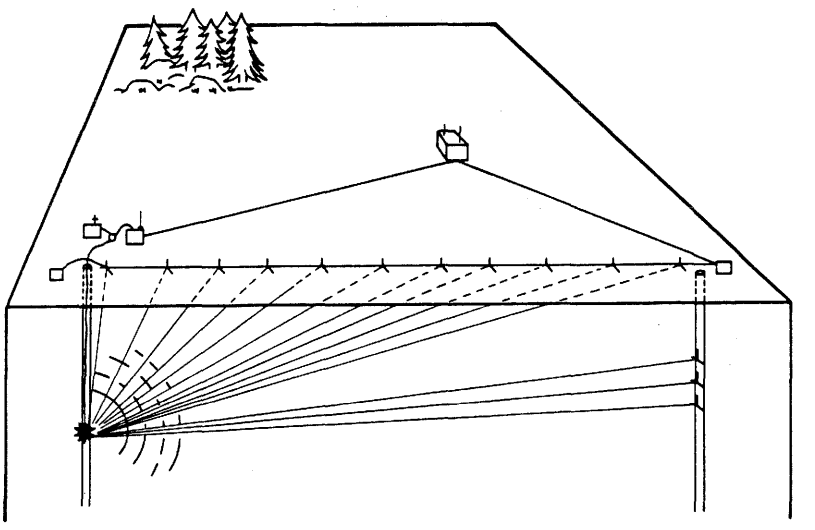

Figure 1-1. Principle of seismic crosshole measurements.

1.4 FIELD CONFIGURATION

When seismic tomographic analysis is performed using the crosshole method the experiment setup is usually as depicted in figure 1-1.

Two boreholes are drilled at each end of the area of interest. A seismic source is placed in one borehole and a receiver in the other. Rays can be sent through the whole area by varying the depths of the source and the receiver. In our system we also place receivers on the surface as this gives a substantial improvement of the tomographic results (11).

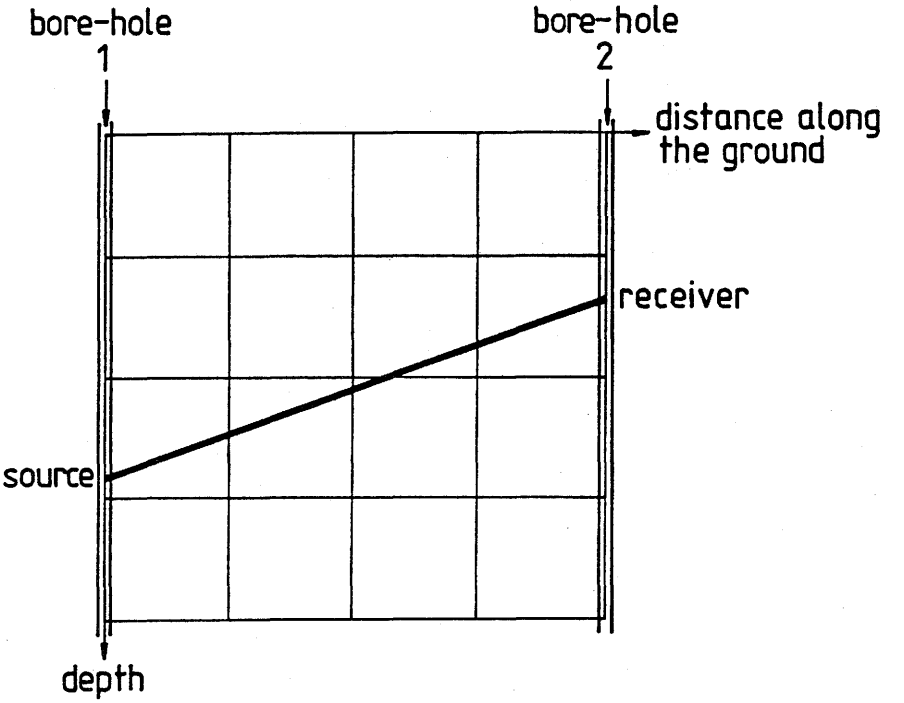

Figure 1-2. Seismic crosshole section with cell decomposition and an example of a raypath.

In short the method amounts to letting a great number of seismic rays pass through the area of interest. In the analysis the area is divided into small cells, rather like the elements of a matrix (Figure 1-2). The measured traveltime for a certain ray can then be regarded as a weighted sum of seismic velocity parameters for the cells which are traversed by the ray.

2 SEISMIC MEASUREMENT SYSTEM

2.1 DESIGN CONSIDERATIONS

When designing a seismic system for crosshole measurements at distances from tens of metres to thousands of metres several parameters are important. The most important factor is the required frequency response of the system. This can be estimated from the formula for the attenuation of seismic spherical waves:

$$A = \frac{A_o e^{\frac{-\pi f r}{Q\ V}}}{r}$$

A - Amplitude at distance r
A_o - Source parameter
f_o - Frequency
r - Distance from the source
Q - Quality factor of the rock
V - Velocity

Typical values for good crystalline rock is 100 for the Q-factor, and 6000 for the seismic velocity. If one calculates the frequency when the amplitude has fallen with a factor 1/e (the so called skin-depth) one arrives at a frequency of 3.8 kHz at 50 m distance, and a frequency of 190 Hz at 1000 m.

A system for seismic borehole measurements consists of the following parts (Figure 2-1):

- A seismic source which generates seismic energy
- Seismic receivers
- Amplifiers and filters
- Timing system
- Data-recording and analysis system

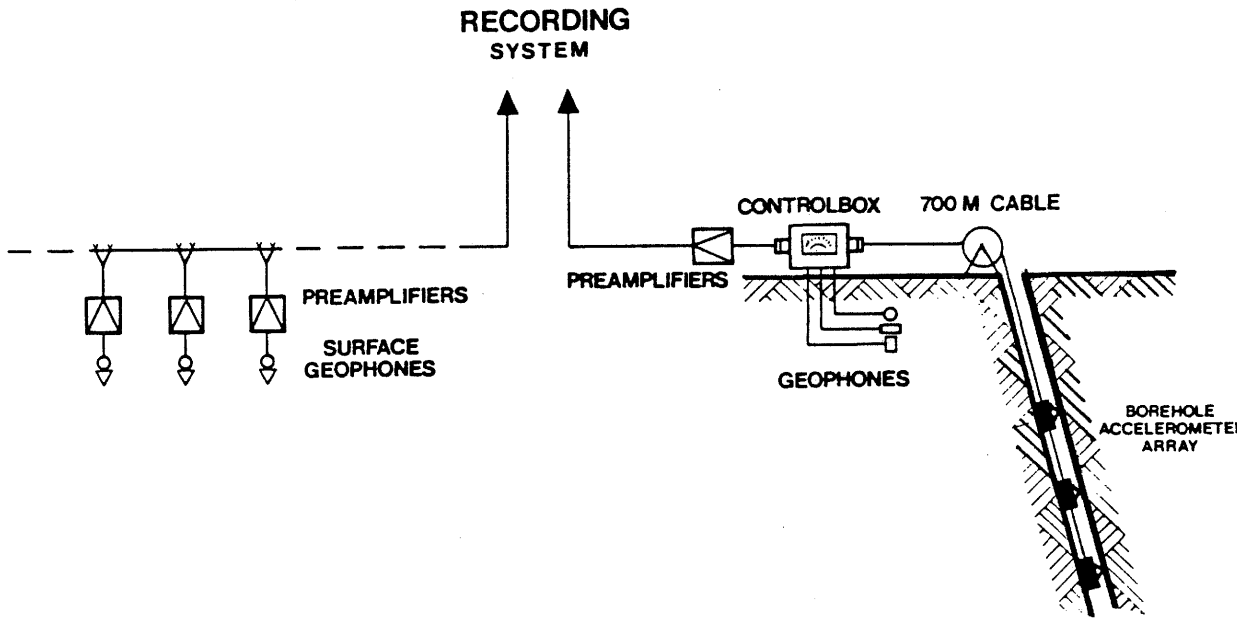

Figure 2-1. Main parts of a seismic borehole measurement system.

2.2 THE SEISMIC SOURCE

2.2.1 Demands On The Source

The purpose of the seismic source is to generate seismic energy of such energy and shape that it can be detected throughout the area under study. Preferably a single-pulse source is used since it gives a signal which is easier to detect. The source should generate S-waves as well as P-waves since the former are more sensitive to the ground-rock structure.

The demands on the seismic source can be summarized as follows

- Energy output of sufficient strength for detection at 1 km distance
- High repeatability
- Non-destructiveness
- Tolerance to large pressures
- High-frequency output
- Small size (to fit in slim boreholes)
- Exact timing-signal

2.2.2 Source Alternatives

Today there are a number of seismic energy sources commercially available which fulfil most of the requirements listed above.
Examples are airguns, vibrators, sparkers and piezo-electric transmitters.

The airgun is often used in off-shore exploration seismics. It has a powerful output and is non-destructive. However, the requirements of operation in slim boreholes and at great depths can not be met by existing airguns. The construction of a suitable airgun was beyond the scope of the present seismics crosshole research programme.

The vibrator is a pneumatically or hydraulically driven device with the same limitations as the airgun. However, a special on-stroke hydraulic "hammer" has been constructed. It can be used in slim boreholes (described in (8)). Unfortunately, the output is only suitable for measurements up to 200 m distance. This is adequate for the small-scale seismic experiment but not sufficient for the large-scale measurements.

Sparkers and piezo-electric sources have been successfully used for borehole seismic measurements (desribed in (22)). These sources too have an unsufficient output for large-scale measurements, however.

Explosives have been used for generation of seismic waves since the beginning of seismic geophysics. The main advantages are the high energy output (4 kJ per gramme of explosive paste), the short pulse rise-time and the repeatability.

In exploration studies explosive charges of a few hundred grammes are usually used. But previous experiences from borehole measurements show that much lower charges can be used (9),(17). We call the use of such small charges (1 to 100 gram) micro-explosions, to indicate the difference from standard explosions (Figure 2-2).

A drawback with the explosive-paste source is to our opinion the cost ineffectiveness. In practice it is difficult to shoot more than three to four shots per hour. A thorough measurement requires at least two hundred shots to be fired. Hence, the measurement time for a complete study will be several weeks.

Alternative explosive sources have therefore been studied. One possibility is to use gas instead of paste as the explosive medium.

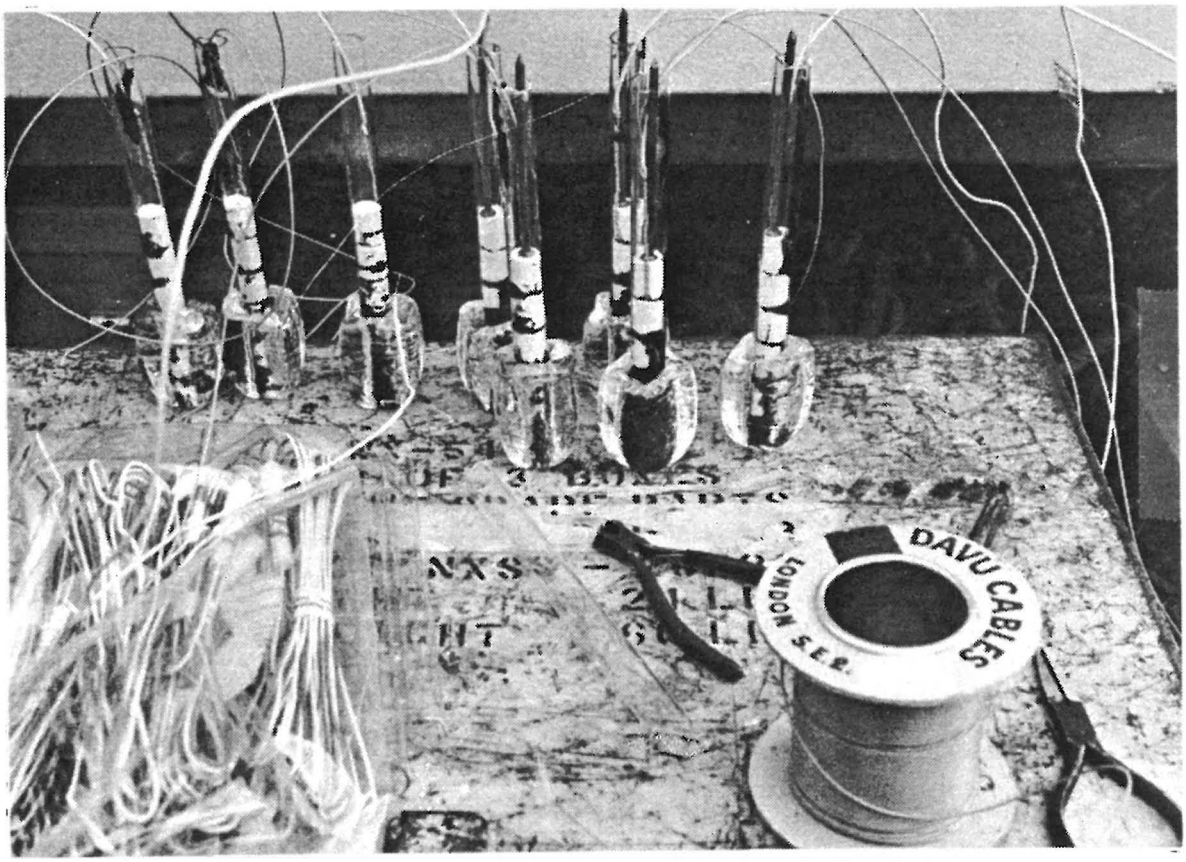

Figure 2-2. Charges of octol in glass devices for use in slim boreholes.

Such a device, which we call the gas exploder has been built and tested (3). The gas exploder utilizes detonations from a mixture of hydrogen and oxygen. The advantage of using a gas exploder would be

- Faster shot series in deep wells
- Fast and easy stacking which allows lower energy in each shot
- No chemical effects on the borehole water

It consists basically of two main parts. One contains the equipment for the detonations and is lowered into the hole. The other is the control board for feeding the downhole equipment with gas and initiating the detonations.

The gases are fed through separate hoses down to the detonation chamber (a steel pipe) before they are mixed (Figure 2-3).

As the detonation front reaches the water it gives rise to a shock wave that propagates into the water. To obtain accurate timing of the instant of detonation the shock wave is recorded with a pressure gauge which is located about 12 cm below the bottom of the pipe.

Theoretically, the energy content of the gas exploder at a water depth of 10 m is equivalent to 22.5 g of explosive paste. At a depth of 100 m it is equivalent to 125 g.
The prototype has been tested down to depths of about 100 m in a pit and in a borehole. The pit was 6 m in diameter and the borehole 110 mm. Seismic recordings were collected at various recording distances. The recorded energy output was lower than that obtained from the theoretical computations but still adequate to provide a sufficient recording range (Figure 2-4 and Figure 2-5).

Unfortunately, there were safety problems with the prototype device. It was considered beyond the scope of the Stripa Phase II project to solve these problems and go ahead to build a practically useful device.

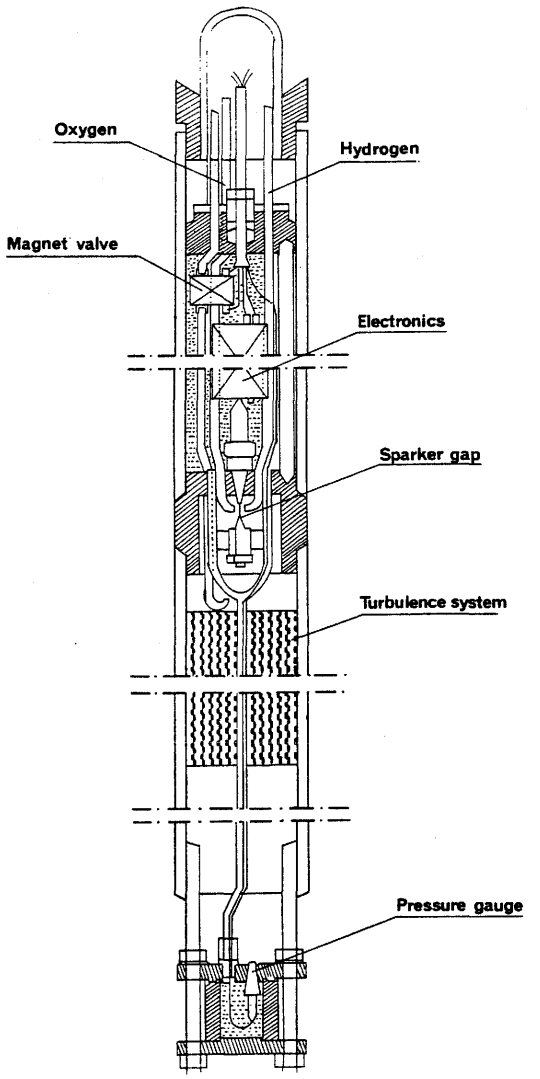

Figure 2-3.
Schematic drawing of the downhole gas-exploder equipment.

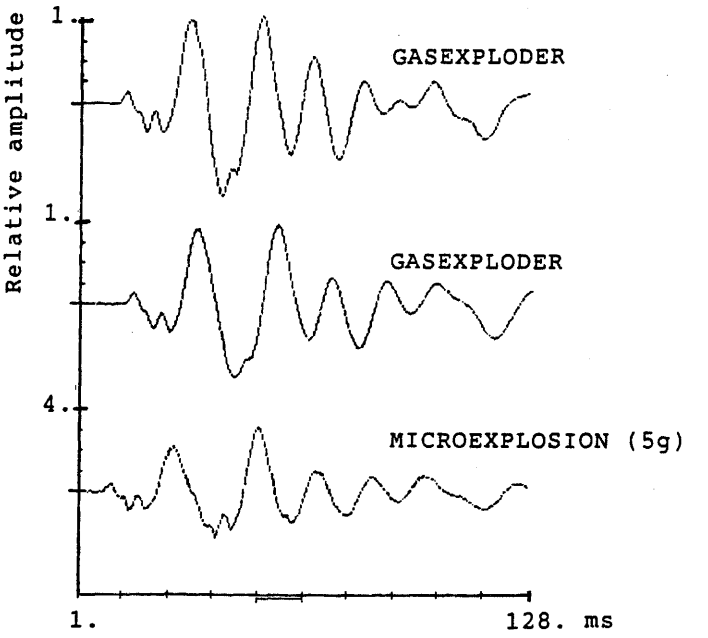

Figure 2-4. Comparison between records at one geophone position from gasexploder and microexplosion (5 g) shots (note the different amplitude scales). All shots were performed at 2 m depth in a pit with a diameter of 6 m. Recording distance was 40 m.

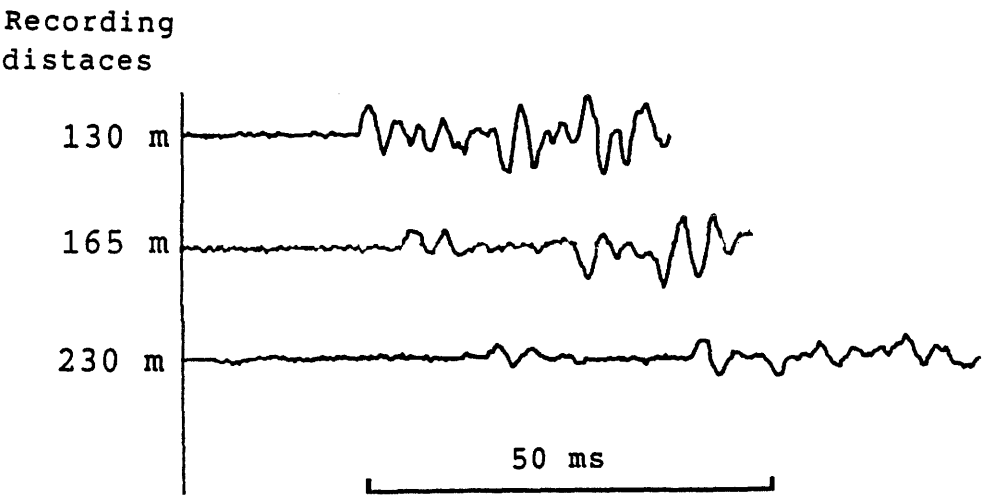

Figure 2-5. Examples of recordings at different geophone positions from a gasexploder shot. Shotdepth was at 85 m in a borehole with diameter of 110 mm.

2.3 TIMING SYSTEM

An essential part of seismic measurements is the determination of traveltimes, i.e. to determine the time it takes for the seismic wave to travel from the shot-point to the receiver. The time when the explosion occurs must be known with great accuracy. This function is provided by the timing circuit.

A properly designed timing system has the following characteristics:

- It has a unified (preferably TTL level, 0-5 V) output suitable for the data-recording electronics
- Timing should be independent of source strength Differences in rise-time or amplitude should not influence the trigger point

2.3.1 The Trigger Circuit

The trigg-pulse, marking the time when the seismic energy was released, can be extracted in several ways.

We have constructed a mechanical trigger device (Figure 2-6).

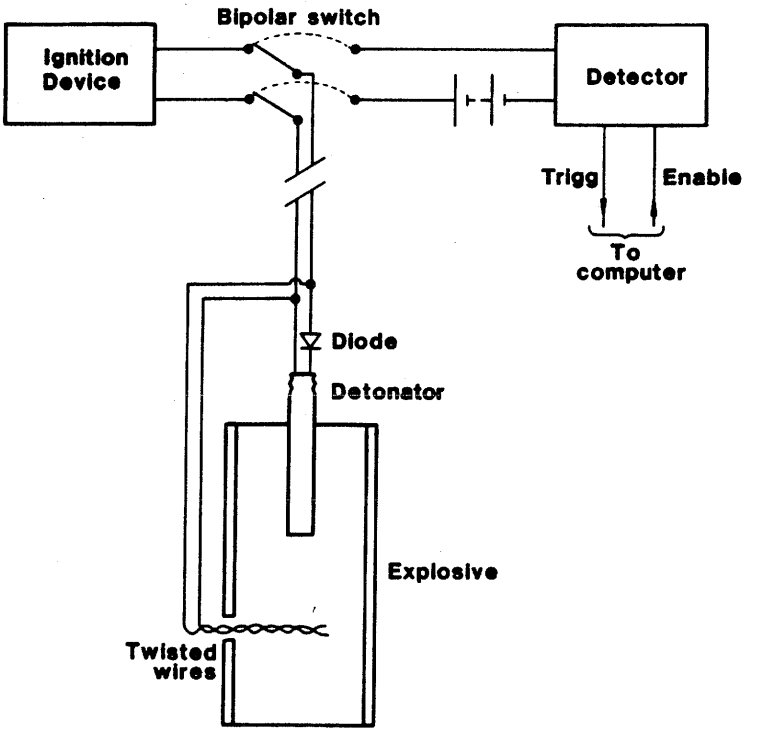

Figure 2-6. Schematic drawing of the charge and trigger arrangement.

The circuit operates on the principle that a contact is made between two insulated wires twisted together. The wires are welded together when they are reached by the shock-wave from the explosion. This gives a very distinct contact closure in contrast to the opposite arrangement, i.e. to let the explosion cut off a piece of wire. In the latter case the plasma which is formed in the explosion will make the circuit conduct even after the wire has been broken.

A special arrangement with a two-way switch and a diode, together with detonators with a delay of six seconds made it possible to use the same pair of wires for both the timing signal and the ignition device.

The circuit operates as follows: When firing, the ignition device is connected to the detonator. Then, during the six seconds when the detonator is burning, the switch is flipped to make connection between the twisted wire pair and the detector box.

2.3.2 The Detector

In principle the detector is a current sensor which senses the change in current when contact is formed between the twisted wires (Figure 2-6). Its output is a TTL-level pulse to the computer. The output is used to inform the recording system that a shot has been fired. It is also connected to an analogue channel and sampled in the same way as the signals from the seismic receivers (Figure 2-14).

The detector unit has an enable/disable input, which is controlled by the recording system. The detector is thus insensitive to incoming spurious pulses as it is enabled just before the shot is fired.

2.4 SEISMIC RECEIVERS

2.4.1 Surface Receivers

In a seismic tomography measurement it is desirable to have as many receivers as possible. Two different types are used, one on the surface and one in the boreholes (Figure 2-1).

For measurements on the ground, commercially available geophones are suitable (Figure 2-7). A frequency response of up to 1 kHz is sufficient since the uppermost ground layers act as a low-pass filter, cutting away the higher frequencies in the seismic signal.

When measurements are carried out in mines, where surface receivers can be put in galleries, a higher

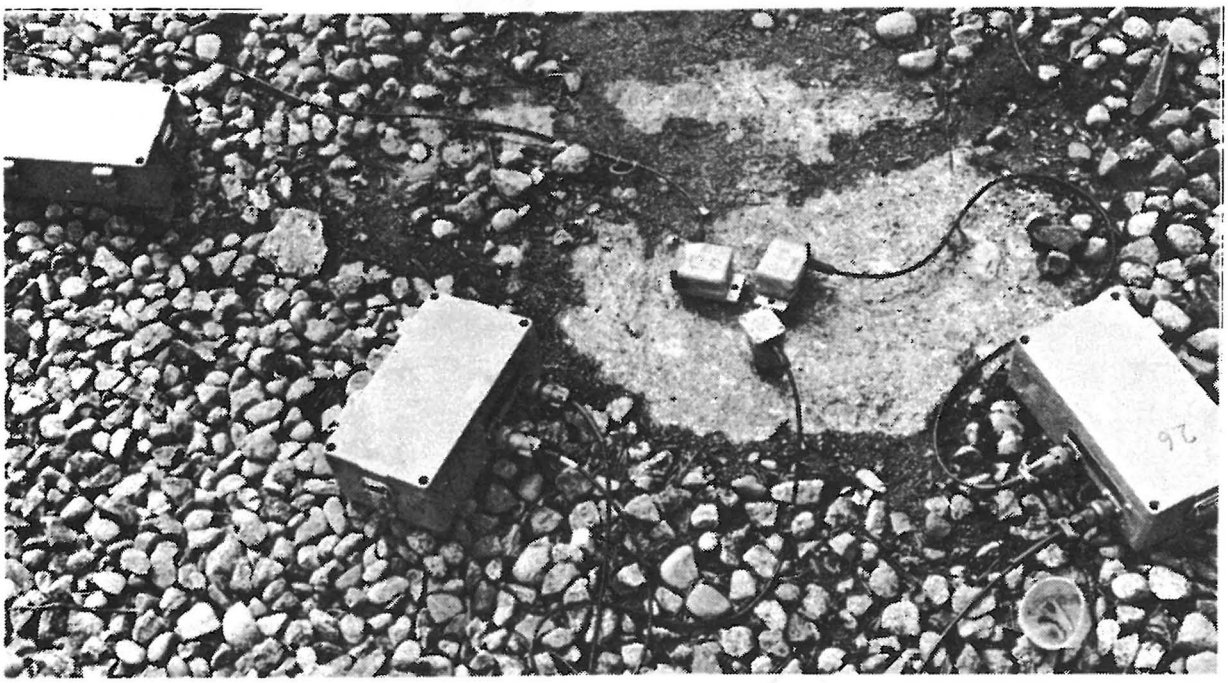

Figure 2-7. A three component geophone set including preamplifiers.

frequency response can be utilized. We then use accelerometers with an upper limit of 8 kHz.

A detailed description of the receivers is given in Appendix 1.

2.4.2 Borehole Receivers

For measurement in slim boreholes no commercially available equipment exists. We have therefore built a series of receiving units (Figure 2-8).

The harsh environment in the deep boreholes puts some special demands on the receivers.

Our units have the following characteristics:

- Each unit has three accelerometers for measurements in the three principal directions
- They can be used in both slanted and vertical boreholes down to a depth of at least 1000 m
- Each unit has a locking knee, which ensures good mechanical contact between the receiver and the borehole wall (Figure 2-9)

Up to four units can be mounted together to form an

Figure 2-8. A borehole receiver array.

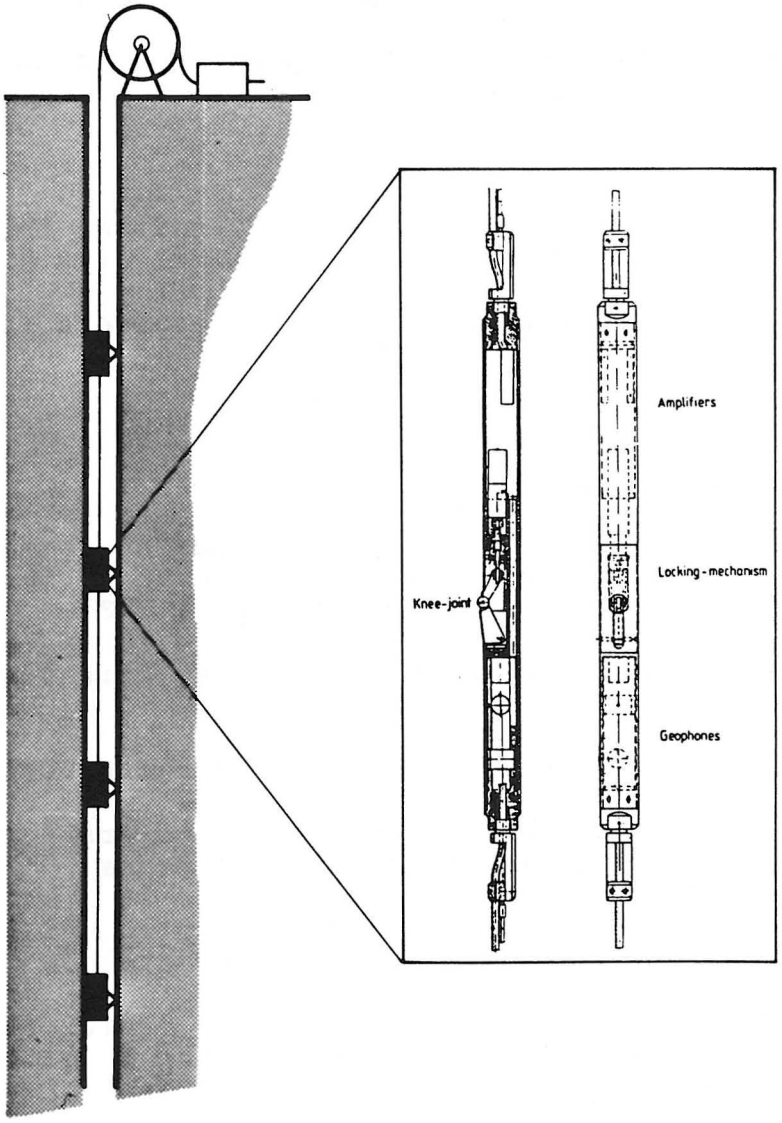

Figure 2-9. Outline of a borehole unit design.

array.

The advantage of using an array is two-fold: First it decreases the measurement time as more signals are recorded in each shot. Second, very accurate comparisons can be made between different parts of a borehole by using signals from different units but from the same shot.

The receiver array is connected to a cable which is reinforced with two steel wires. The cables are wound on a motor-driven winch for fast repositioning (Figure 2-10).

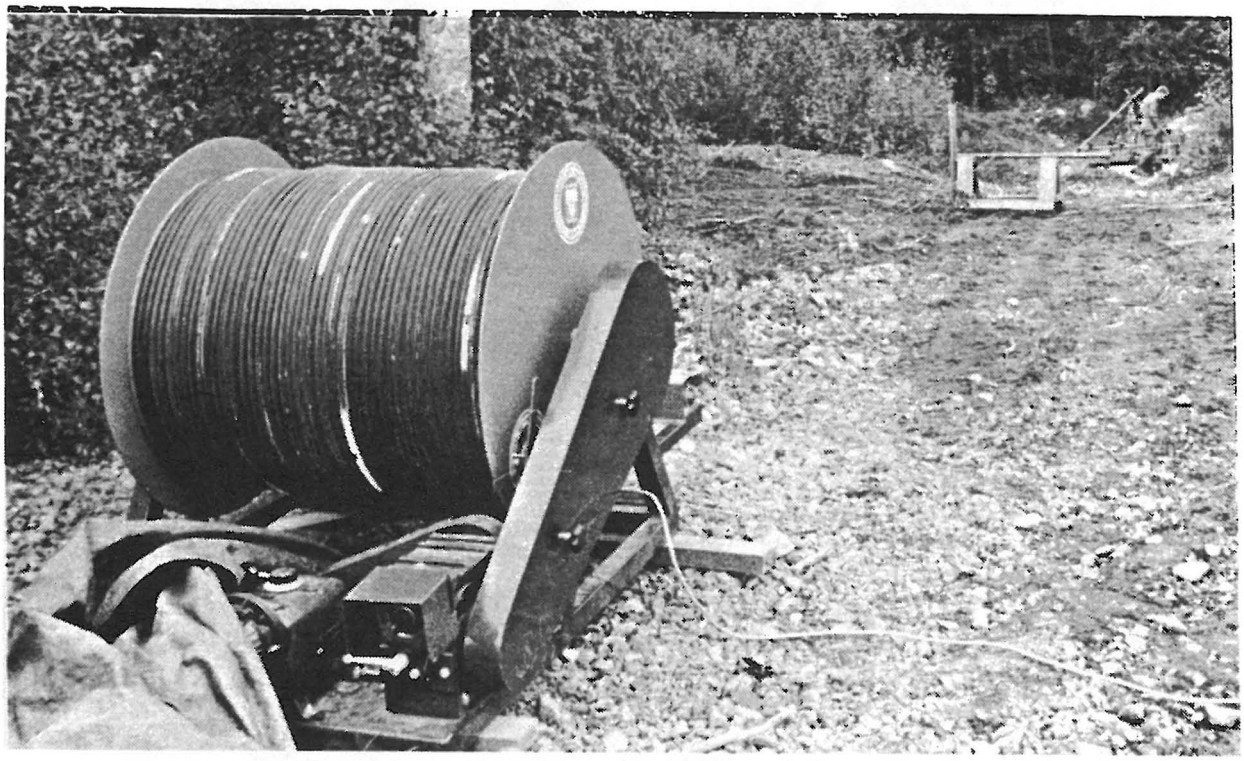

Figure 2-10. A cable winch.

At present, seven receiving units have been built. Three winches have been acquired, which means that measurements can be carried out in tnree boreholes simultaneously. Such measurements are especially valuable for 3-D seismic tomography.

2.5 DATA RECORDING SYSTEM

A versatile data-recording system is most essential when new experimental techniques are being developed. In addition to the normal requirements on a field recording system it must be possible to alter the experimental conditions if an unforeseen situation arises. It is also desirable to have the possibility to perform data reduction and analysis in the field, in order to spot errors as quickly as possible.

We have chosen to develop a system of our own. It is based on a PDP 11/34 mini-computer with various peripherals (Figure 2-11).

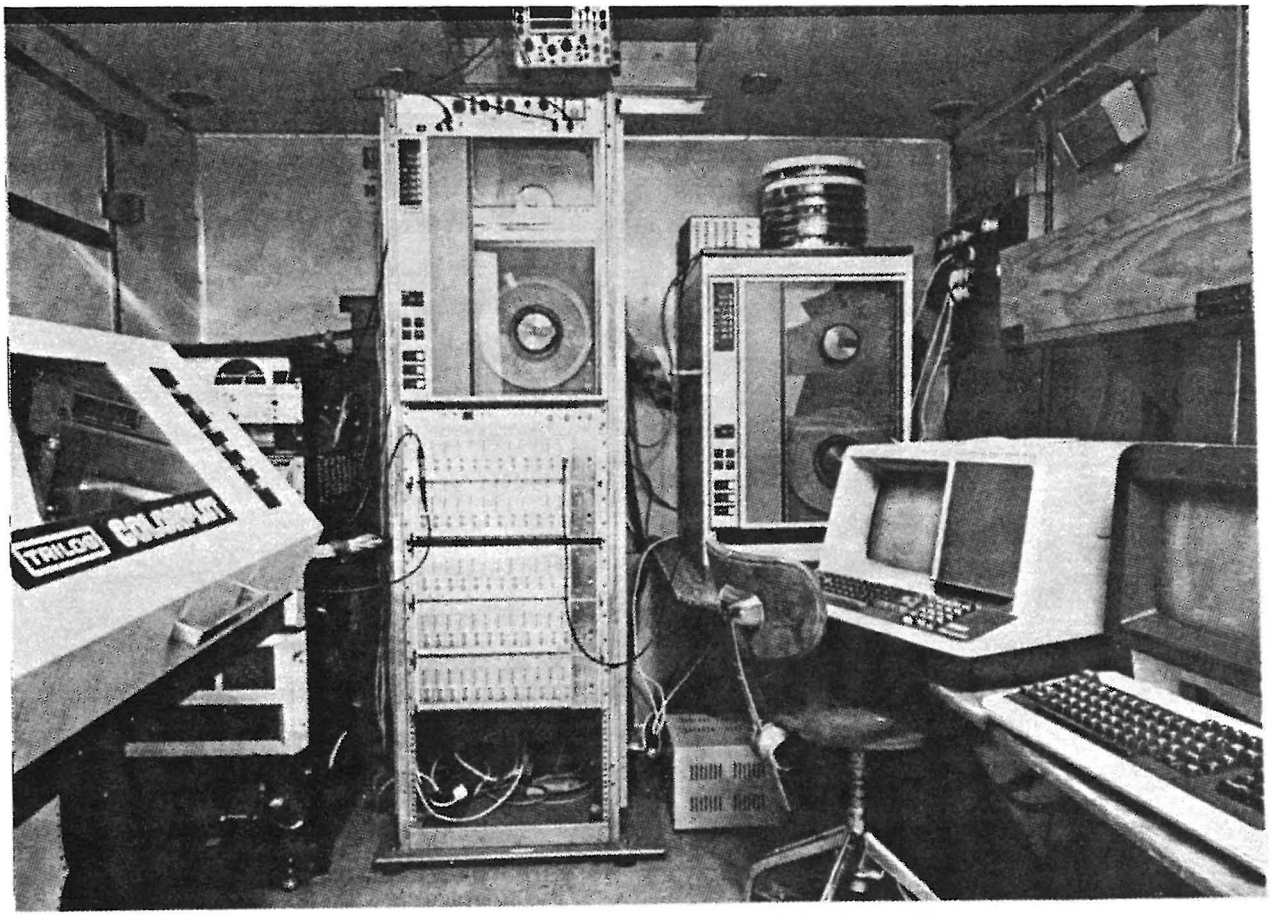

Figure 2-11. The Mobile Seismic System (MOSES) set up in the laboratory van.

The reasons for this are the following:

- A standard mini-computer is much cheaper
- The commercially available systems are very specialized and cannot be used for program development

- A standard computer can be used for other purposes besides field-data recording

- Service and spare parts are much more readily available for a standard system

- A standard computer can be updated and enhanced gradually as new peripheral equipment becomes available. A special system is more rigid and will be obsolete in a shorter time

2.5.1 Field computer configuration

In order to make a data acquisition system from a standard computer it must be expanded with various extra peripherals (Figure 2-12). The standard peripherals have to be selected carefully as they are to be operated in a harsh environment, quite different from the normal air-conditioned computer room.

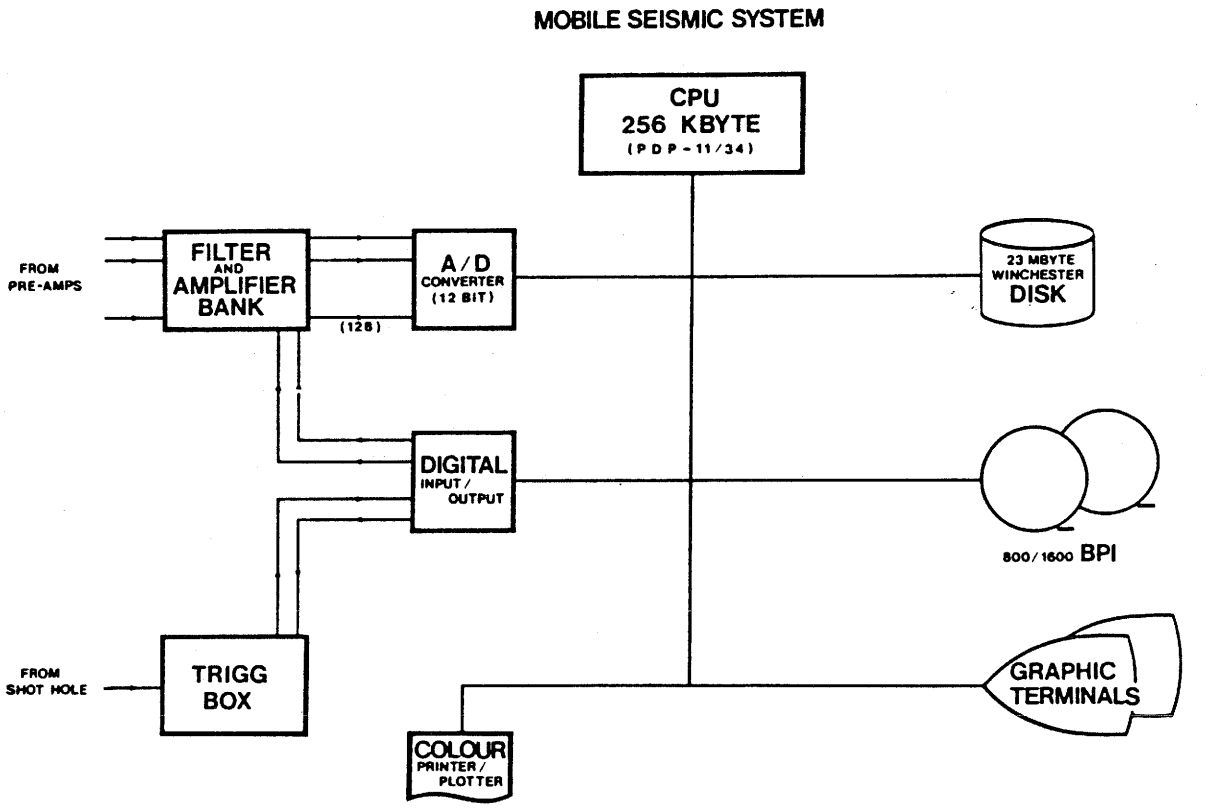

Figure 2-12. The main parts of a seismic data acquisition system.

The secondary storage, usually disc memory, is often the most fragile part. Therefore we have selected a

Winchester-type disc, which has proven to be very rugged. It is completely sealed, which means that it is not disturbed by the dust and dirt which cannot be avoided when operating in the field.

In addition to the disc memory a backup medium is required. The alternatives are cassette and open-reel tape drives. For our system we choose industry compatible magnetic tape, which facilitates the transport of data to other computers.

The tape drives have mechanical tension arms, instead of vacuum columns, to avoid environmental problems.

The real-time subsystem is the most important part of the field computer.

The present computer was selected mainly because of its ability to interface to all kinds of laboratory equipment. The analogue signals are sampled by a special microprocessor controlled subsystem called the LPA (16). It has two twelve bit A/D (analogue-to-digital) converters with a maximum sampling rate of 150 000 samples per second. The total number of analogue channels is 128.

The trigg-pulse detector, the amplifier and the filter controls are interfaced by DR-11C parallel digital ports.

2.5.2 Amplifier And Filter Electronics

The amplifiers and filters were designed and built at FOA. The main design points were

- Battery-powered pre-amplifiers with low power consumption
- Main amplifiers with integrated filters
- Compact design
- Only one signal cable per amplifier bank

Five banks of twelve amplifiers each have been built.

The gains can be set from 0 to 48 dB in steps of 6dB. The high-pass filter can be selected from 0 to 100 Hz. The low-pass filter, which also acts as an anti-aliasing filter, can be set from 100 Hz to 10 kHz.

The filters have a slope of 24 dB per octave.

2.5.3 Field Computer Software

The programs are of two types, real-time programs and data-analysis programs (Figure 2-13).

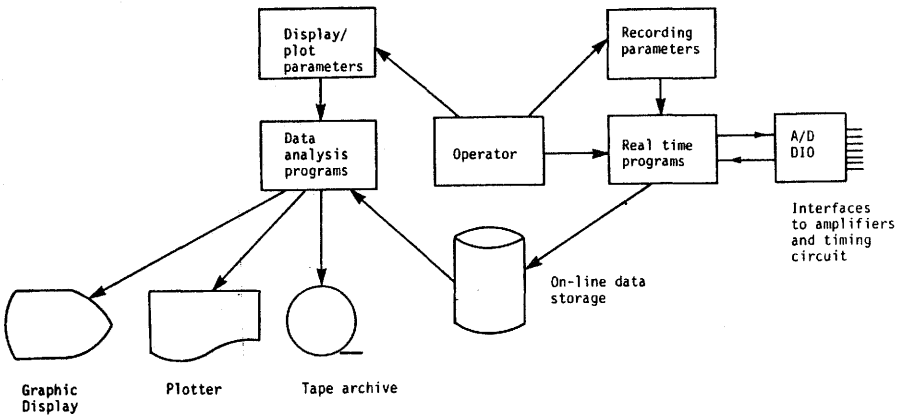

Figure 2-13. Layout of the field computer software.

The real-time programs deal with the actual sampling of the A/D converter, stores the data onto disc memory or magnetic tape and controls the settings of the filter and amplifier banks.

The operating system, RSX-11M (19) has many facilities for multi-programming and inter-task communication.

The system is organized so that specific real-time functions are isolated to separate programs. This modular structure minimizes the work if parts of the hardware are changed as only a small module has to be re-programmed.

All relevant parameters (sampling rate, number of A/D channels, gain and filter settings etc) are stored in tables. Hence the real-time programs do not have to interact with the operator. The operator interaction is carried out by separate, menue-oriented programs.

A special technique, called pre-event sampling, is utilized to ensure maximum accuracy for the shot-time determination. When the computer has been started to record a shot, but before the shot has been fired, data is stored in a circular buffer. Upon receiving a signal from the trigg-pulse detector, the data are stored in a memory buffer until all space is used. This means that some data are recorded before the shot was fired. By feeding the detector signal to one of the analogue channels the arrival of the trigg-pulse can be clearly seen (Figure 2-14). As the rate of sampling is

controlled by a crystal oscillator with high precision, the time between the shot and the onset of the seismic signal can be determined very accurately.

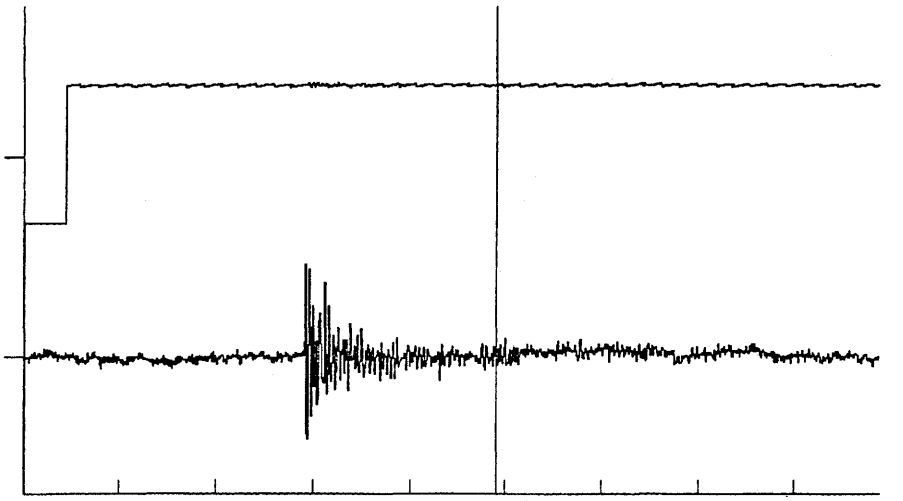

Figure 2-14. Record sections, showing one accelerometer signal and the trigg pulse detector signal from a shot.

3 FIELD EXPERIMENTS AT THE LARGE-SCALE TEST SITE

3.1 INTRODUCTION

The main purpose of the large-scale experiment was to apply the seismic crosshole method at distances up to 1000 m.

A triangular area, with a borehole in each corner, was selected. The aim was to investigate the obtainable resolution at large distances, up to 1000 m, and also to carry out measurements in three dimensions.

Furthermore, new source-receiver combinations (the so called VSP geometry with sources at the surface) were tested.

3.2 DESCRIPTION OF THE LARGE-SCALE TEST SITE

The large-scale test site at Gideå is situated in the northern part of Ångermanland about 30 km north-east of Örnsköldsvik (Figure 3-1).

The site has been investigated and described by the Swedish Geological Co. in a number of studies (1),(2),(18). Some of the main characteristics obtained from these investigations are outlined in the map in Figure 3-2. The bedrock consists of migmatized gneiss of north-eastern structural strike and small dip. Dolerite dikes appear across the area, usually having an east-western strike and widths of less than 1 m. Two dikes in the central part of the area are 2-10 m wide. The map in Figure 3-2 indicates the positions of eleven local fracture zones. The properties of these fracture zones have earlier been examined by means of 13 core-drilled holes and 24 percussion-drilled holes. The widths of the fracture zones were then found to vary from 1 to 24 m.

The crosshole measurements were performed in a rock volume bounded by the three core-drilled holes Gi1, Gi2 and Gi11.

It appears from this map that three dominating fracture zones (I - III) are crossing half of the test area. The width of zone I has been estimated to about 25 m, zone II to about 15 m and zone III to 10 - 12 m. All boreholes are slanting and uncased. The three core-drilled holes Gi1, Gi2 and Gi11 have a length of about 700 m and are 56 mm in diameter. The percussion-holes 6, 13 and 21 (used as seismic source holes) are between 90 m and 150 m long with a diameter of 110 mm.

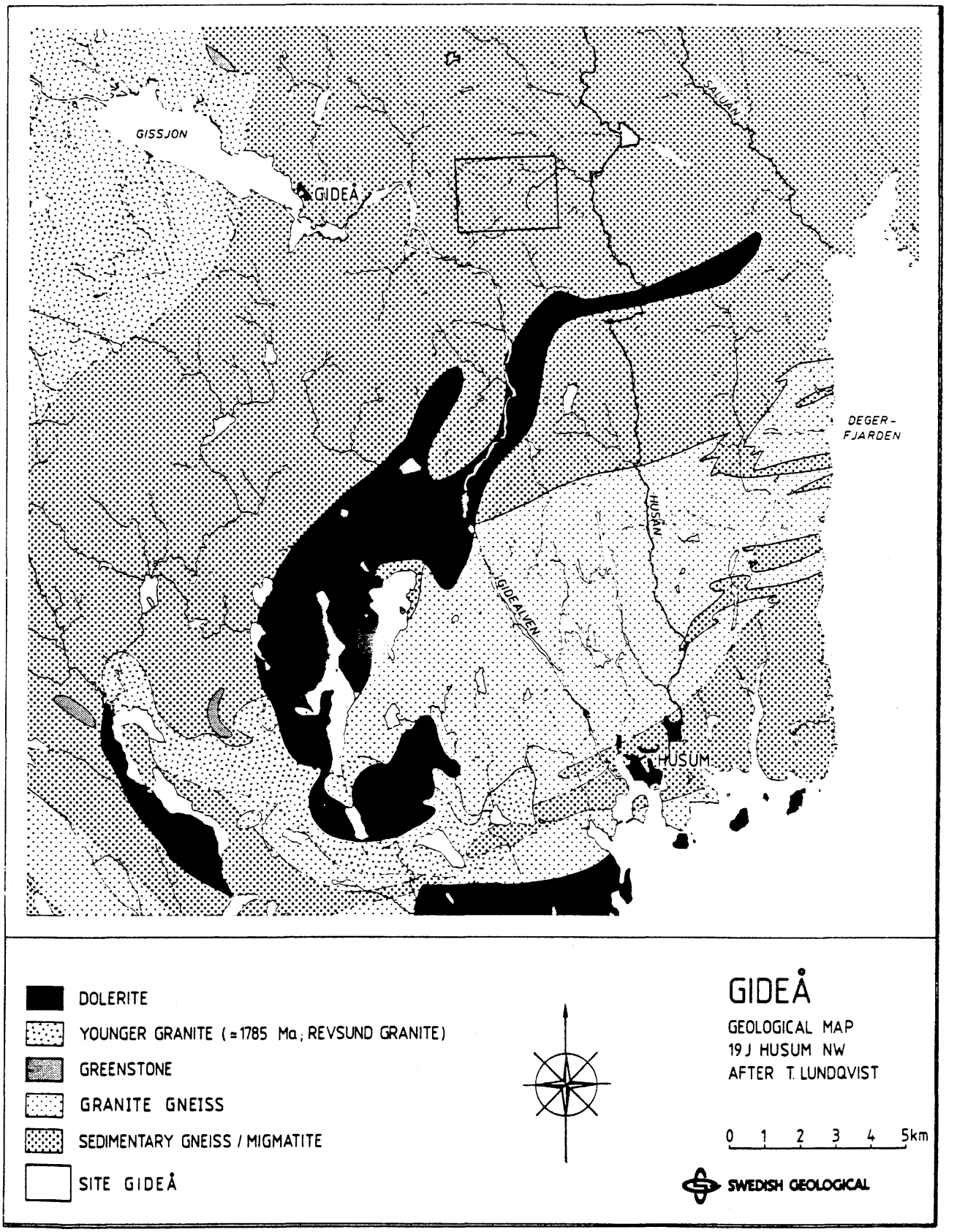

Figure 3-1. Regional geological map including site Gideå.

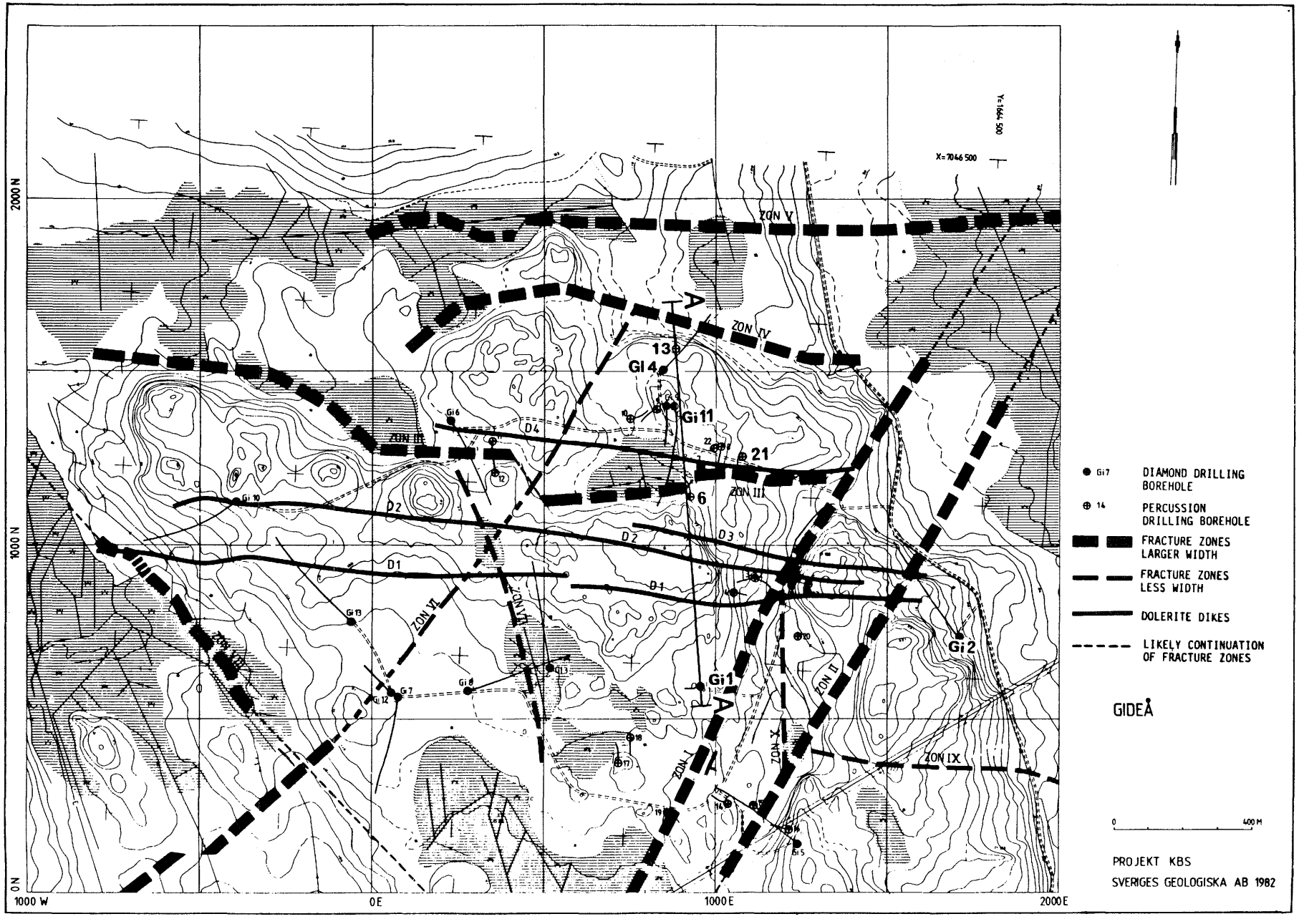

Figure 3-2. The Gideå site.

The distance between the top of the recording holes are 1050, 800 and 750 m. The difference of the surface topography altitude at the measurement positions along the three lines is within 24 m. The topography variation within the area (about 0.4 square kilometers) is 24 m and and it consists mainly of outcrop, except for the central part.

3.3 TECHNICAL DETAILS ON THE EXPERIMENT

The section was surveyed on two occations, in October 1983 and during seven weeks in June and July 1984.

Two different techniques were used, explosions at the surface (VSP geometry) and explosions in the borehole (traditional crosshole geometry).

The surface explosions were fired in 1.5 meter deep holes (diameter 30 mm), drilled along the lines between the three core-drilled holes. The explosive charges were made from a penthyl-based explosive ("M46") with yields of 62 g. Just before the shots were blasted the holes were filled with water in order to ensure good coupling to the ground.

Fourteen shot-points were placed between the holes Gi1 and Gi2, eleven points between Gi2 and Gi11 and three points between Gi1 and Gi11. Five to ten shots were fired in each ground-hole and simultaneously recorded in all three core-drilled holes. The number of shots per hole was determined by the local rock quality. A new hole was drilled if the recorded amplitudes dropped too low.

The recording positions in the borehole were generally spaced with a separation of 10 m. Examples of sections recorded at a depth of 520 m in hole Gi2 from various shot positions are given in Figure 3-3.

The explosions in the boreholes were fired in three percussion-drilled holes (6, 13 and 21) and the three core-drilled holes Gi1, Gi2 and Gi11.

In the percussion-drilled holes cylindrical charges of 30 - 62 g of the paste M46 were used. In the core-drilled holes the explosive paste "Octol" was used to prevent chemical contamination. The charges were 50 g for all shots (Figure 2-2).

It was found that at recording distances up to about 500 m, a yield of 30 g usually provided a sufficient signal-to-noise ratio.

The position accuracy of a microexplosion is estimated to be within 0.1 m. The explosions were properly centred with a glass device to minimize the effects on the walls of the boreholes and to generate reproducable seismic signals.

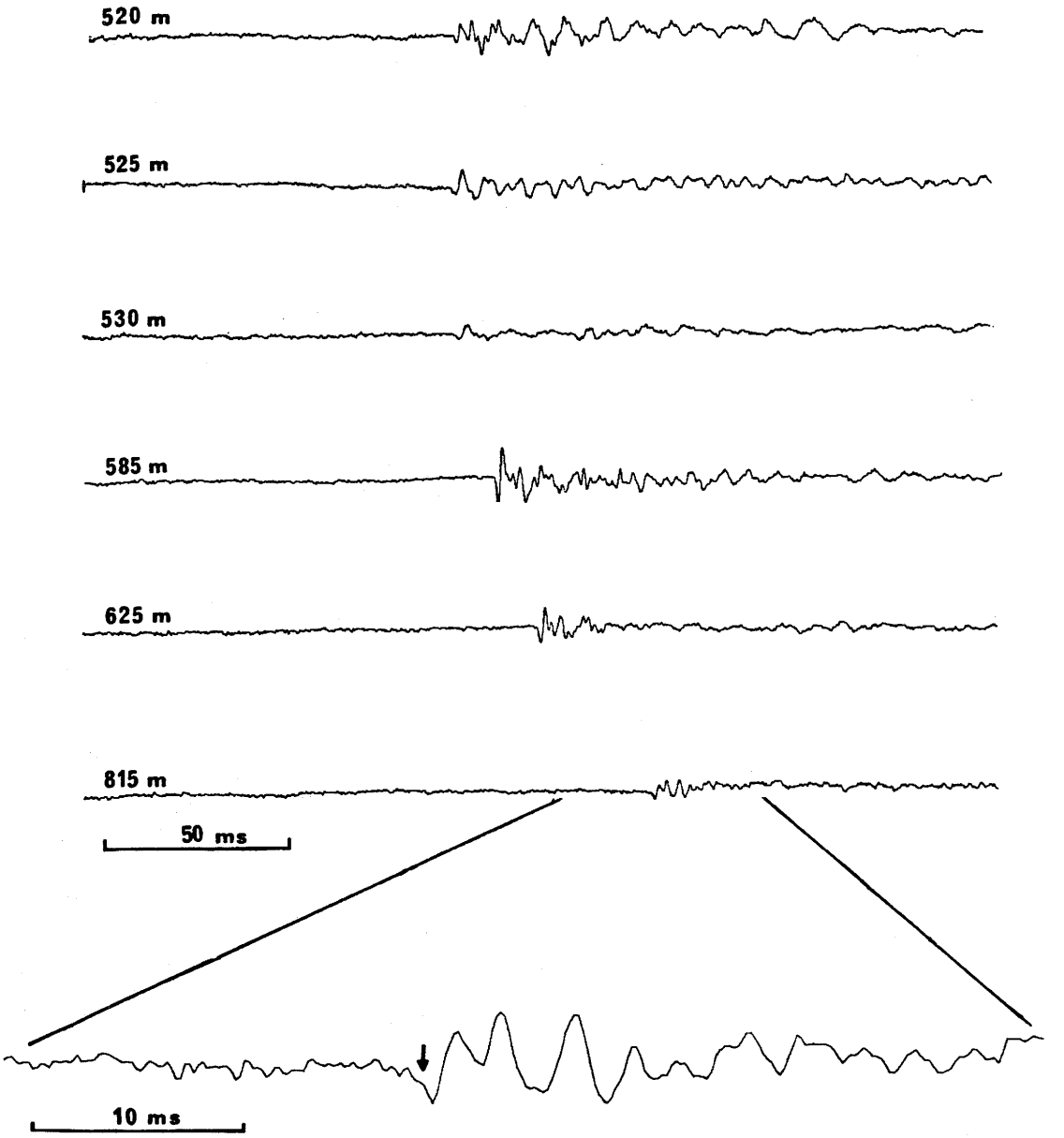

Figure 3-3. Recordings at a depth of 520 m in Gi2, (horizontal component), from surface shots at different positions along line Gi1 to Gi2. The shots at 815 m is shown in both normal and expanded scale.

The shot series in hole Gi2 was interrupted after only two recorded shots at 544 m and 300 m depth, because of an obstruction which was found around 340 m depth. It was not possible to clean the hole and no more measurements or shot firings could be done below this depth.

The holes Gi1, Gi2 and Gi11 were used both for measurements and as source holes, but firing and measurements were never performed simultaneously in one hole. The deep shots in the core-drilled holes were also recorded at geophones located on the surface. Charges fired on the surface were only recorded with

the borehole accelerometers.

The seismic signals were picked up by one accelerometer array in the borehole Gi2 and by another array and single-element unit alternating between holes Gi1 and Gi11. The deep shots were also recorded by geophones on the surface close to the line between the top of hole Gi1 and near the top of hole 13.

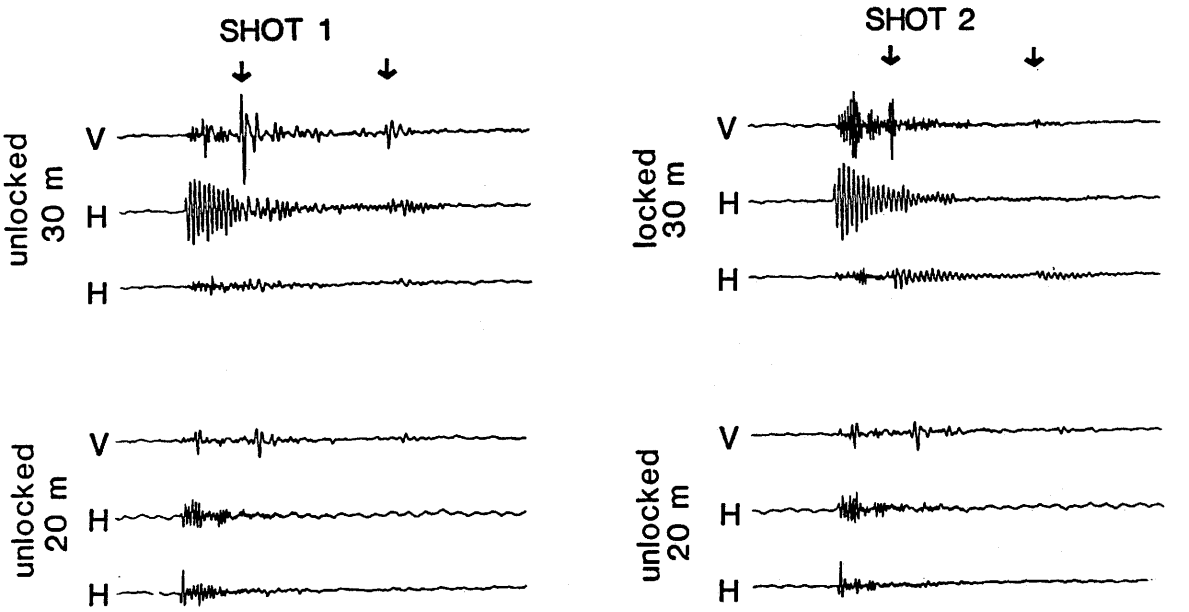

Figure 3-4. Comparison between records from locked and unlocked borehole accelerometer elements. Shotdepth was at 149 m in hole 13. The records from the unlocked element at 20 m are reference records for the two shots. The locking of the element at 30 m depth at shot 2 reduces the tube waves (marked with arrows) and increases the frequency content of the recordings, especially on the verical-component.

All these geophone locations are in outcrop and the spikes of the geophones were wedged into hand-drilled holes (diameter 17 mm, depth 40 - 50 mm). Three-component geophone sets were used at four locations and vertical-component geophones at the other 23 positions along this line. All surface geophones were calibrated relative to each other.

For the borehole recievers it was found that the signal quality was somewhat better when they were clamped against the borehole wall. Figure 3-4 shows a

comparison between records from locked and unlocked borehole-accelerometer elements. The shot-depth in hole 13 was 149 m. The records from the unlocked element at 20 m are reference records for the two shots. The locking of the element at 30 m depth at shot 2 reduces the tube-waves and increases the frequency content of the recordings.

The locking of the receivers also reduce the tube-wave signals observed on the vertical-component recordings. In the holes Gi2 and Gi11 the receivers were locked unless the borehole loggings indicated fractures.

The recording system was normally operated at a sampling rate of 3.3 kHz (i.e. 0.3 ms sampling) with 30 channels.

A special test was performed with shots at five depths in hole 17 with a reciever at 410 m depth in hole Gi11.

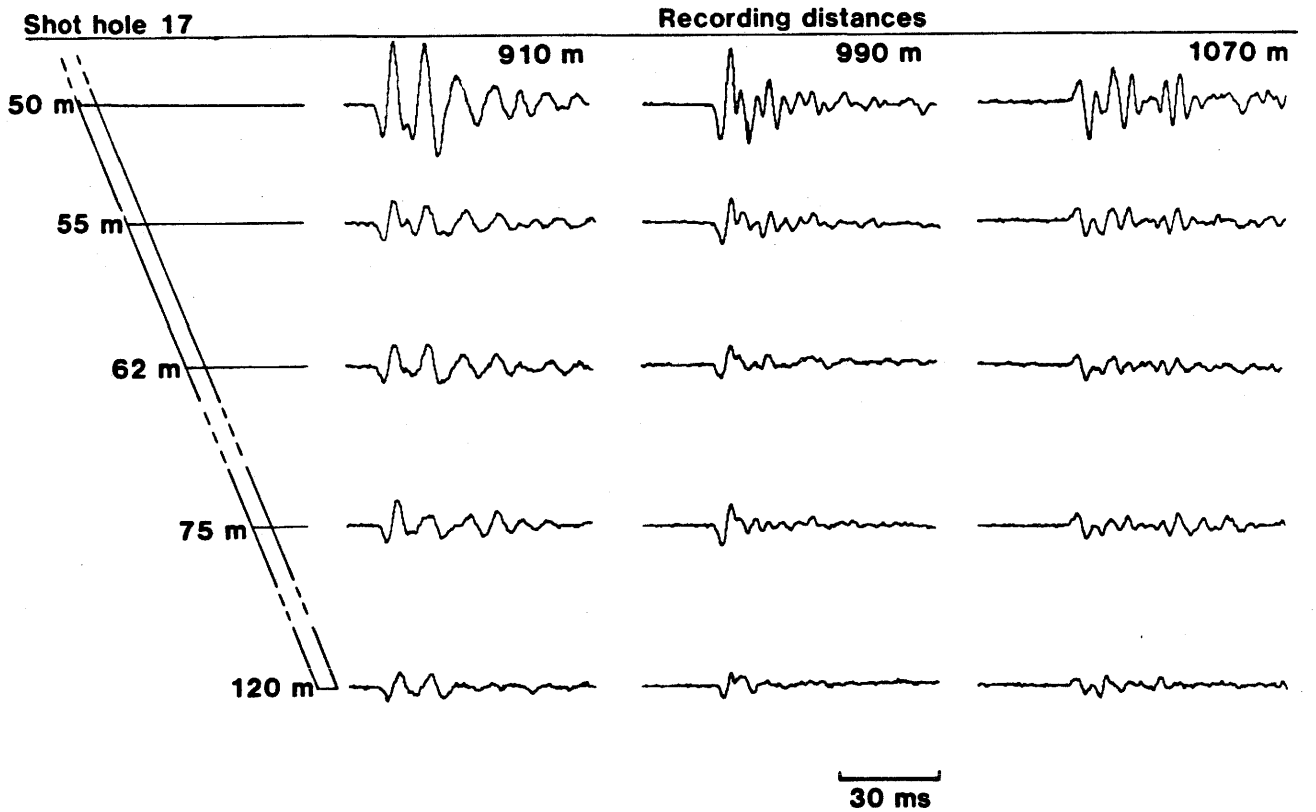

Figure 3-5. Examples of recordings from the shot series in hole 17 with a receiver at 410 m in Gi11. Observe the big difference in amplitudes from the shots at 50 m and 120 m.

The purpose was to test if yields less then 50 g provide sufficient energy for distances over 1 km in this area. An earlier study in the Stripa mine had indicated that no damage is done to the borehole if the yields are less then 50 g.

It was verified that a 50 g micro-explosion would be a sufficiently strong source for these distances. When analysing this test a special feature was observed. The amplitudes recorded from different shot depths in the hole showed great differences (Figure 3-5). This is probably due to a zone of less homogeneous rock just below 50 m depth in hole 17 which attenuates and reflects signals from below.

3.4 ANALYSIS AND RESULTS

3.4.1 2-D Analysis Procedures

The 2-D tomographic analysis was made in two parts. One coarse analysis between the boreholes 13 and Gi1 was performed, and one in more detail between the holes 13 and 6 (Figure 3-6). In this way we can make a comparison between two independent tomographic solutions from different subsets of a common data-set.

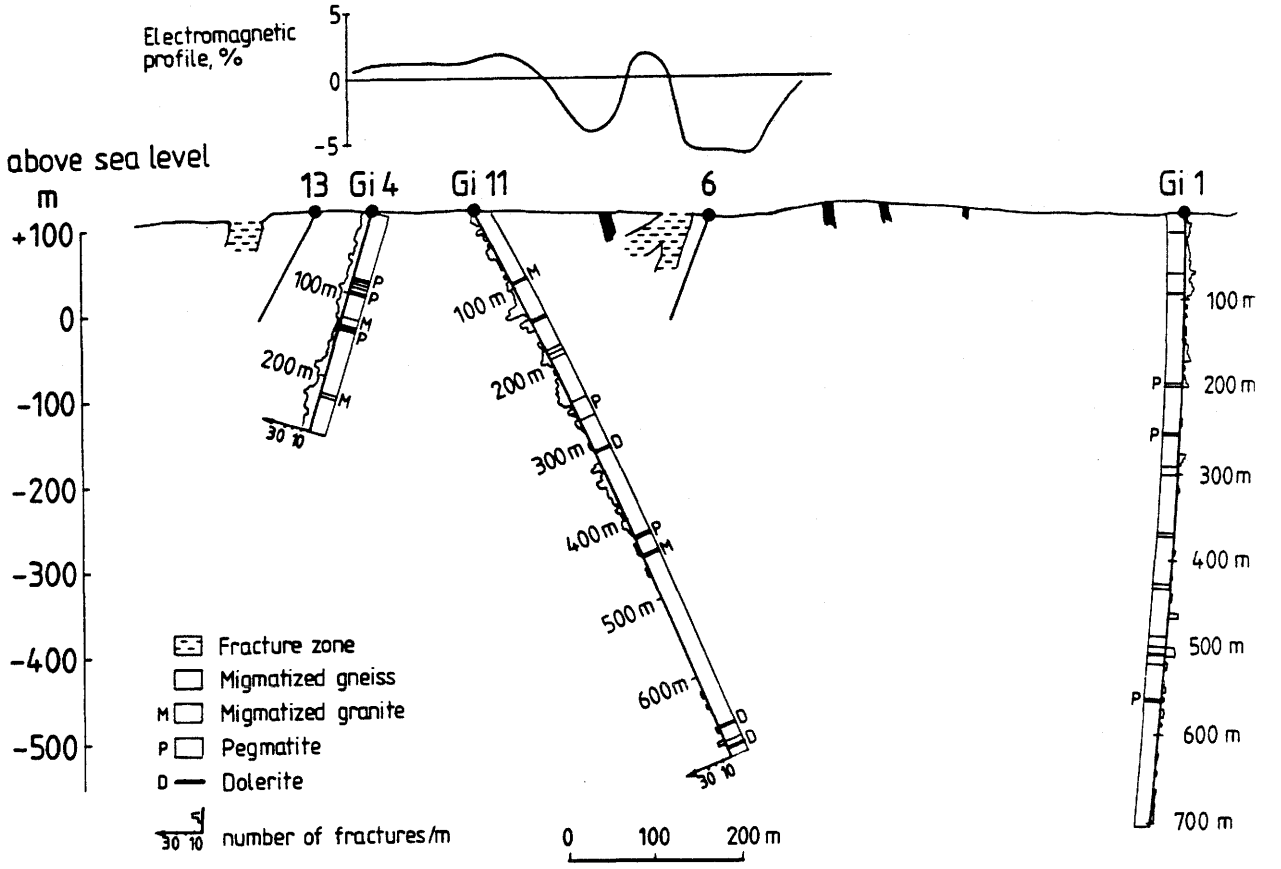

Figure 3-6. Projected vertical section view showing the borehole locations. General geology and fracture frequency are indicated for the three cored drilled holes. An electromagnetic profile and the features from surface geology are also outlined.

Since shots and geophones are not situated in the same plane the cross-section becomes the projection of the positions of the shot points and geophones onto a

plane. A linear equation system was solved for the unknown cell-slownesses. A description of the method is given e.g. in (11),(12),(13),(14).

The error in the measured traveltimes is estimated to be less than 0.2 ms.

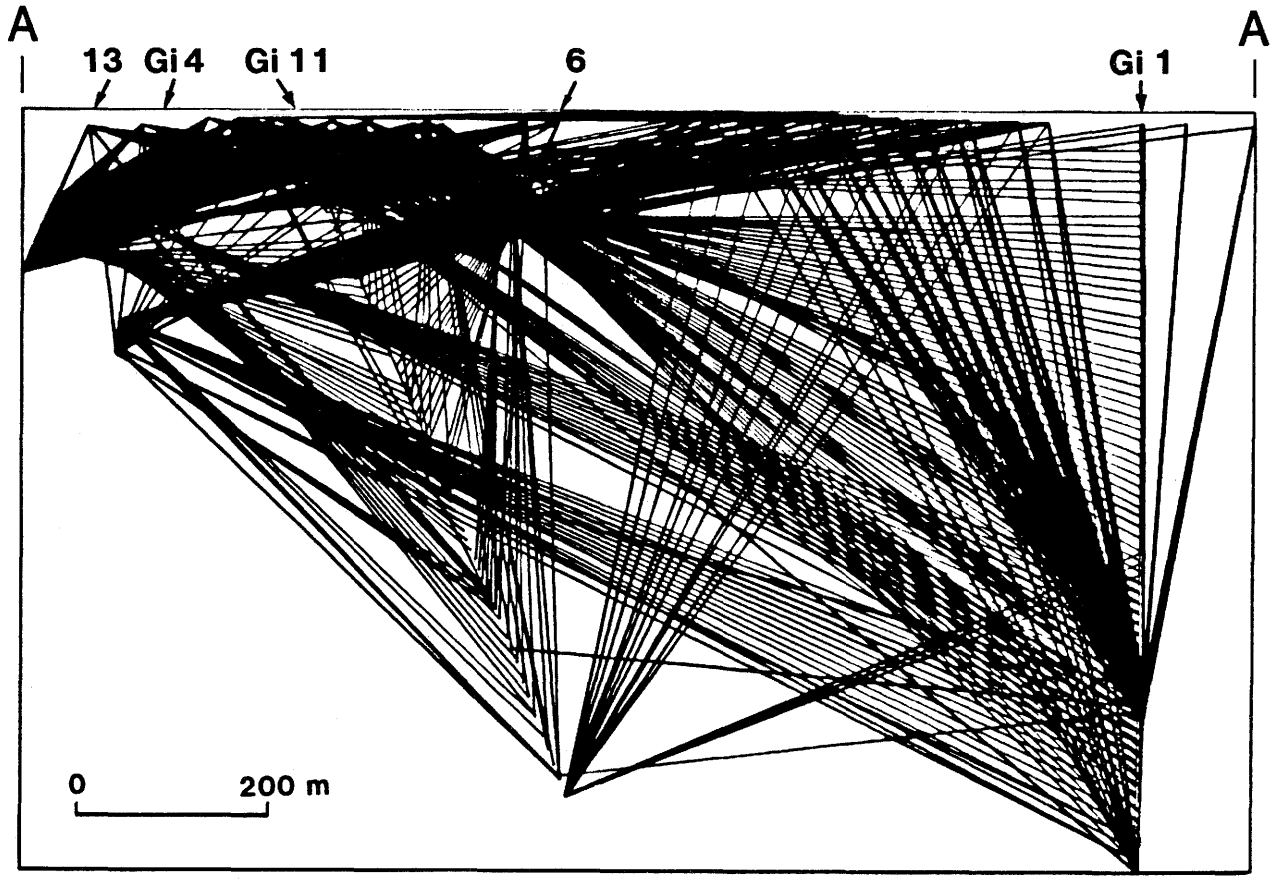

Figure 3-7. Projected vertical 2-D section view showing source to receiver ray paths.

Figure 3-7 shows the 800 ray-paths over the whole vertical section including hole Gi1. The selected subset of 467 rays which only covers the area between holes 13 and 6 is shown in Figure 3-8. In this detailed section several of the longest paths disappear.

The result from the tomographic inversion made from all the traveltimes over the whole section is depicted in Figure 3-9. A decomposition into squares of 25 m was used, leading to 968 unknown parameters. Approximately 200 iterations with the Conjugate Gradients (CG) method were performed.

In the detailed subsection a decomposition into squares of 10 m side was used, leading to 1865 unknown parameters. Approximately 170 iterations with the CG-method were performed. The results from the tomographic inversion of the resulting traveltimes is shown in Figure 3-10. (Note that the velocity scales are not the same in the two Figures 3-9 and 3-10).

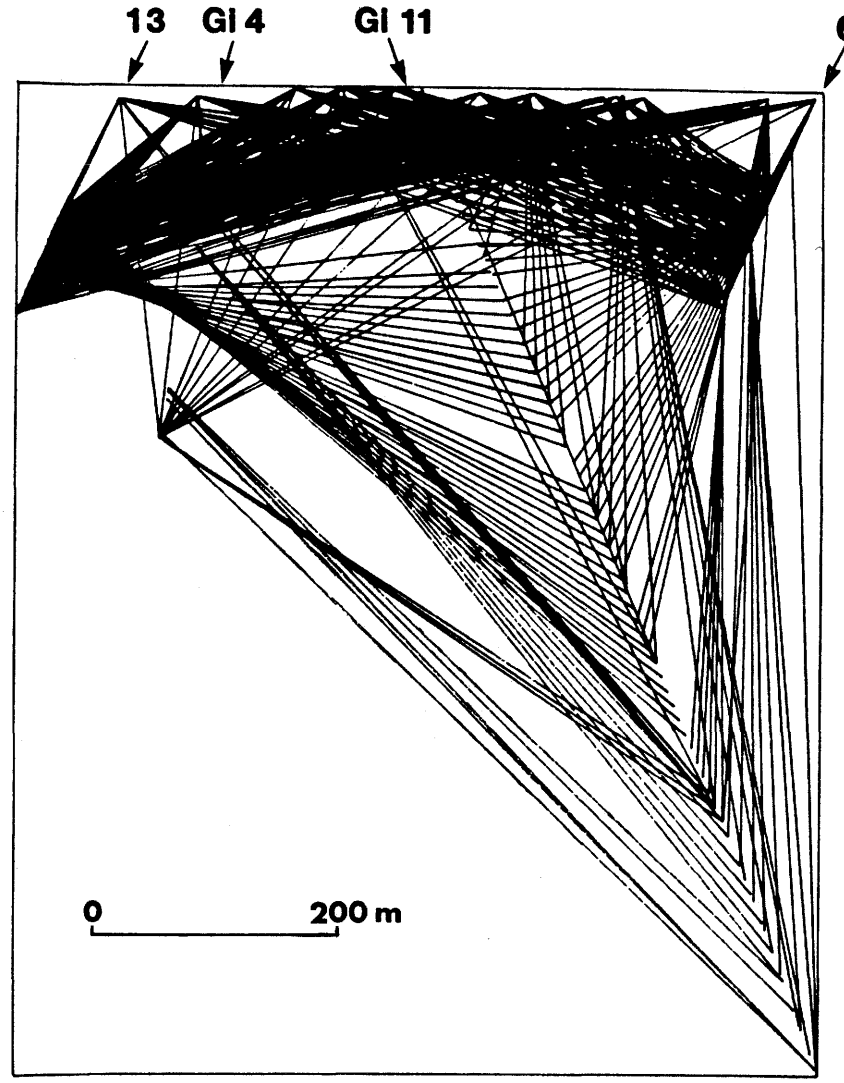

Figure 3-8. Raypattern for the partial section between the holes 13 and 6.

As expected, there are no contradictions between the two results. Because of the smaller cell size the detailed subsection gives more details in the velocity pattern. As short paths are often most significantly affected by low-velocity zones, it is interesting to observe that the distortion in the detailed picture is not more severe.

Some features can be found in the experimental pictures. The depth dependence of the velocity is obvious. The velocity is about 5 km/s at the surface and about 6 km/s at 500 m depth. Two low-velocity regions cross each other about 100 meter below the surface at the top of hole Gi11. Another quite clear pattern is a structure strongly related to the ray-pattern.

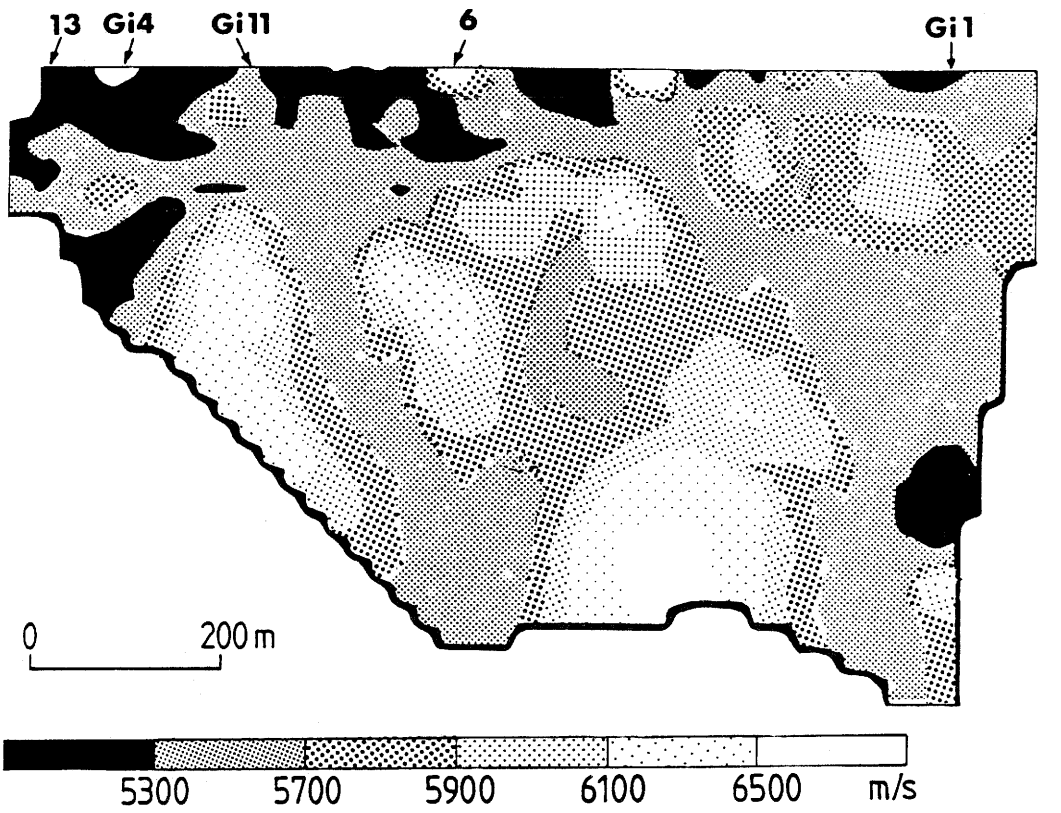

Figure 3-9. Tomographic map of the whole crosshole section between holes Gi1 and 13.

3.4.2 Discussion

As can be seen in the following examples, (figures 3-11 to 3-17) the structure is not uniquely determined by the experimental data set. It is therefore important to compare the experimental result with results from calculations on theoretical models. From the other geophysical measurements in the area, an interpretation in terms of thin fractured strips has been suggested. It is therefore of interest to investigate theoretically how such strips would be mapped by the present inversion procedure and see if results compatible with the data could ensue.

As a start, the region between holes 13 and 6 is considered. A first example is shown in Figure 3-11. A laterally homogeneous velocity model was assumed. The depth dependence is given to the right (a smooth increase between the bars from 4.55 km/s to 6.05 km/s).

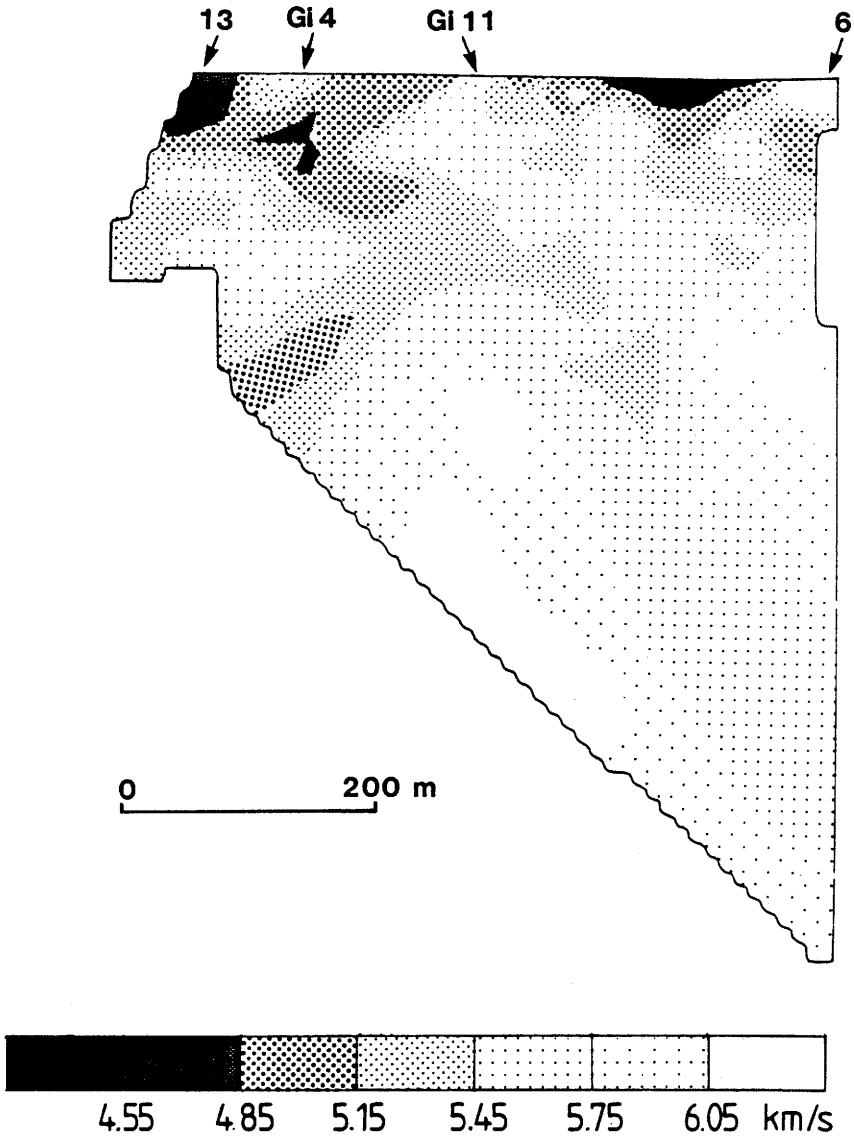

Figure 3-10. Tomographic map of the partial crosshole section between holes 6 and 13.

The reconstruction is reasonable although some wiggles in the level curves are present because of smoothing and neglection of ray-bending in the inversion. A comparison with Figure 3-10 does indeed indicate that the true structure is more complicated. Figure 3-12 is as Figure 3-11 except that a low-velocity rectangle and a low-velocity strip were included in the model (smooth transition zones at the boundaries). Note that low velocities appear in the upper right part as in the experimental result (Figure 3-10). The image of the strip will be smoothed and it is difficult to follow its extension downwards because of the less dense ray-coverage there. Nevertheless, very clear indications of its existence are obtained. In Figure 3-13 the direction of the strip was different but, in principle, similar observations can be made. A comparison with the experimental result is interesting. In Figure 3-14 both the strips are present.

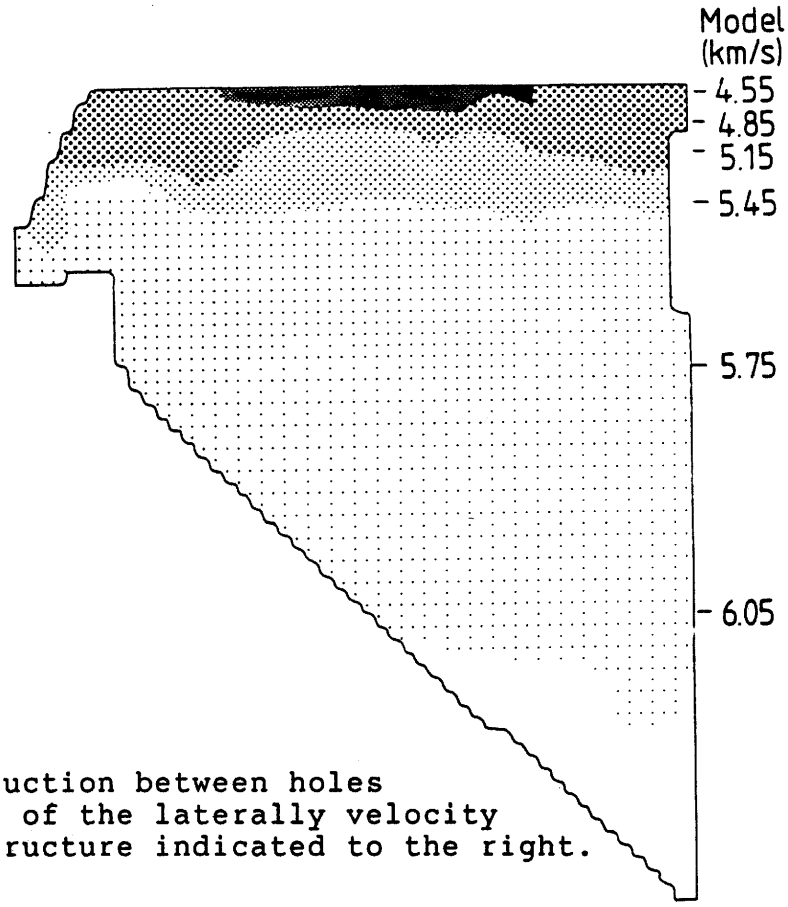

Figure 3-11. Reconstruction between holes 6 and 13 of the laterally velocity model structure indicated to the right.

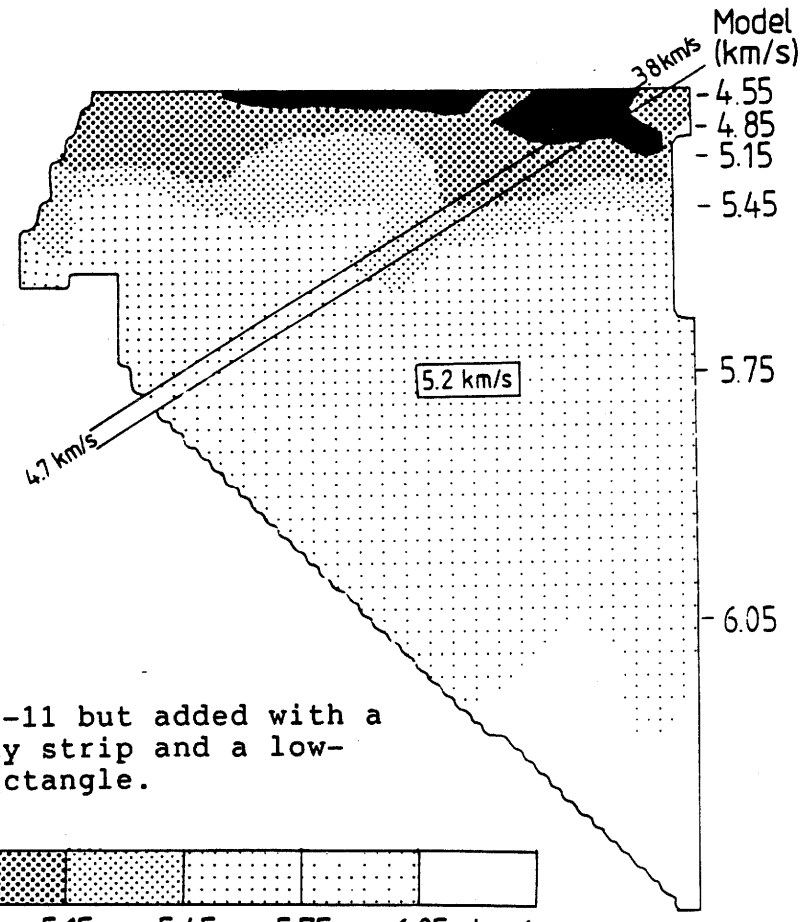

Figure 3-12. As Figure 3-11 but added with a low-velocity strip and a low-velocity rectangle.

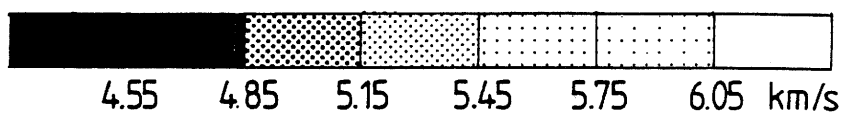

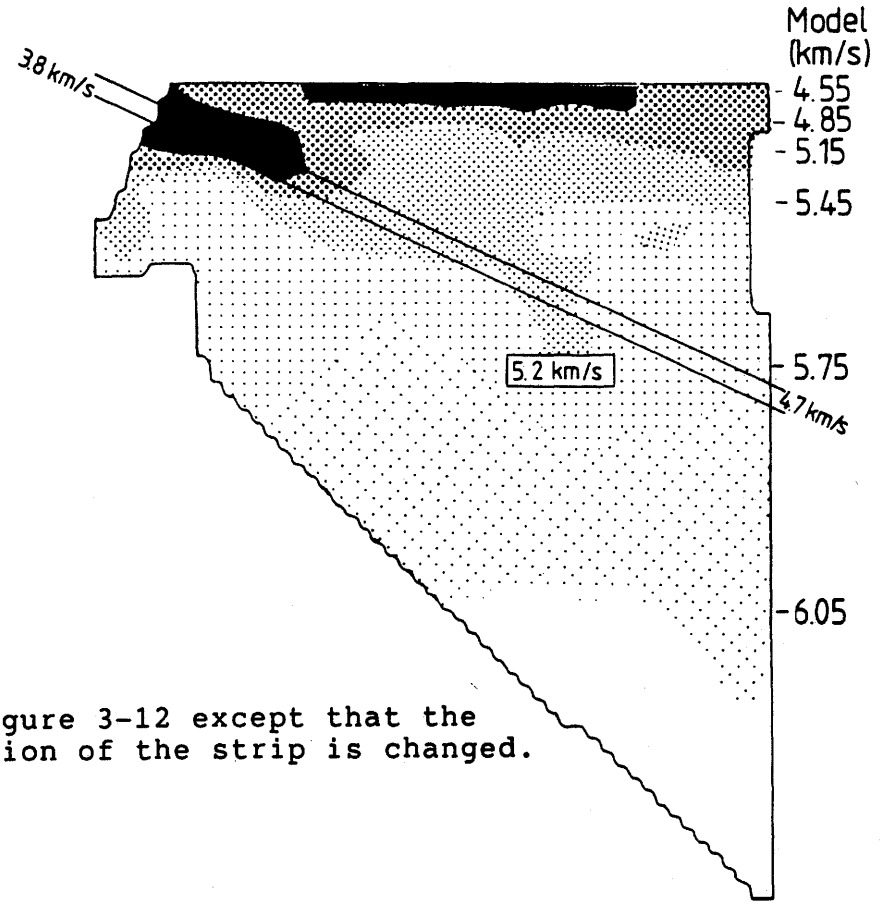

Figure 3-13. As Figure 3-12 except that the location of the strip is changed.

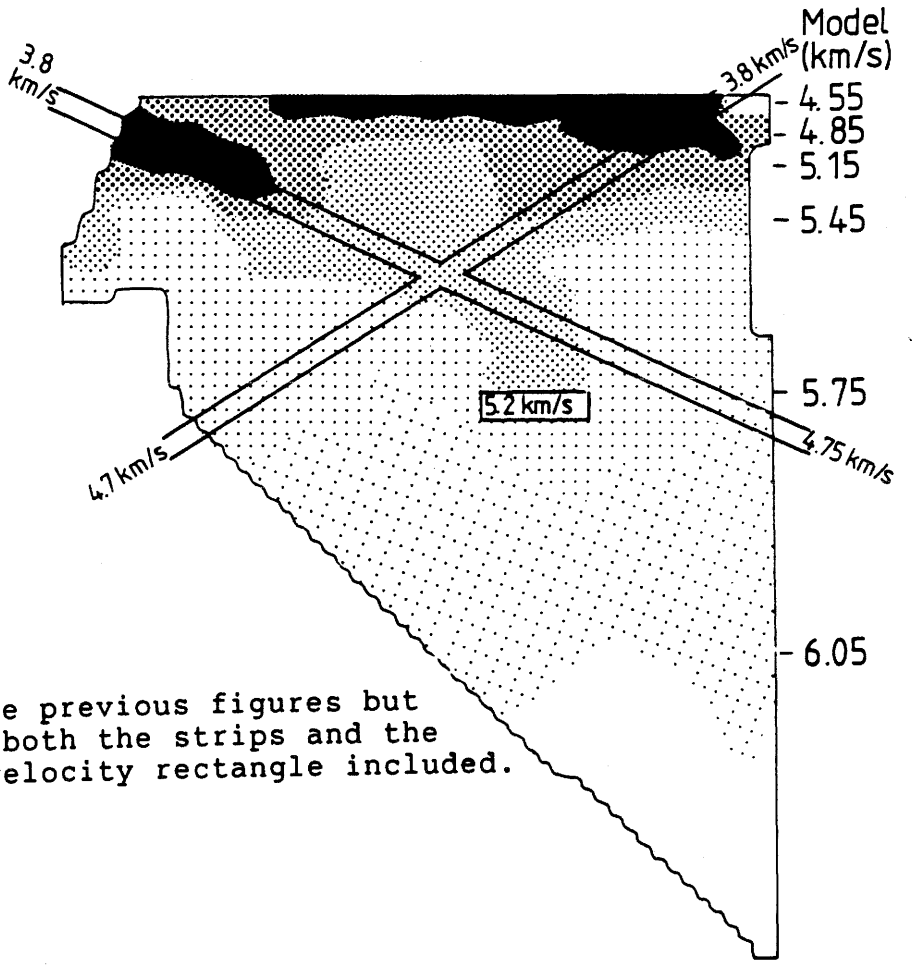

Figure 3-14. As the previous figures but with both the strips and the low-velocity rectangle included.

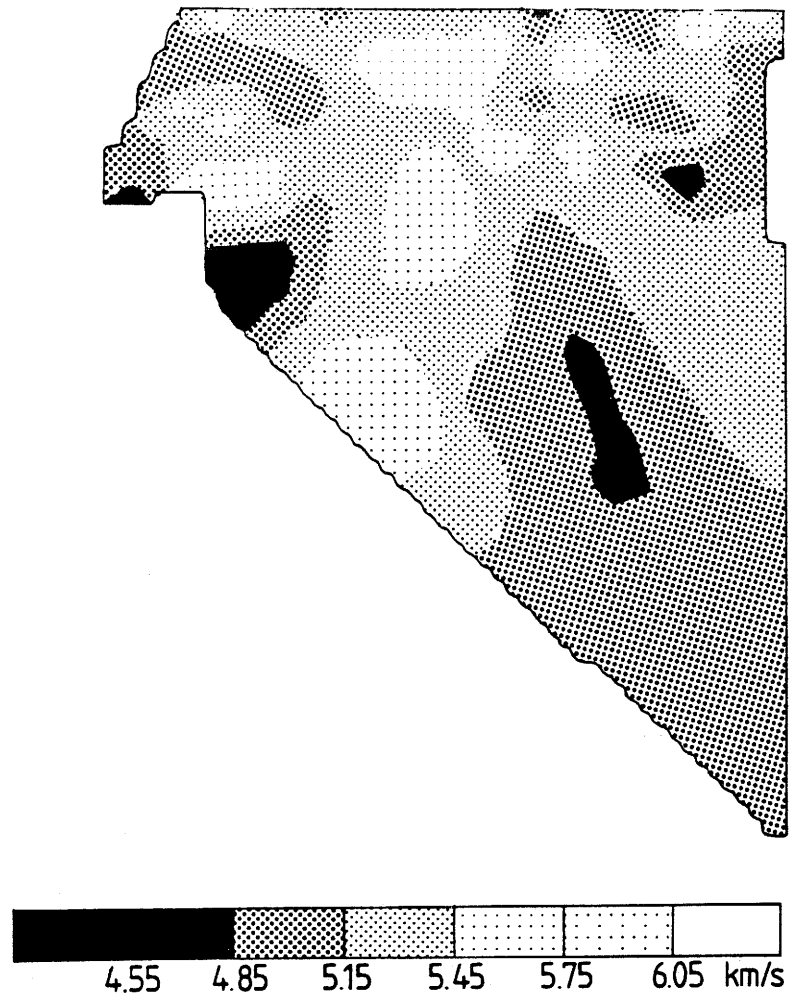

Figure 3-15. Artifacts obtained in the reconstruction of an anisotropic velocity structure between holes 6 and 13. The maximum velocity in the horizontal direction.

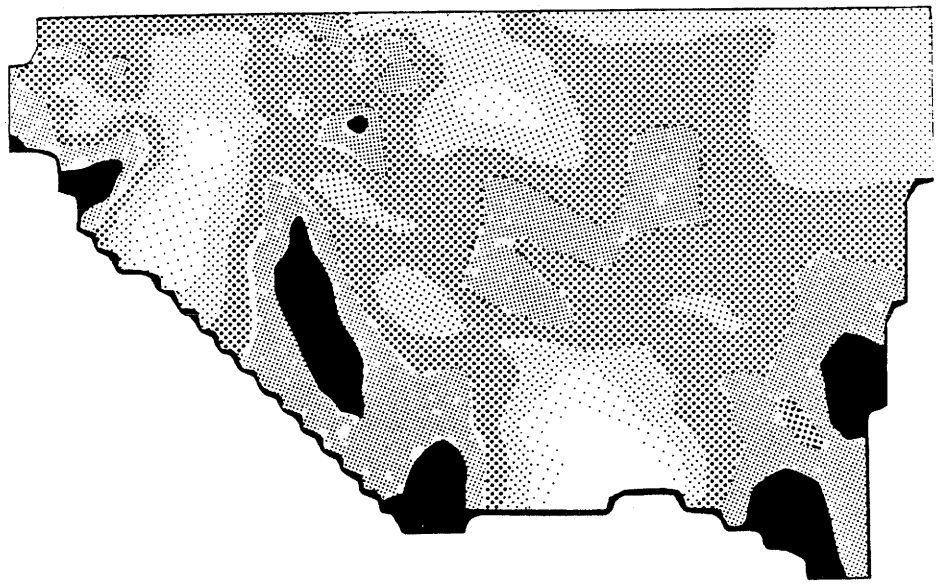

Figure 3-16. Artifacts obtained in the reconstruction of an anisotropic velocity structure between holes Gil and 13. The maximum velocity in the horizontal direction.

The Gideå site is dominated by sedimentary gneiss of varying degree of migmatization. The gneiss foliation structure has in general a small dip. This almost horizontal schistosity is also intensified by small horizontal joints in the rock mass. Most likely such a schistosity will cause velocity variations in different directions, an anisotropic effect. Synthetic traveltimes for a homogeneous velocity structure designed with a horizontal velocity of 5400 m/s and a vertical velocity of 5140 m/s were computed. The reconstruction is shown in Figure 3-15. Artifacts appear because different parts of the region are dominated by rays in different directions. A comparison with the experimental picture in Figure 3-10 shows good agreement for many features. The model does not include any depth dependence of the velocity. Hence, the weathered layer appearing in the upper part of the experimental result could not be reconstructed.

Synthetic traveltimes for an anisotropic velocity model designed in the same way as the previous model in Figure 3-15 (with a horizontal velocity of 5400 m/s and a vertical velocity of 5140 m/s) were also computed for the whole section including hole Gi1. The result from the reconstruction is shown in Figure 3-16. As can be seen from a comparison with the experimental result in Figure 3-9, most features related to the ray-pattern are accounted for.

Figure 3-17 shows the result from an inversion of a model structure including one low-velocity strip. The strip is dipping about 20 degrees, crossing the section

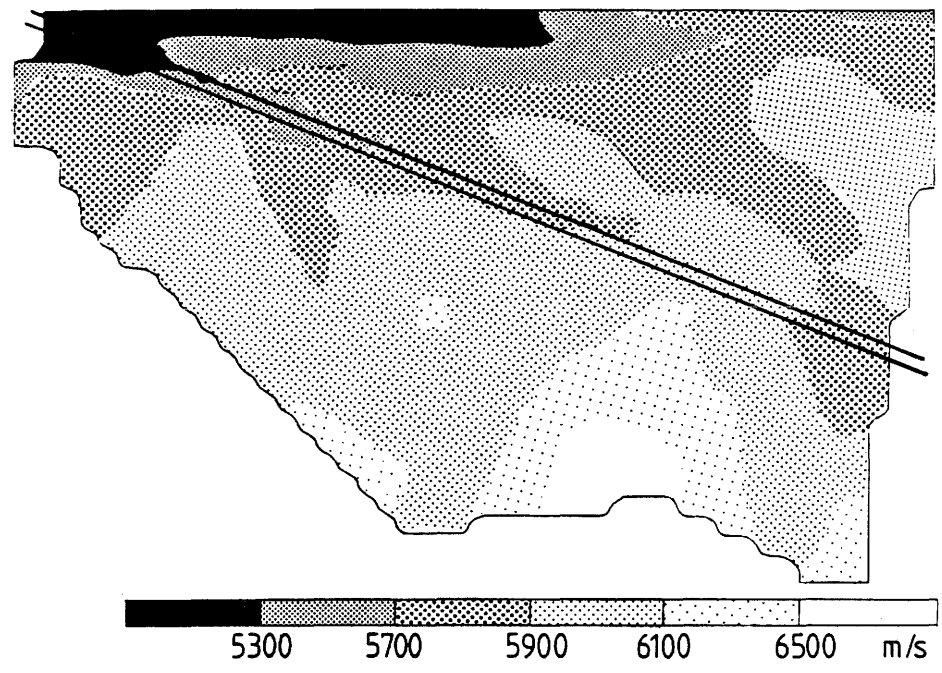

Figure 3-17. Reconstruction from a 2-D model with one low velocity strip, between the holes Gi1 and 13.

from the upper left corner. This model also includes the velocity variation with depth. It is clear that either model alone does not fit the experimental data very well. However, if the models from Figures 3-16 and 3-17 are taken together a reasonable fit is obtained.

3.4.3 3-D Tomographic Analysis

An extended 3-D tomographic inversion of the data has also been performed, using a decomposition into cubes of 25 m side. To illustrate the 3-D inversion results the figures show a number of plane cuts through the volume. Traveltime data was available mainly for source-receiver combinations with the source at the surface and the receivers down in each borehole. The data-set included 1824 rays crossing the volume. As can be seen from Figure 3-18 it is obvious that the cell velocities at each hole and at the surface can be estimated rather well while those downwards in the middle present much greater difficulties with this ray coverage set. A coarse structure can be seen down at about 225 m depth (Figure 3-19), but the residual errors are quite large, making interpretations difficult.

In order to investigate the possibilities to localize the extension of a feature within a volume, synthetic traveltimes were computed. A 3-D velocity model including depth dependence and a low-velocity strip has been inverted using the experimental geometry. Our model includes a low-velocity strip dipping about 40 degrees to the south-east, corresponding to a fracture zone of a width of 25 m. In the reconstruction shown in Figure 3-20, five top layers separated by 50 m are outlined. The image of the strip is smoothed and it is difficult to follow its extension below the 175 m layer because of the less dense ray-coverage there.

Both the experimental and the synthetic result indicate the difficulties to reconstruct features at depth using typical 3-D crosshole ray-geometries. These difficulties are due to the sparseness and the bad angular coverage of the rays that penetrate the deeper parts of the volume. To get favourable circumstances one would need access to the bottom in order to have source points or receivers there. This could be achieved for example by using curved boreholes meeting at depth and enclosing the volume. It should also be noted that a large number of boreholes are required to allow for a sufficient number of horizontal ray directions. Taken together, these demands are quite severe and make 3-D crosshole measurements for routine purposes too expensive.

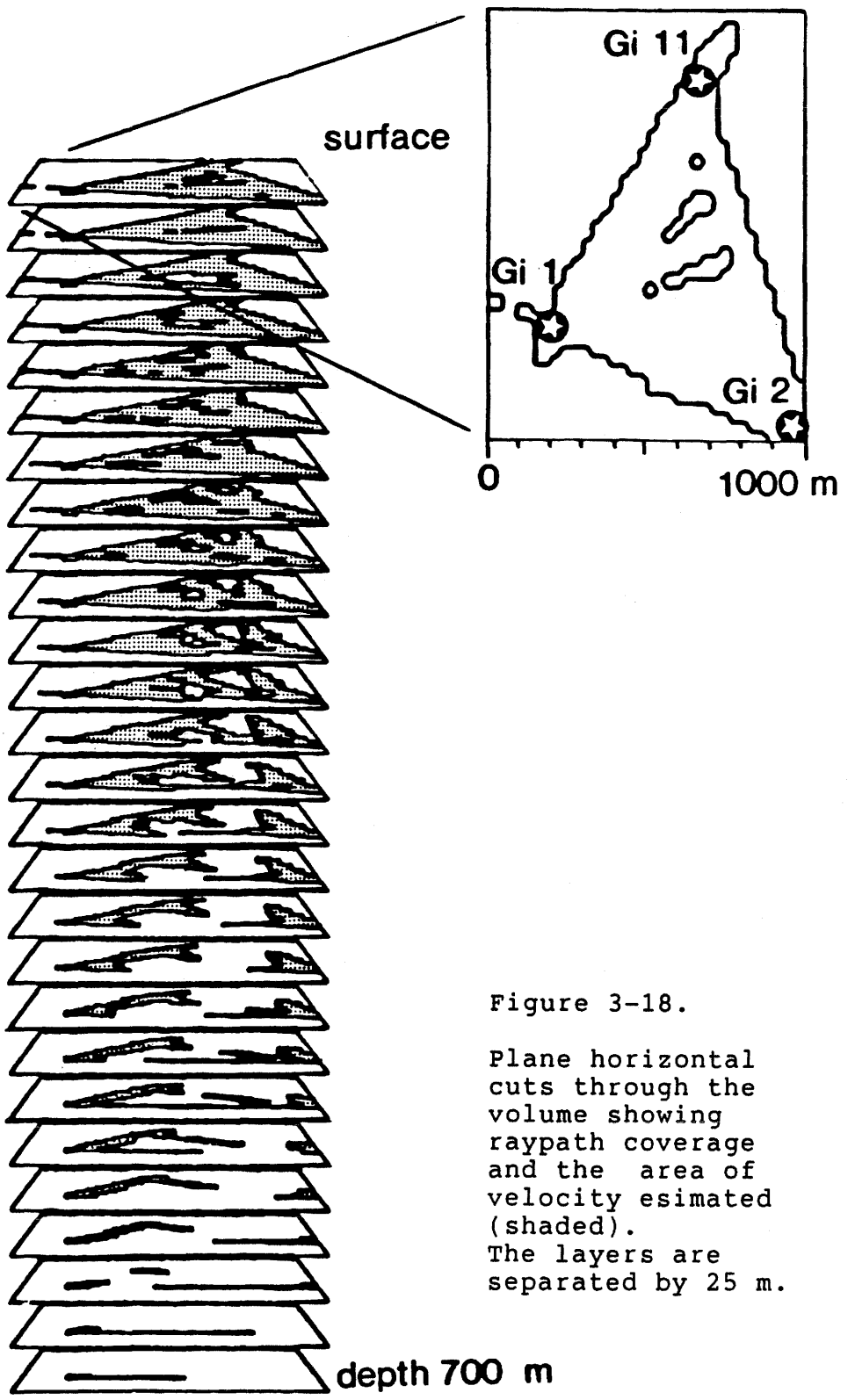

Figure 3-18.

Plane horizontal cuts through the volume showing raypath coverage and the area of velocity esimated (shaded). The layers are separated by 25 m.

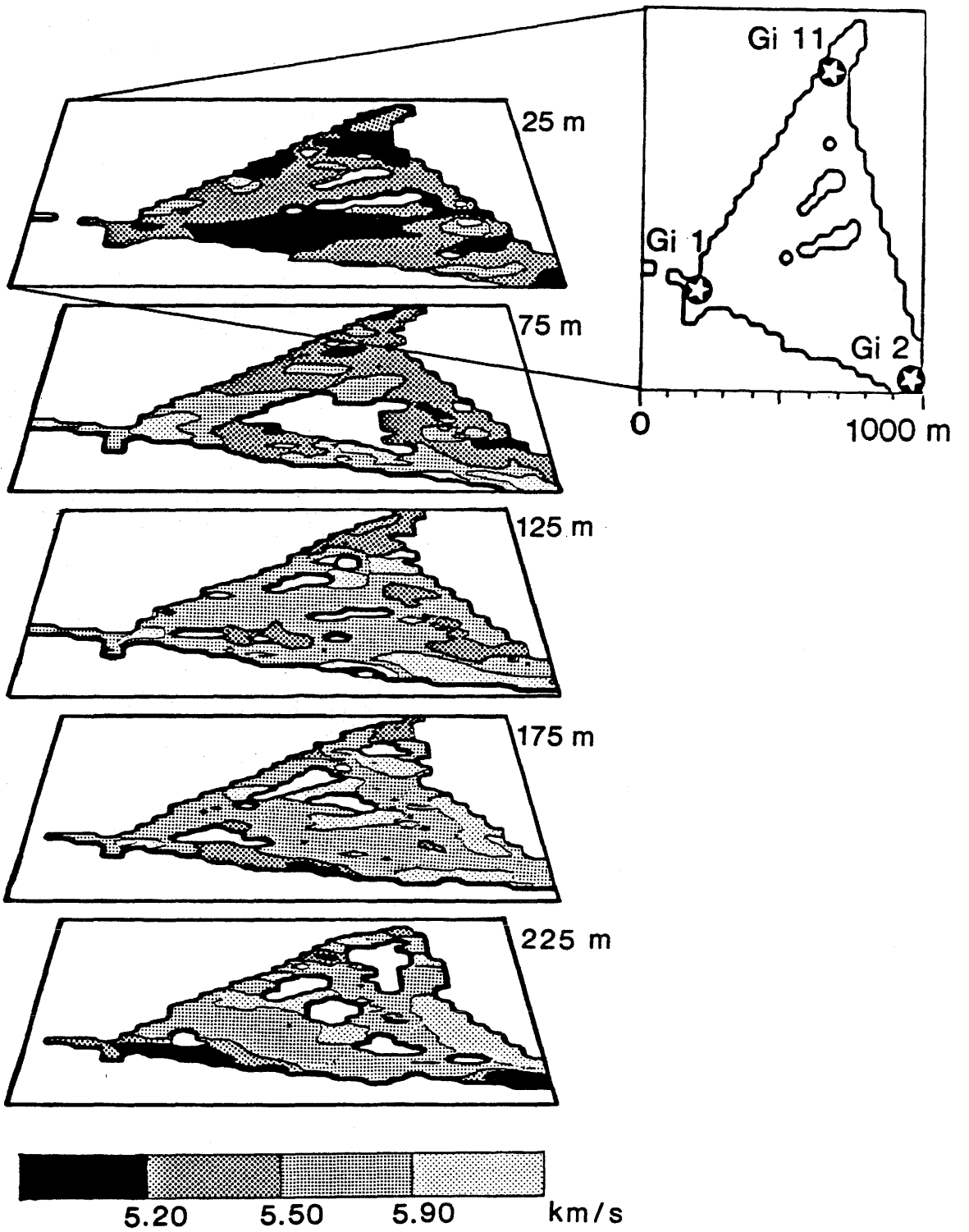

Figure 3-19. Velocity structure to 225 m depth. The layers shown are separated by 50 m.

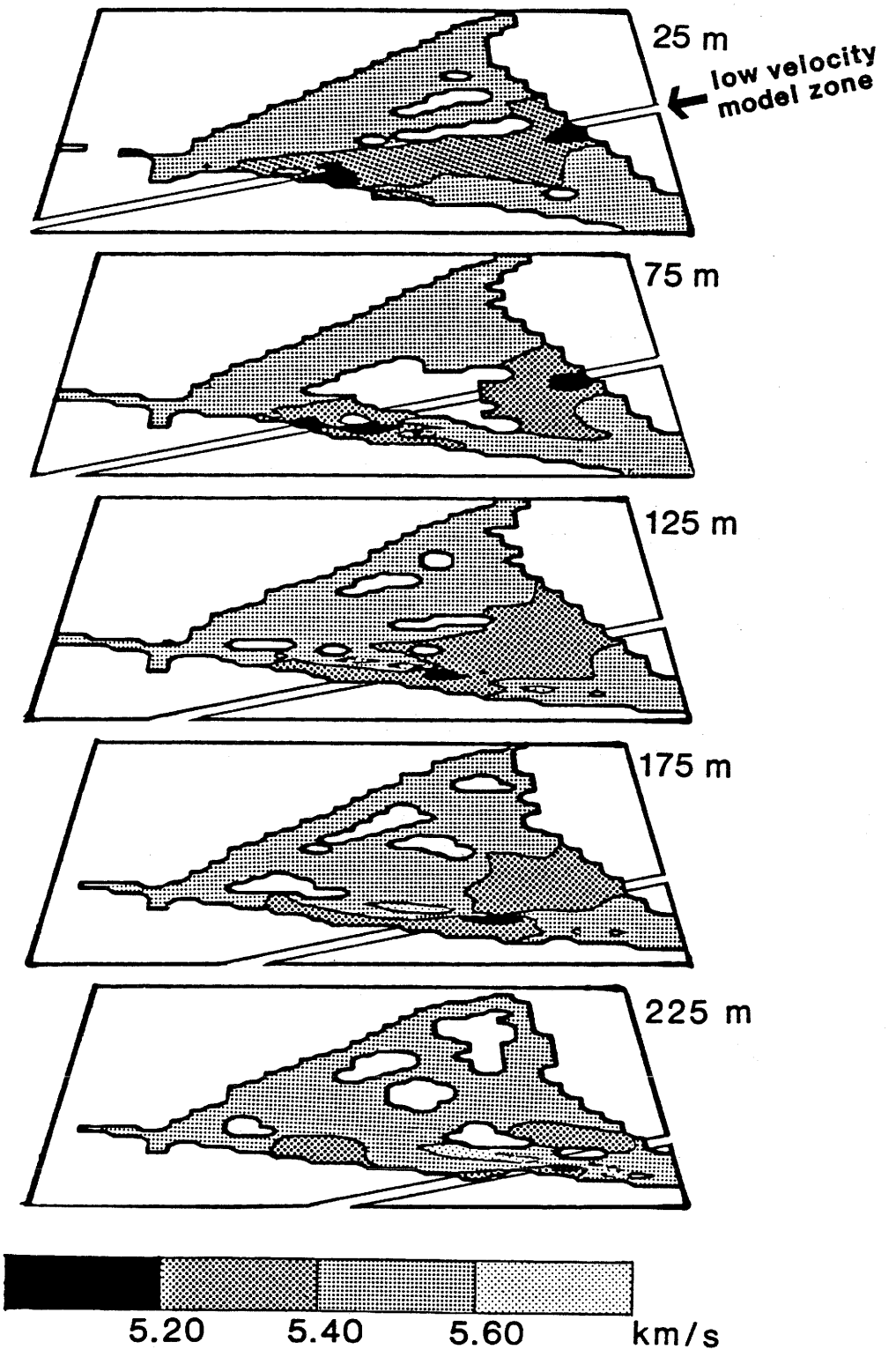

Figure 3-20. Velocity structure to 225 m depth from a model with one low velocity zone. The layers shown are separated by 50 m.

3.5 TUBE-WAVES

Tube-waves have been observed on several recordings at the vertical component of the borehole accelerometers. This type of waves can be generated by a compressional wave passing a discontinuity in the borehole, (21).

The sections in Figure 3-21 show vertical-component records from hole Gi11 at depths ranging from 20 meters to 340 meters. The shot depths are from 149 meters to 100 meters in hole 13. The tube-wave signals can be followed from one depth to another which is indicated by the lines in the section. Signals from three apparent sources can be observed at 70 m, 150 m and 250 m. These depths are in agreement with fracture zones detected by core mapping.

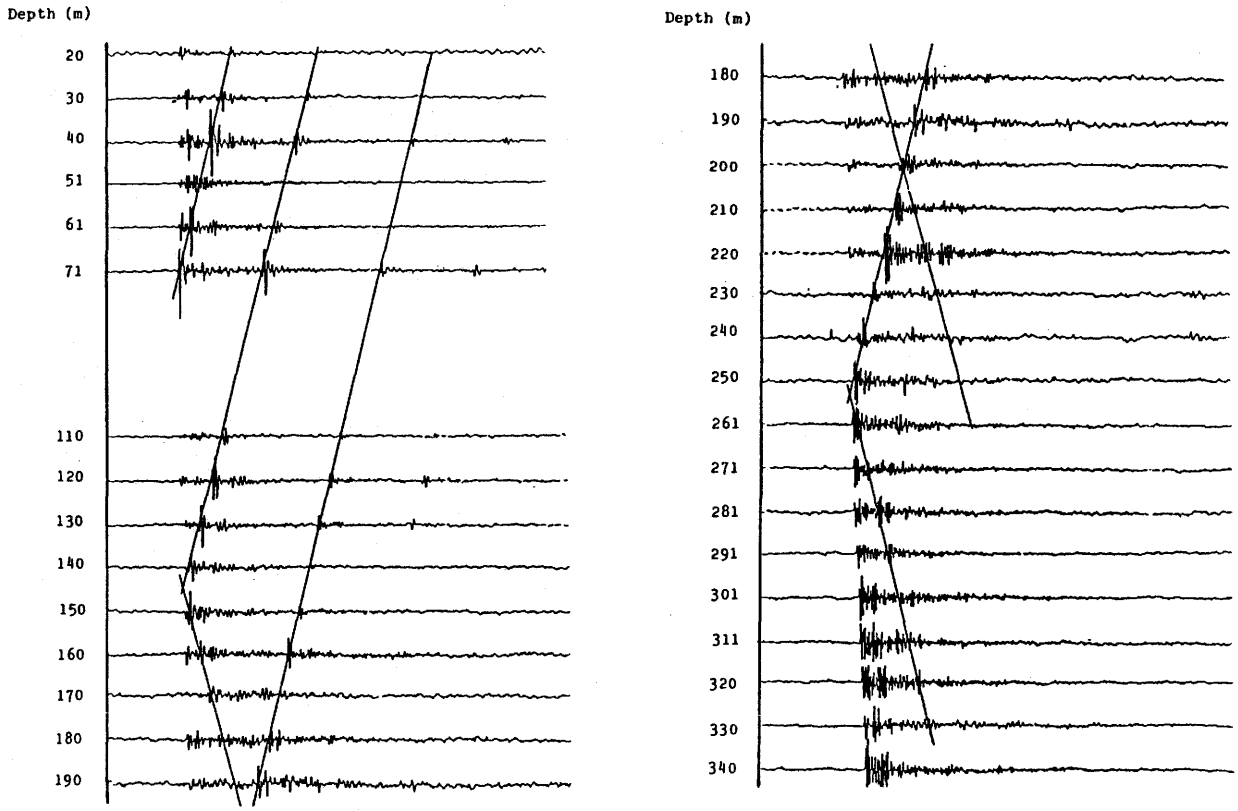

Figure 3-21. Vertical component recordings as a function of depth. The shot depth in hole 13 is from 149 m to 100 m. Tube wave sources at a depth aroun 70 m, 150 m and 250 m in hole Gi11.

3.6 CONCLUSIONS ON LARGE-SCALE SEISMICS

The large scale field tests show that crosshole seismic measurements can be made for large sections. The seismic system designed for the Stripa II Project has proven to be useful for recording of seismic signals at distances up to 1 km.

The analysis of the data from the large-scale seismic experiment has pointed at some problems which we believe are particularly important for such measurements:

- anisotropy
- ray-bending
- boreholes bending out of the plane.

The problem of anisotropy may be treated by allowing the velocity to vary with direction. This leads to more unknown parameters, however, and the interpretation becomes less certain.

Ray-bending can be accounted for by iterative ray-tracing. The calculations will be much more time-consuming, but in principle the problem can be solved.

The third problem should be avoided by proper planning at the time of drilling. When the boreholes at the large-scale test site were drilled, however, crosshole measurements were not intended or even known.

Elaborate analysis techniques can compensate for some of the deficiences mentioned above. Still it is only possible to get the coarse structure of the area under study. Model calculations provide a useful tool to aid the interpretation of some of the features found in the experimental data, particularly when anisotropy is involved.

Large-scale 3-D measurements are even more problematic, as demonstrated by the 3-D experiment performed. It is exceedingly difficult and expensive to get a ray-coverage of such density that a meaningful tomographic analysis can be made. With the current test it was only possible to depict one or two features. A comparison to off-shore reflection seismic measurements indicates the size of the problem: A typical "3-D gather" consists of thousands of recordings from several hundreds of channels. Such large data volumes are of cource not possible to record with the current crosshole technology.

4 FIELD EXPERIMENTS AT THE SMALL-SCALE SITE

4.1 INTRODUCTION

In the small scale experiments, carried out at the Stripa mine, two sections were measured.

The measurements were performed in the granitic pluton which outcrops in a supracrustal belt with structures striking mainly in NE-SW direction (Figure 4-1). Due to the relatively mild tectonism since the intrusion, the Stripa granite is generally unfoliated. It is a grey or reddish, fine to medium grained, relatively uraniferous rock. It shows abundant fracturing and deformation on a microscopic scale and frequently on a megascopic scale as well (6).

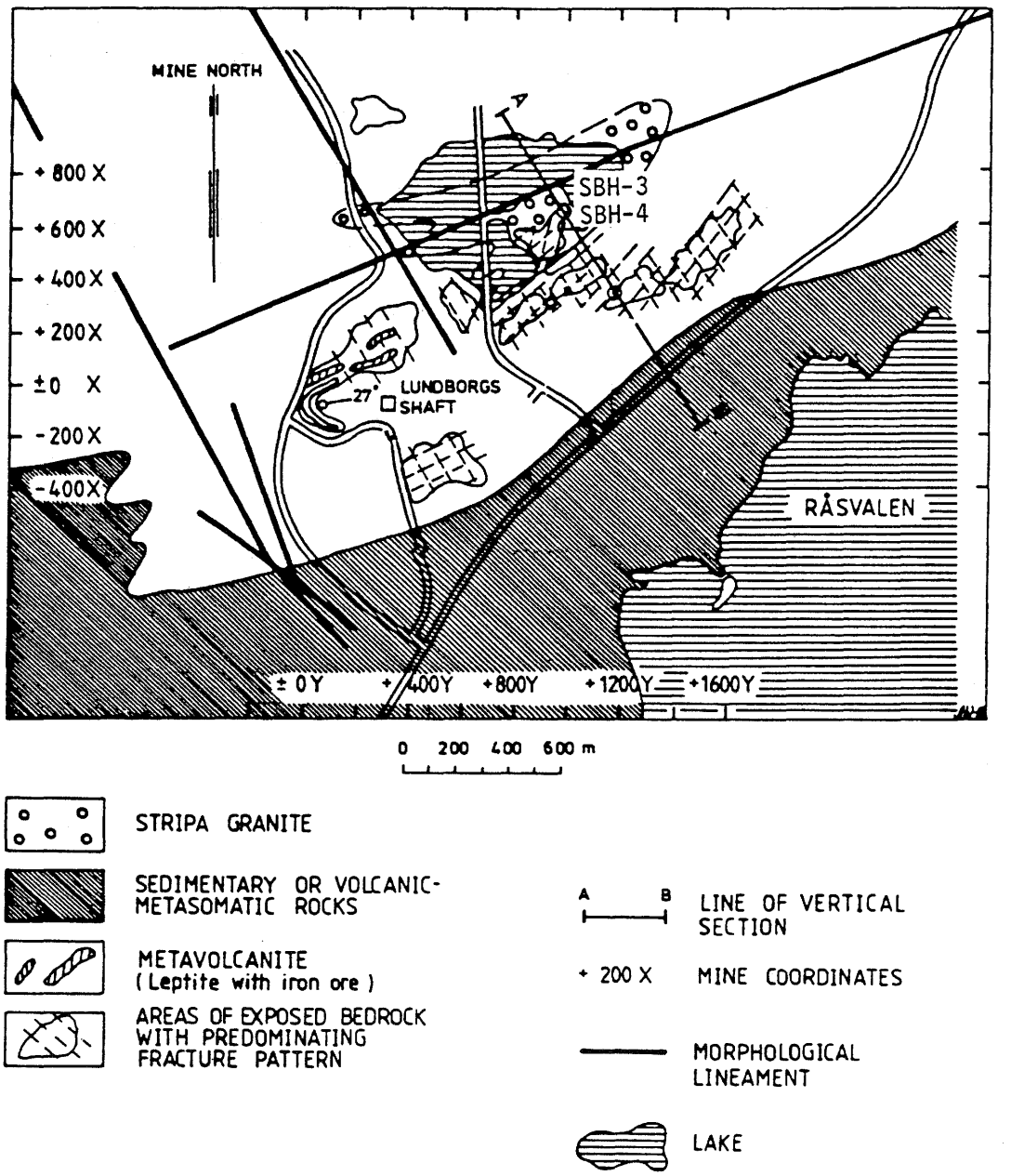

Figure 4-1. Geologic map of the Stripa area.

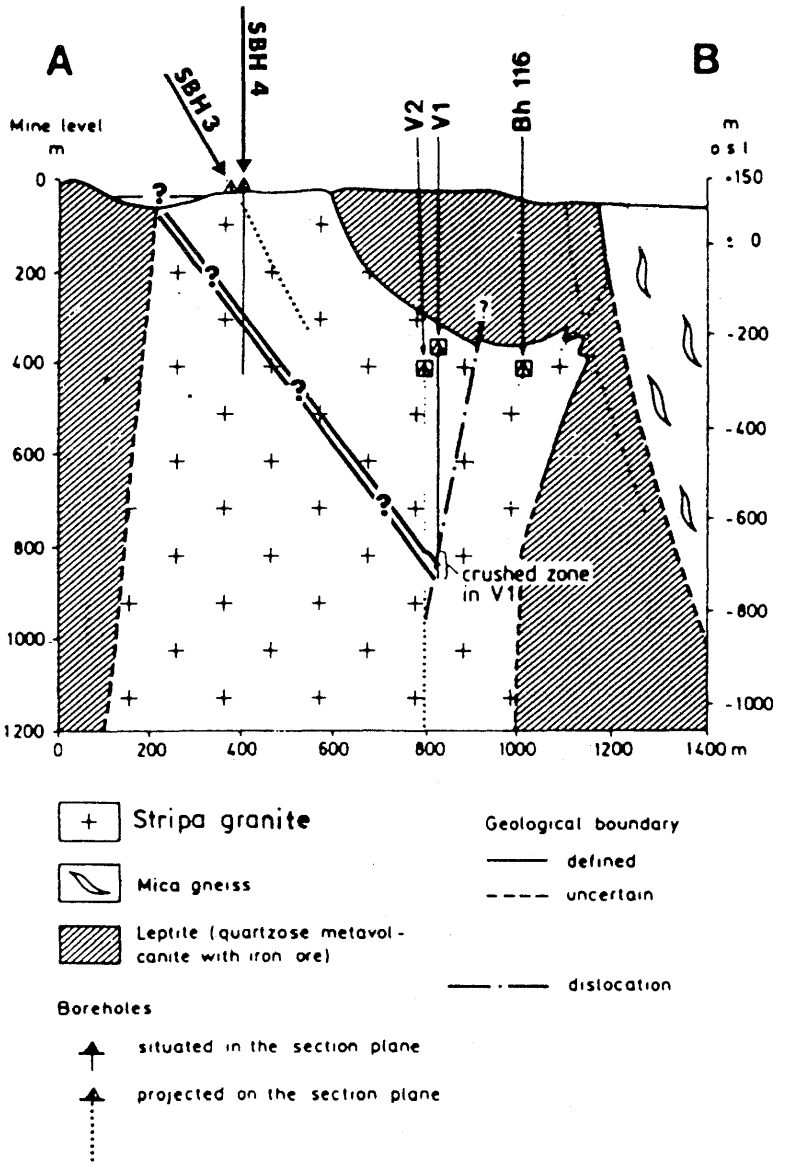

Figure 4-2. Vertical section through the investigation area.

The purpose of the first experiment was to see if the large fracture zone, observed in the underground mine, reaches the surface within the crosshole section. The zone can be traced at 505 m in the bottom of the hole V1, which is drilled in the mine at the level of 360 m below the ground (Figure 4-1 and Figure 4-2).
One direction of the zone suggests an intersection at 370 m ,in the bottom of the vertical SBH-4 borehole, drilled from the surface, (15).

The second experiment was carried out in the fan-holes at the crosshole site at 360 m level in the Stripa mine. The purpose of these measurements was to complete the fan-hole surveys.

A hydrophone receiver was also tested in the fan-holes.

4.2 SITE FOR THE EXPERIMENT

The first experiment was performed between the vertical SBH-4 hole and the slanting (50 degrees) SBH-3 hole, both drilled from the same location at the surface. The holes are 372 m and 315 m deep, respectively (Figure 4-2).

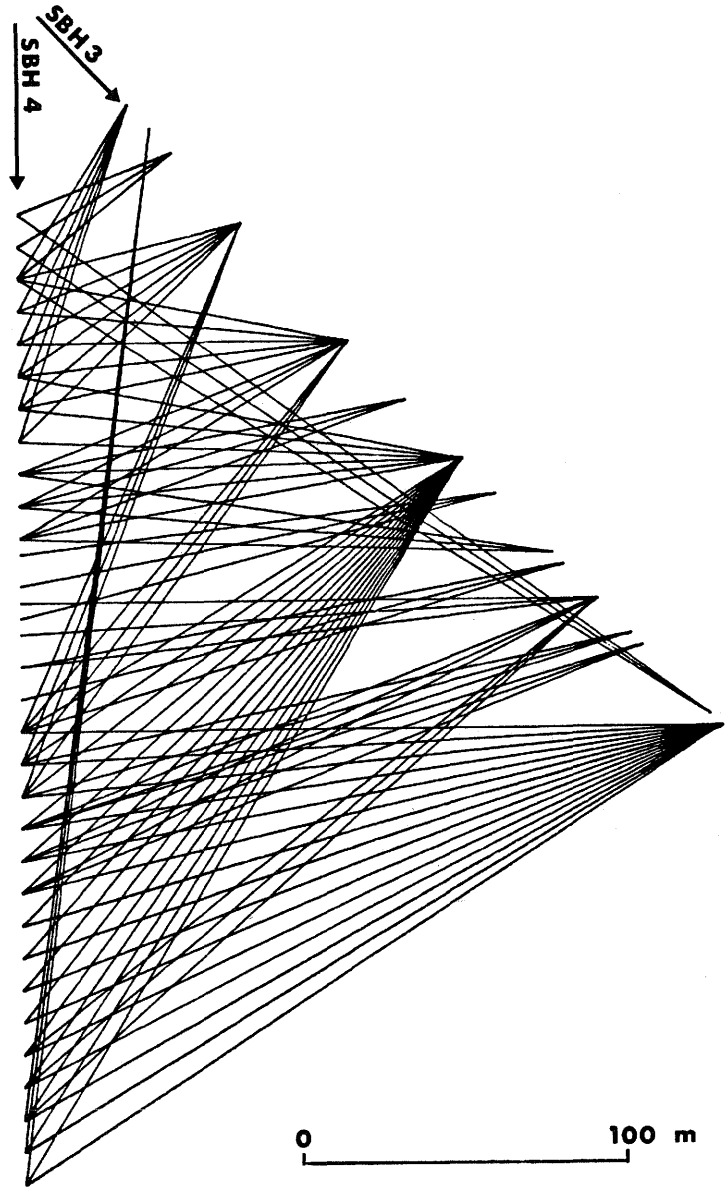

Figure 4-3. Projected vertical section view showing source to receiver ray paths.

Micro-explosions were set off in hole SBH-3 at 15 different depths down to the bottom at 315 m. The section was surveyed with a chain of three accelerometer probes in hole SBH-4 and some 100 rays were recorded (Figure 4-3). No surface geophones were used.

The second experiment was performed between the F5 and the F6 hole. The holes are 200 m and 250 m deep, respectively, with 10 degrees and 40 degrees inclination from the horizontal plane. Both holes are directed 122 degrees towards south-east (Figure 4-4).

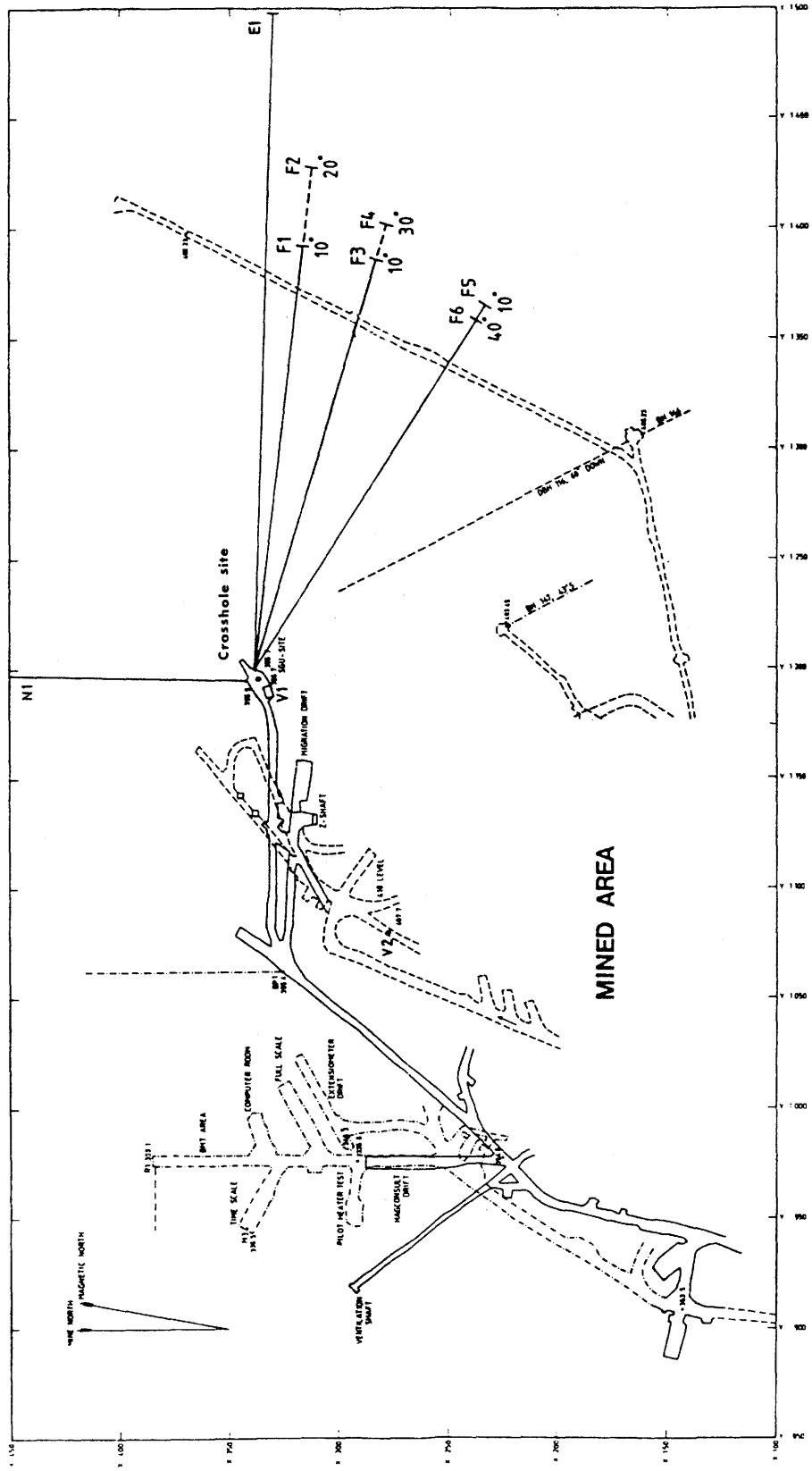

Figure 4-4. Map of the Stripa mine at 360 m level. Fanholes F1-F6.

Source charges of 1 and 5 grammes of explosive were used in the borehole F5. The distance between each source point was usually 5 m. The measurements were made with a chain of three receiving units placed in hole F6. The chain was moved in steps of 5 m. In total nearly 500 rays were recorded (Figure 4-13).

The sampling frequency throughout the test was 12 kHz. The section in Figure 4-5 shows axial-component records from hole F6 at depth ranging from 135 metres to 185 metres.

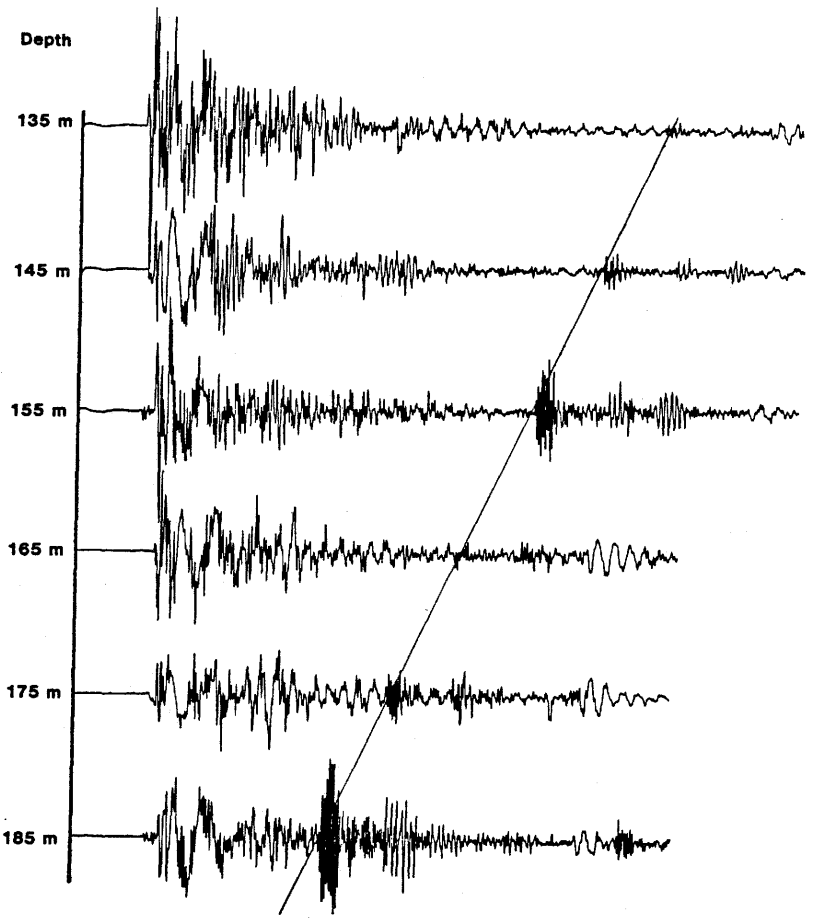

Figure 4-5. Record sections from 135 to 185 meters depth in hole F6. A tube-wave source is indicated at a depth around 208 meter.

4.3 EXPERIMENTAL RESULTS

4.3.1 Section SBH4 - SBH3

Figure 4-6 shows the velocity structure calculated for the section SBH4-SBH3.

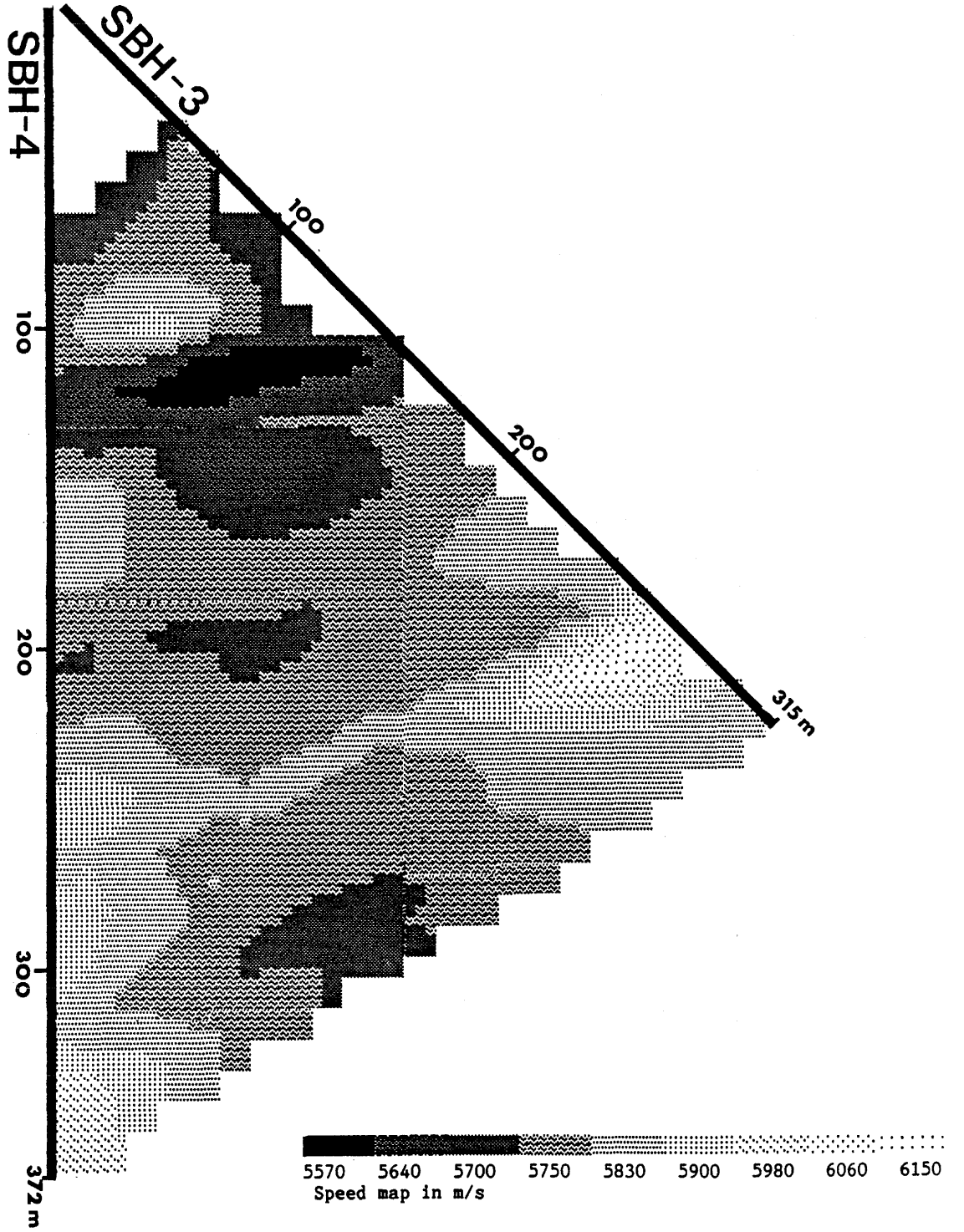

Figure 4-6. Velocity structure from experimental data.

A decomposition into squares of 10 m was used in the tomographic analysis. The main feature which can be seen is an almost horizontal a low-velocity zone crossing the SBH-4 borehole at a depth of 140 m. The zone is also indicated by strong tube-waves. Tube-waves were also recorded at depths of 310 and 340 m. A corresponding low-velocity structure can be seen in the tomogram.

The results from the experimental data have been compared with results from calculations on theoretical models. A first example is shown in Figure 4-7. A laterally homogeneous velocity model was assumed, having an increase in velocity with depth from 5.7 km/s to 5.9 km/s. Figure 4-8 is the same as Figure 4-7 except that two low-velocity strips are included in the model. Note that low velocities appear in the upper part, as in the experimental result (Figure 4-6). The features near the bottom of hole SBH-4 are not reconstructed in agreement with the experimental result. In Figure 4-9 the direction of this lower strip is different.

Results from calculations with a series of anisotropic models designed with an anisotropy contrast of 1 % and varying angles of the anisotropic structure are presented in Figures 4-10 to 4-12. The large difference noticed when comparing the models with the pattern observed in the experimental solution indicates that anisotropy effects most likely do not influence the experimental picture.

The results from these interpretations indicate that the observations in borehole SBH-4 could not be connected to the major fracture zone found in hole V1.

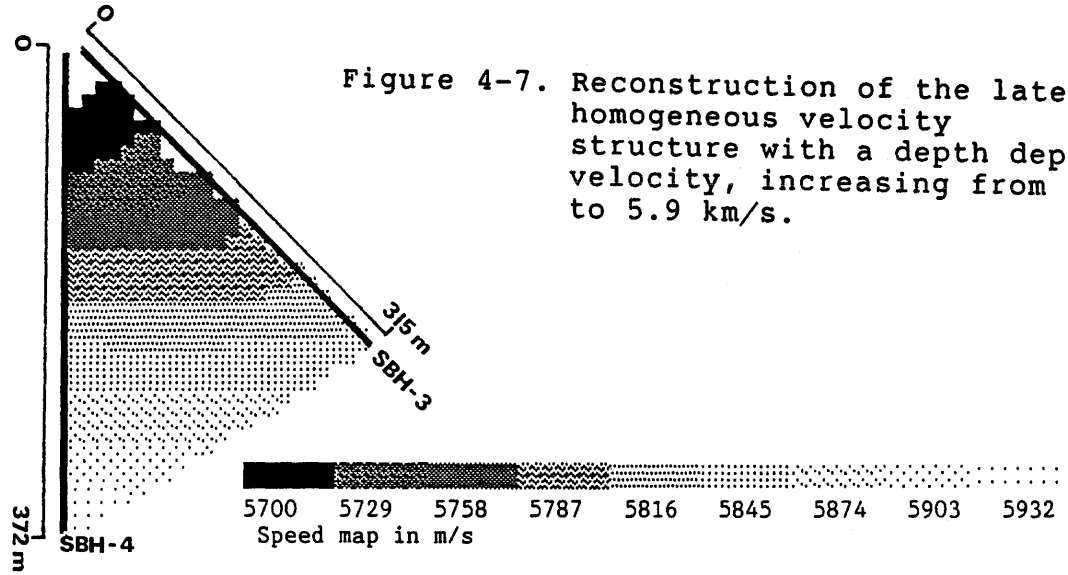

Figure 4-7. Reconstruction of the laterally homogeneous velocity structure with a depth dependence velocity, increasing from 5.7 km/s to 5.9 km/s.

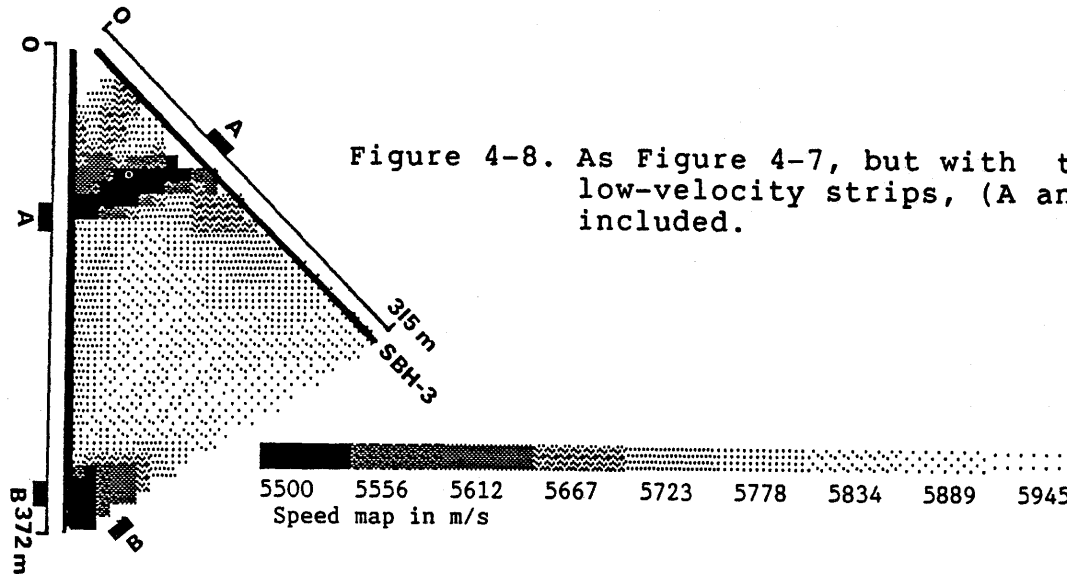

Figure 4-8. As Figure 4-7, but with two low-velocity strips, (A and B), included.

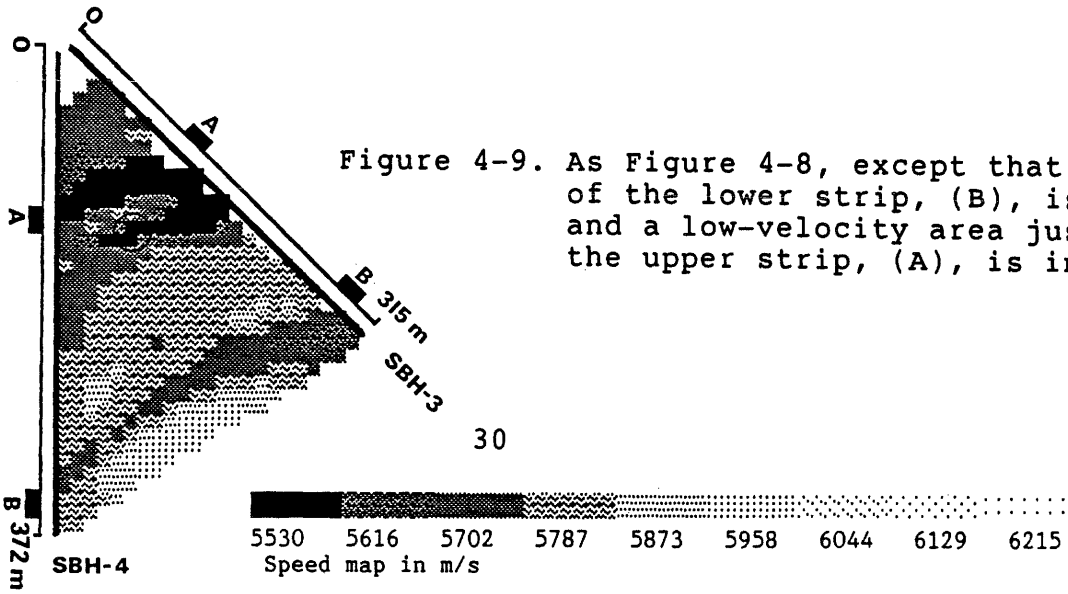

Figure 4-9. As Figure 4-8, except that the angle of the lower strip, (B), is changed and a low-velocity area just below the upper strip, (A), is included.

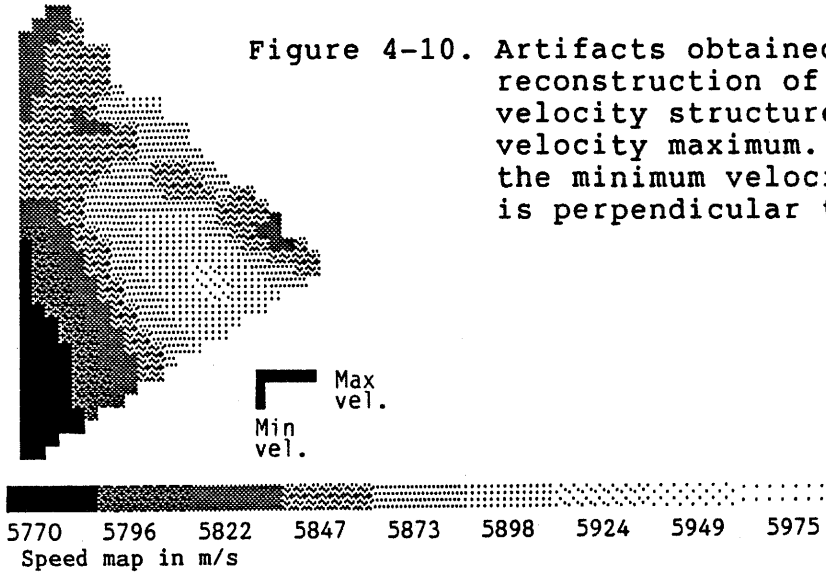

Figure 4-10. Artifacts obtained in the reconstruction of an anisotropic velocity structure with a horizontal velocity maximum. The orientation of the minimum velocity, (contrast 1%) is perpendicular to the maximum.

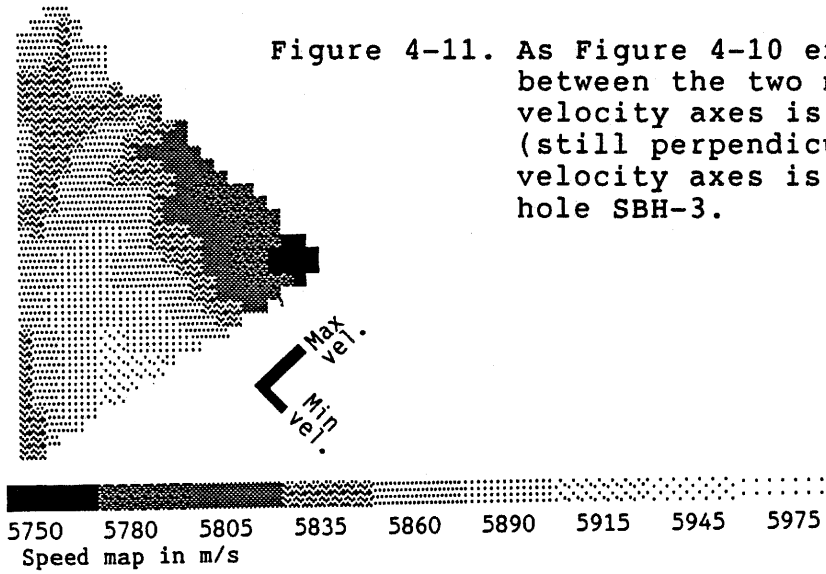

Figure 4-11. As Figure 4-10 except that the angle between the two maximum and minimum velocity axes is rotated 45 degrees (still perpendicular). The minimum velocity axes is almost parallell to hole SBH-3.

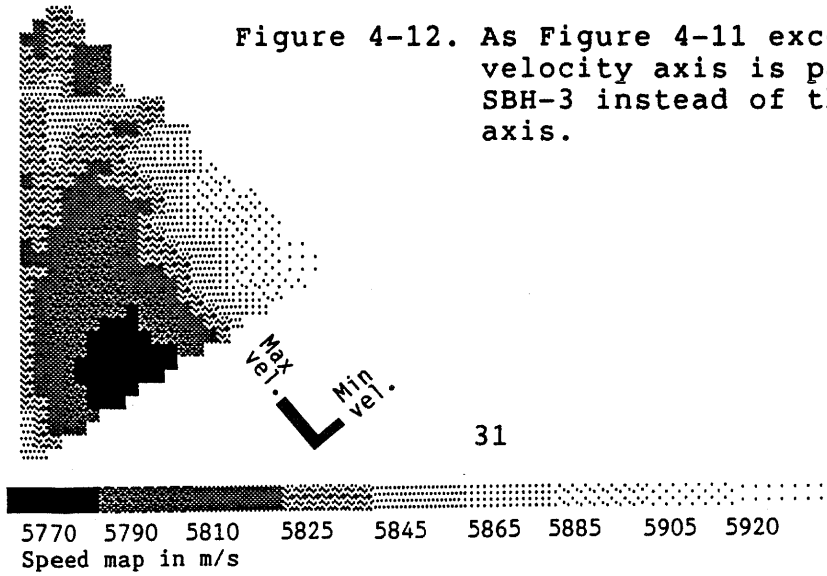

Figure 4-12. As Figure 4-11 except that the maximum velocity axis is parallell to hole SBH-3 instead of the minimum velocity axis.

4.3.2 Section F5 - F6

The results from a straight-ray (Figure 4-13) tomographic inversion of the resulting traveltimes for the section between the holes F5 and F6 is shown in Figure 4-14. This inversion is computed from data recorded down to just 220 m in hole F6. No borehole coordinates were available for the deepest part of the hole F6.

A decomposition into squares of 5 m was used in the tomographic analysis.

From previous investigations at the cross-hole site, (6), (7), seven units of deformed and fractured rock were distinguished, and correlated between the boreholes. The result described below was compared to these units and four zones were defined from the velocity structure (Figure 4-14). The correlations done in the previous investigations have at some locations been revised, since data from later crosshole measurements yielded more information on rock quality between the boreholes.

The minimum velocities appear in the lower right corner of the picture, crossing hole F6 below 210 m. This is the most prominent feature that intersects the area and corresponds to the fracture zone L. Due to the strike, about north-east 45 degrees, and a dip orientated towards west, it does not reach hole F5.

The feature observed along hole F5 between 50 and 100 m depth branches into two zones crossing hole F6 around 50 m and 105 m, (Figure 4-14). This pattern may be created partly by the two zones A and C. Between these two zones A and C a strongly brecciated section with high porosity is known to intersect hole F5 (6),(7), causing a seismic low-velocity area. Because of this brecciation and the short distance between the boreholes in this part of the section it is difficult to separate the two zones and to find the intersecting angle for the zone A.

Another quite wide feature is the low-velocity area intersecting hole F5 between 125 m and 150 m depth. The most clear extension from this feature reaches hole F6 at around 170 - 190 m, in agreement with the zone K.

Along the upper left limit of the section an indication of a low-velocity feature can be observed, but since this zone is too close to the border of the analysed section it is not possible to see the shape of its extension. However, the core maps show a heavily fractured section around 15 m depth in hole F5.

The low-velocity pattern intersecting hole F5 at 190 m is partly an artifact created by the drift intersecting the cross hole section about 25 metres below hole F5 at 170 m depth.

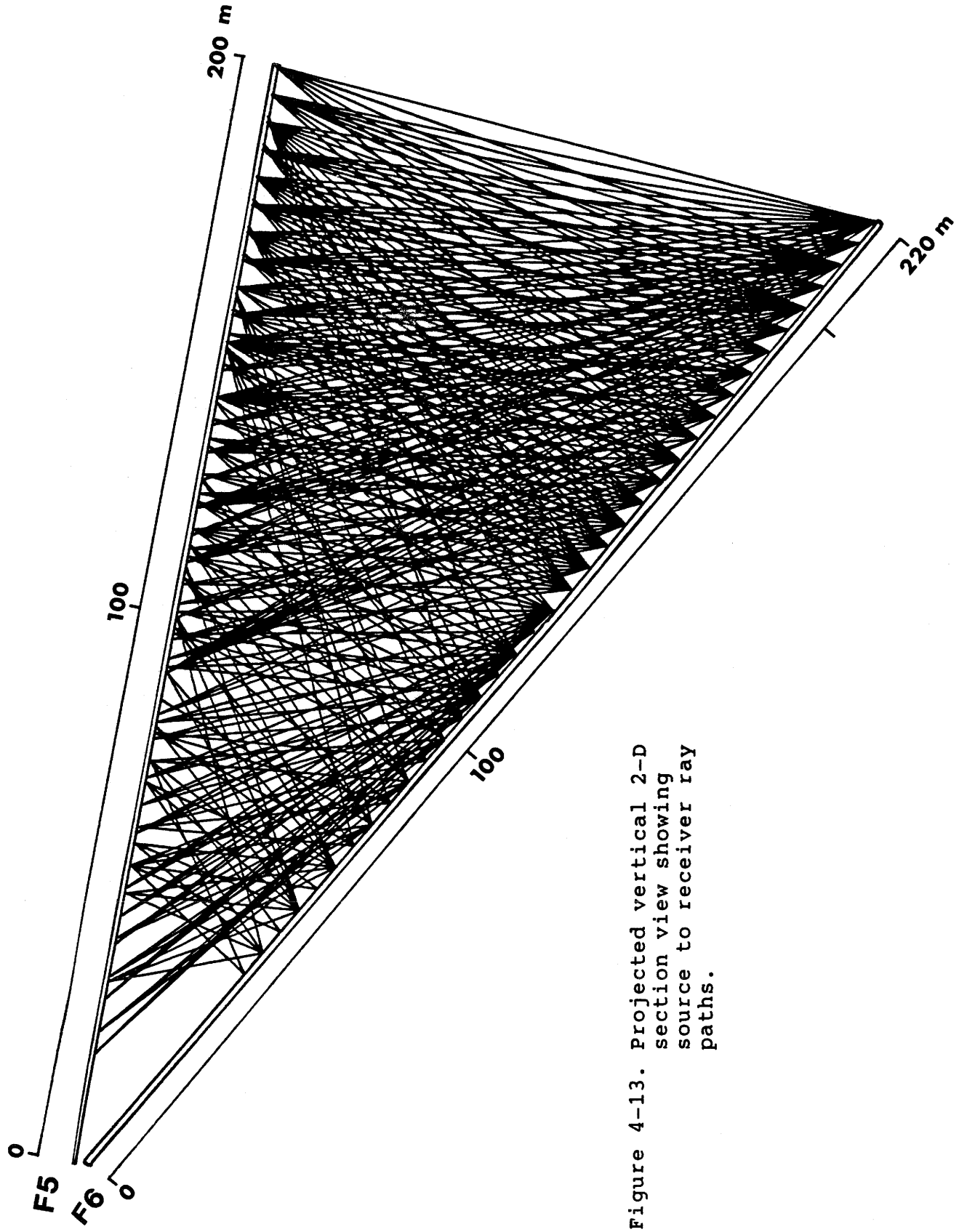

Figure 4-13. Projected vertical 2-D section view showing source to receiver ray paths.

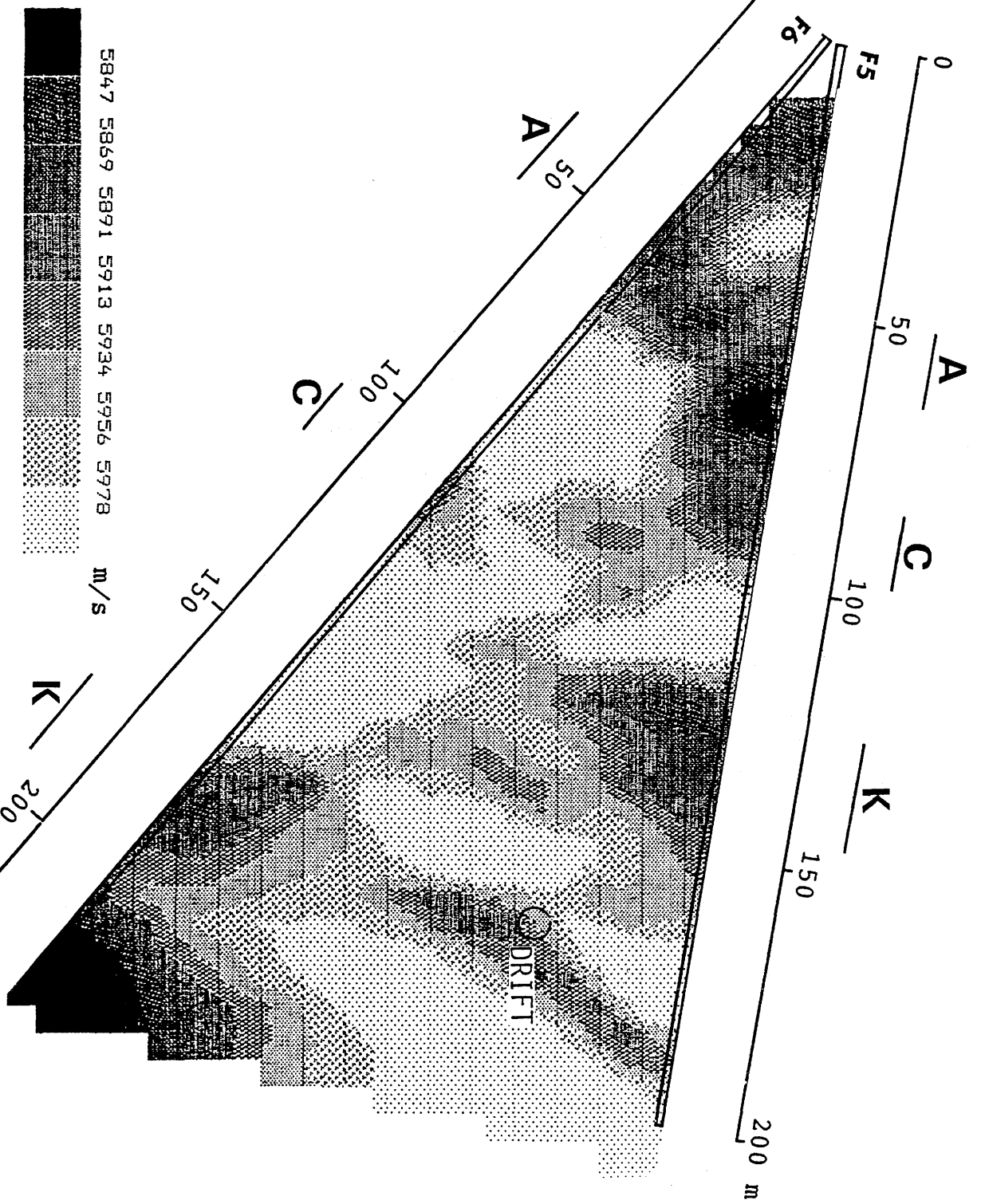

Figure 4-14. Velocity structure for the F5-F6 section, from experimental data

4.4 DATA QUALITY ANALYSIS

Small fractures in the Stripa rock, which is very competent, must be determined from very small traveltime anomalies in the tomographic analysis. This puts strong requirements on data quality, and it is important to make sure that even comparatively small systematic errors are eliminated. Other workers have had problems with time-offset errors in their data (due to the instrumentation). Thus, we will first consider some tests to see if errors of this kind are present in our Stripa data for the F5-F6 section.

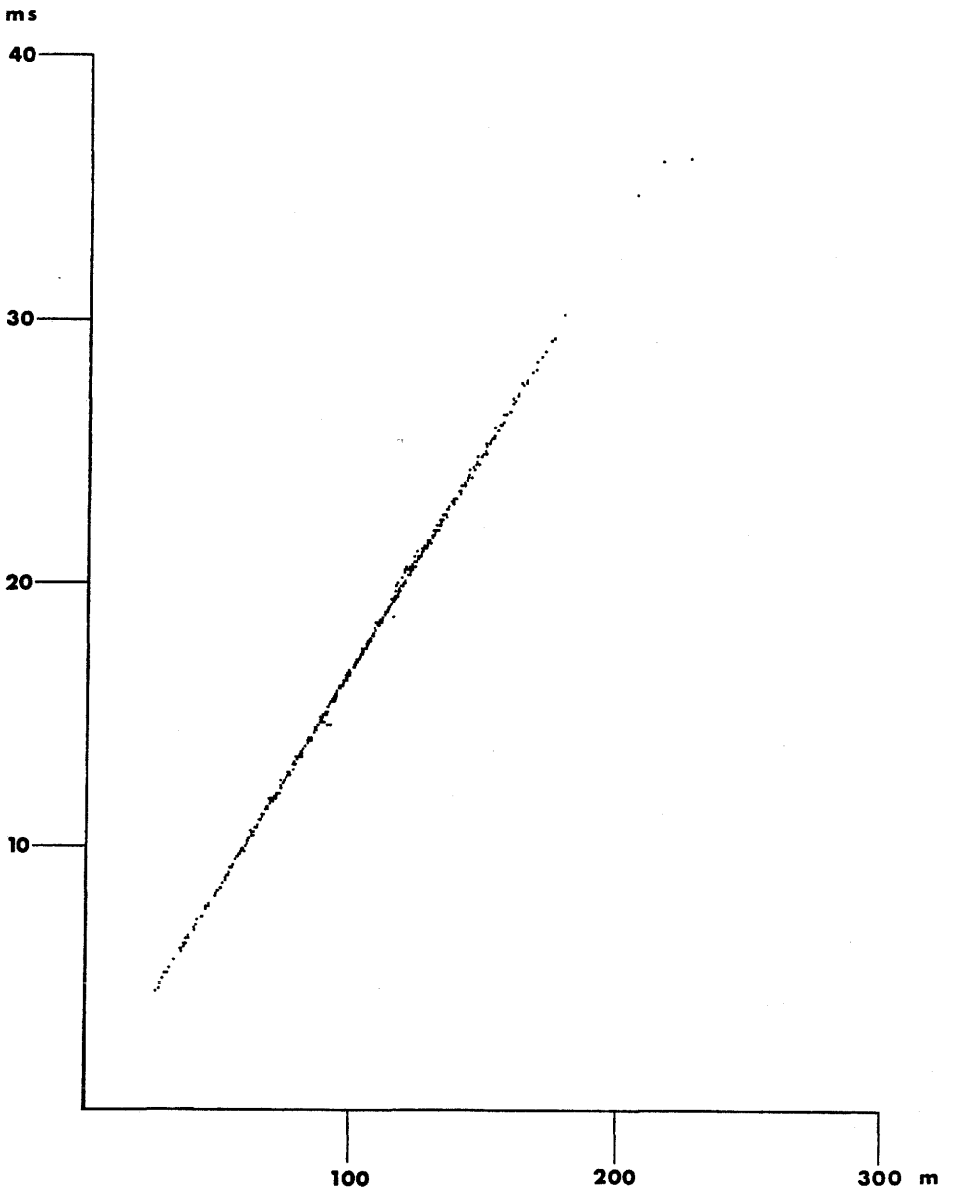

Figure 4-15. Traveltimes as a function of distance.

Figure 4-15 shows our traveltimes as a function of distance. Fitting a straight line to the data points by hand one readily notes that the origin is passed very closely indicating time-offset free data. Figure 4-15 is also interesting because it shows that the deviations from a constant average velocity for all the rays is very small, which indicates that the Stripa rock is homogeneous.

The straight line can of course be fitted to the data in Figure 4-15 by linear regression techniques also. Doing this, we obtained a time-offset of -0.003 ms, which is sufficiently close to zero to be considered insignificant, and a slope (average velocity) of 5.94 km/s. Reducing the traveltime data according to the corresponding straight line and magnifying the time-scale, Figure 4-16 is obtained. A few traveltimes are conspicuously low. This is probably due to a geometric error as a result of the extrapolation of curvature data for borehole F6, see below. Apart from this, however, the spread of the data does not give rise to any suspicions of systematic errors.

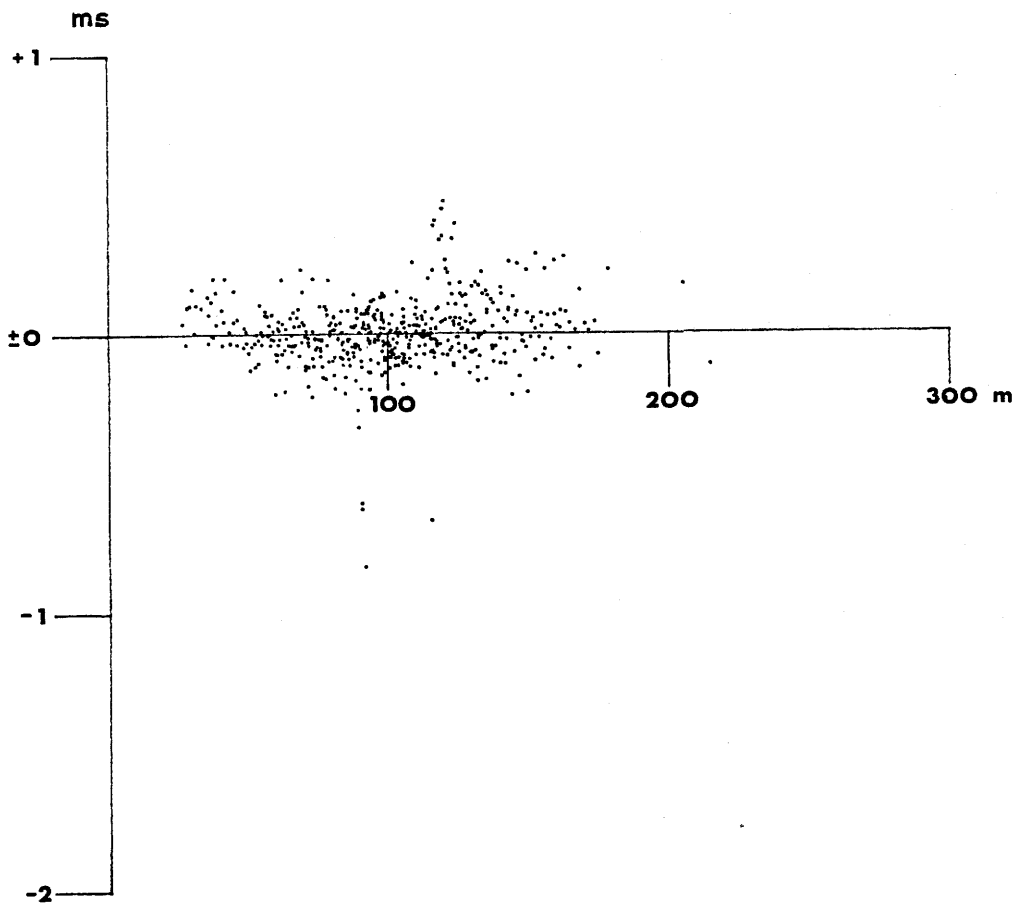

Figure 4-16. Timeresiduals as a function of distance.

In Figure 4-17 the average velocities are plotted as a function of source- and receiver-coordinates in the two boreholes. Of course, the low-velocity regions (fractures and so forth) will be visible in a plot of this kind although in a disguised form. A strip, for example, will appear as a "point" and a "point" will appear as a strip. (Cf. the properties of the slant-stack.) Systematic errors in the data will also be noticeable in this plot although some experience is needed to separate them from the "correct" low-velocity regions etc.

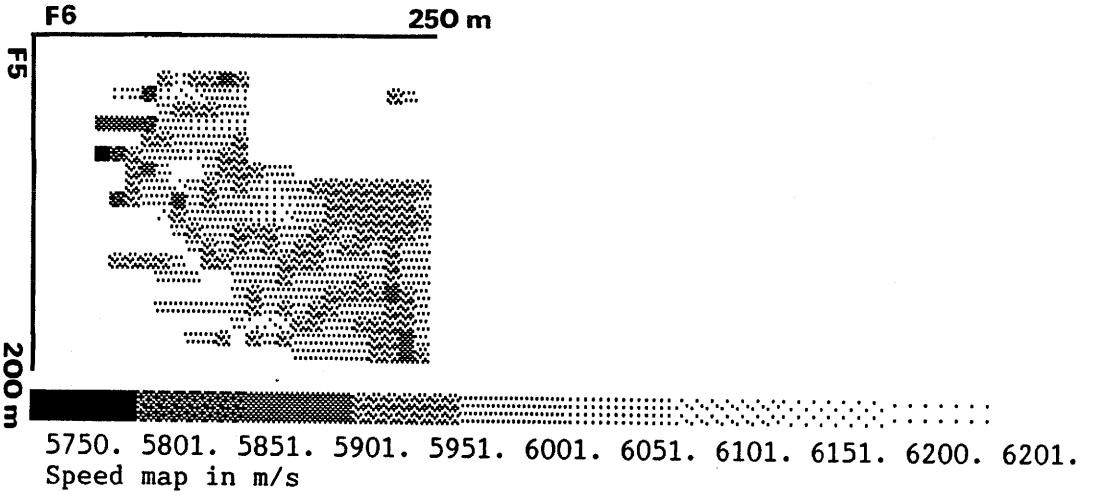

Figure 4-17. Average velocities as a function of source- and receivercoordinates

Looking at Figure 4-17 a conspicuous feature is the low-velocity column in the rightmost part. It may be explained by a low-velocity region at the bottom of hole F6. However, curvature data for the deepest part of this borehole were not available, instead a simple extrapolation was made to obtain the source coordinates needed. Obviously it is not possible to do this extrapolation with sufficient accuracy. (The influence of geometrical errors is discussed on page 62 below).

Another indication of these errors is obtained when data recorded below 220 meter depth in hole F6 are included in the tomographic inversion. Figure 4-18 shows the result of tomographic analysis for all measured rays (493 rays). The ray-paths can be seen in Figure 4-19. Compared to the velocity structure in Figure 4-14 two main differences can be observed. First, a high-velocity area appears around the bottom of hole F6, below 220 meter depth. Second, a stronger diagonal structure is obvious. Using the whole measured data set we get an non-uniform ray-coverage which may cause this diagonal pattern.

In order to see what effect the ray-coverage has on the tomographic image a series of inversions with different ray-geometries have been done. Figure 4-21 shows a subset of 412 rays. This gives a more uniform pattern than when all rays are used. The results from the tomographic inversion from this subset is shown in Figure 4-20.

Figures 4-22 to 4-25 show results of tomographic analysis and ray-paths for 50% and 25% of the rays. A decomposition into squares of 5 m side was used.

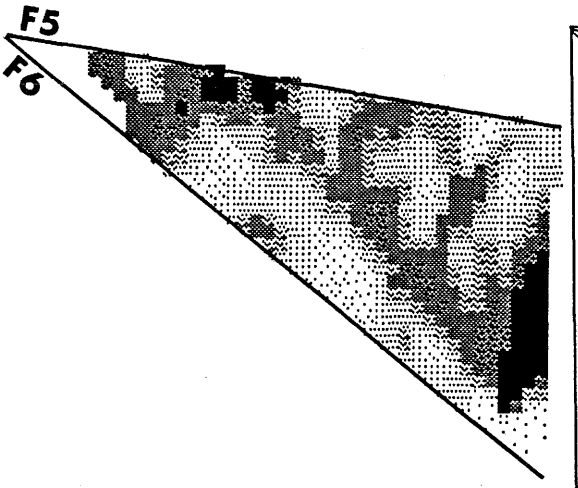

Figure 4-18.
Velocity structure from experimental data from 493 rays.

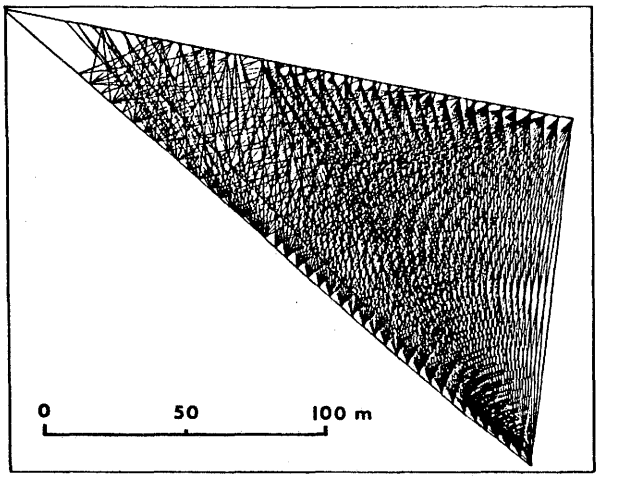

Figure 4-19.
Raypattern from 493 rays

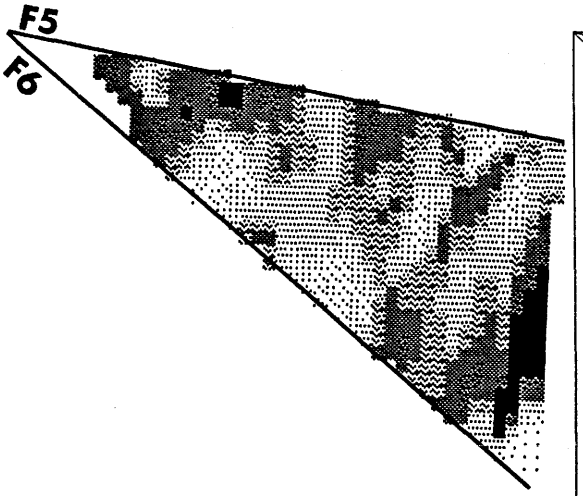

Figure 4-20.
Velocity structure from experimental data from 412 rays.

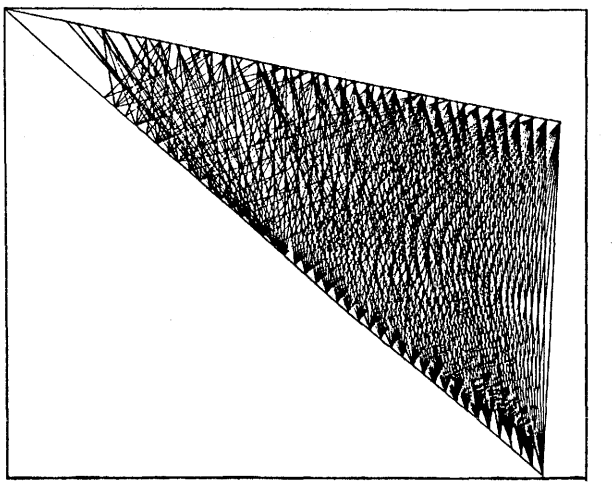

Figure 4-21.
Raypattern from 412 rays

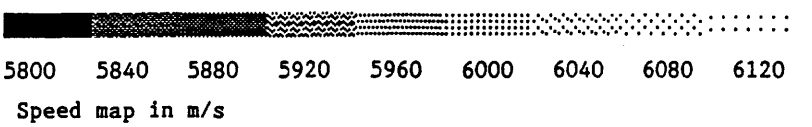

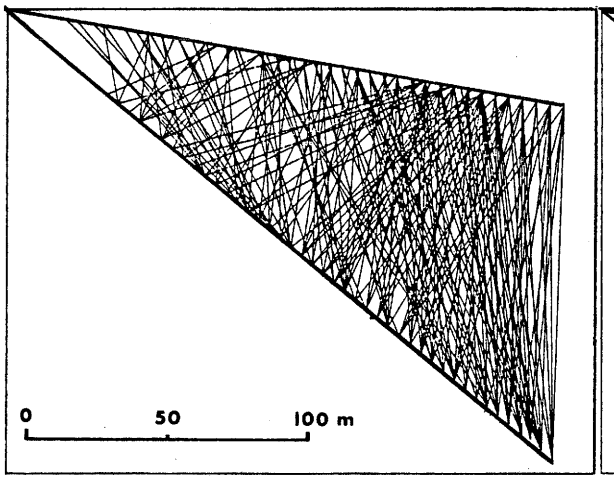

Figure 4-22.
Raypattern from 50%
of the 412 rays.

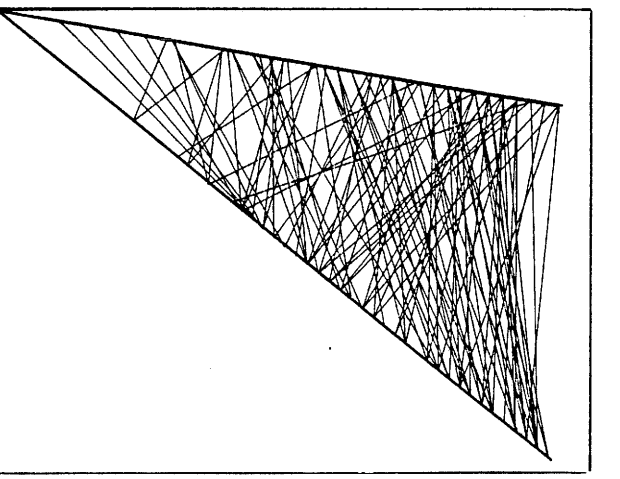

Figure 4-24.
Raypattern from 25%
of the 412 rays.

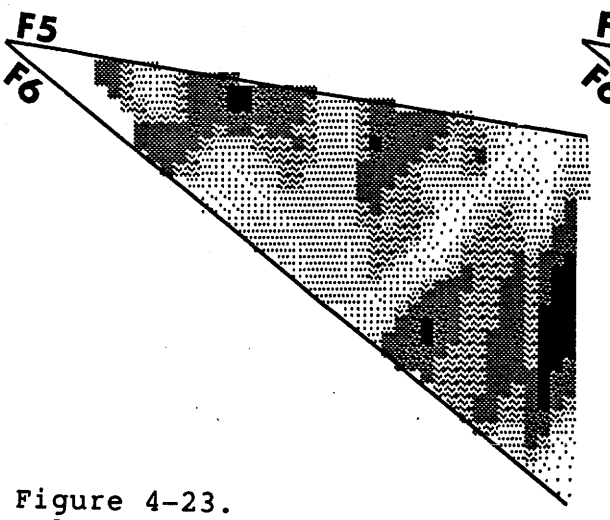

Figure 4-23.
Velocity structure
from 50% of the
412 rays.

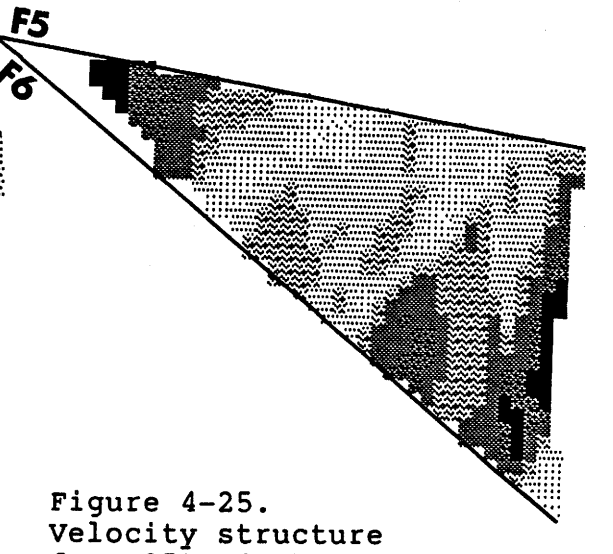

Figure 4-25.
Velocity structure
from 25% of the
412 rays.

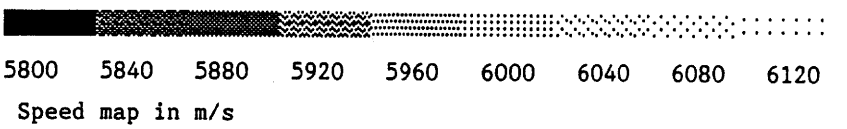

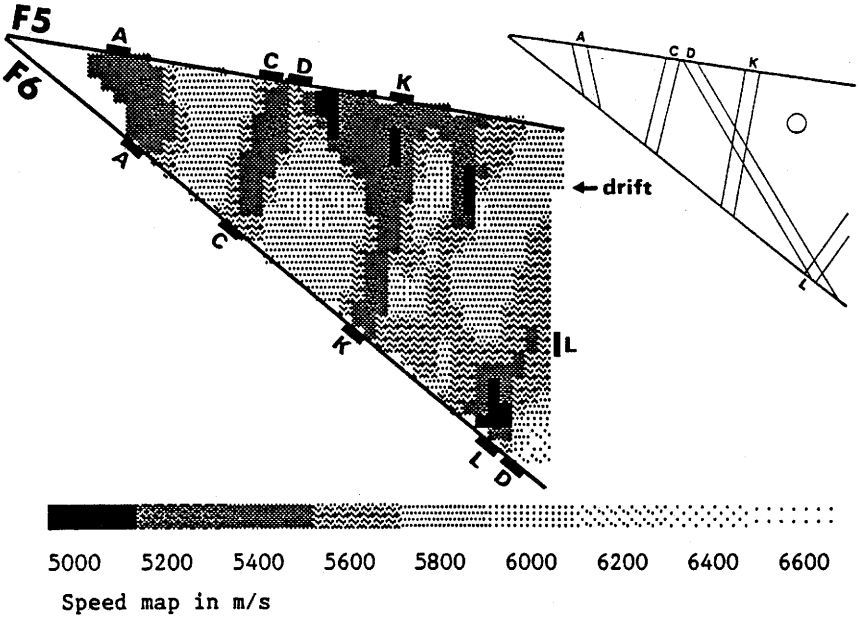

Figure 4-26. Model 1, 493 rays

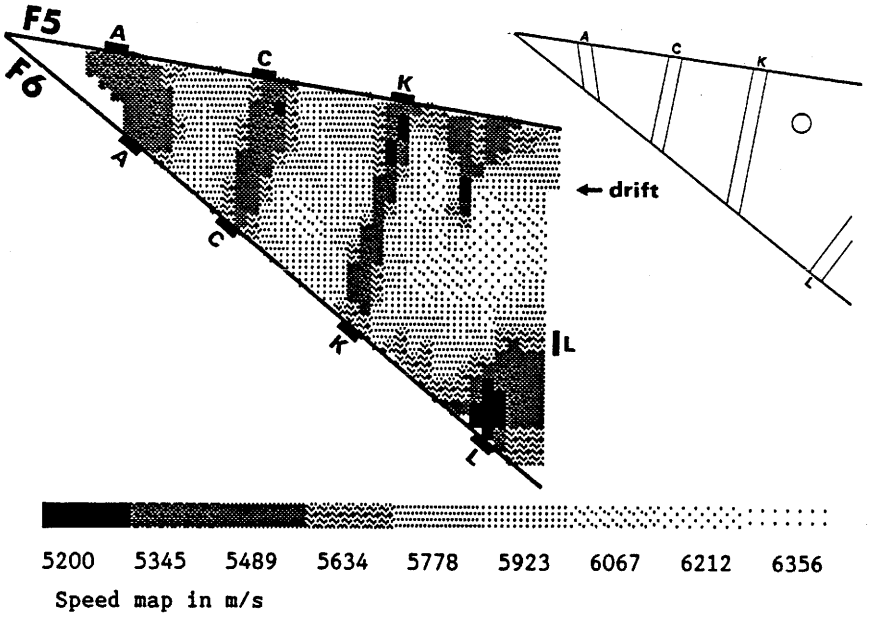

Figure 4-27. Model 2, as model 1 except that 'D-zone' is not included.

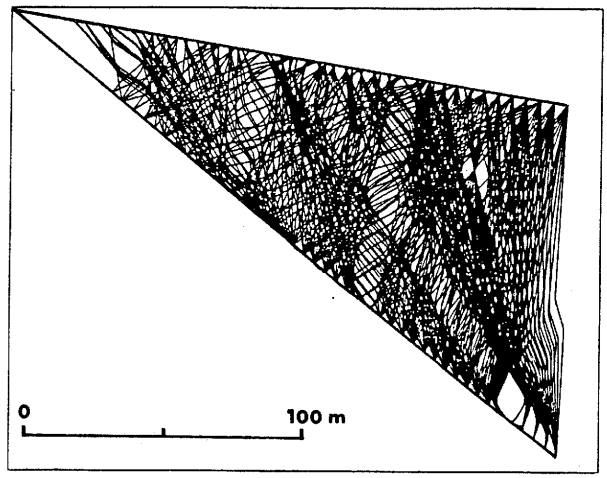

Figure 4-28. Raypaths from synthetic traveltimes.

The experimental data have been compared with results from calculations on theoretical models. Different low-velocity zones have been included in these models. The velocity outside the zones is assumed to be 6.0 km/s. The widths of the zones vary whereas the velocity contrast between the rock and the zones is the same. The tomographic reconstruction from the models are shown in Figures 4-26 and 4-27.

An example of ray-paths obtained from calculations of synthetic traveltimes, with ray-bending taken into account, is shown in Figure 4-28.

A tomographic inversion based on synthetic data from an anisotropic model with an anisotropy contrast of 3-4%, the minimum velocity in the horizontal direction and the maximum velocity in the vertical direction, is shown in Figure 4-29. The model result and the experimental solution show no resemblance.

If anisotropy were present (in a fairly homogeneous rock) this would also manifest itself in Figure 4-17 as rows and columns with gently varying velocities. We do not see any such indications of anisotropy.

In order to investigate the influence of errors in distance and coordinates, a series of "position errors" was introduced in hole F5. By inverting the resulting data in the same way as the experimental ones, the series of maps in Figure 4-30 (a)-(c) is obtained. It is obvious that even a small geometric error of only 0.5 m severely disturbs the quality of the tomographic analysis.

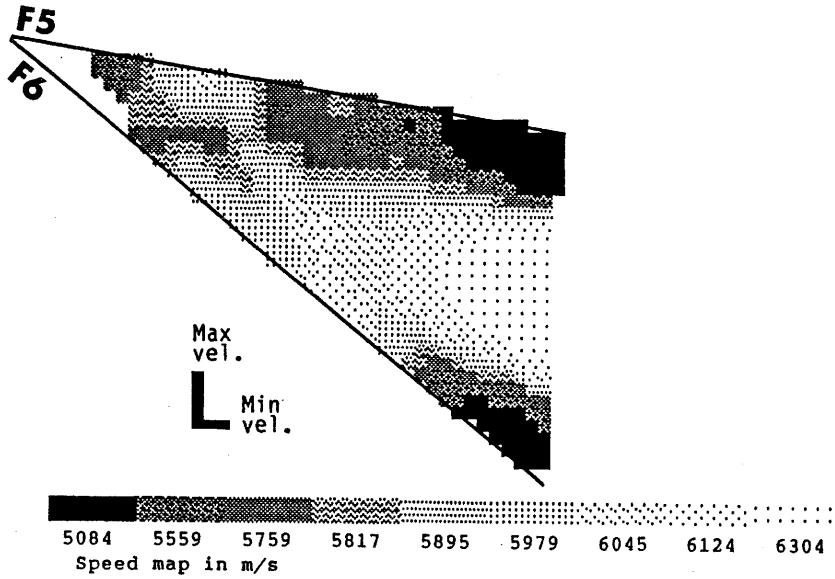

Figure 4-29. Tomographic map on an anisotropic model. The minimum velocity in the horizontal direction and a maximum in the vertical direction.

4.5 THEORETICAL CONSIDERATIONS

4.5.1 Solution by iterative methods

When the number of unknowns is large, the direct solution of the tomographic equation system by Gaussian elimination will be too demanding. In this case iterative solution methods can be used. They are also of great interest for use in the field where less capable computers are available. A comparison of the performance of the three iterative methods SIRT, ART and CG (see (14)) is given in Figures 4-31 and 4-32. Figure 4-31 (a)-(c) shows the result after ten iterations and Figure 4-33 (a)-(c) when convergence has been reached.

The different rates of convergence for SIRT, ART, and CG are apparent, CG being the fastest procedure. However, the main pattern is visible for all methods. The main difference is that the velocity contrasts are lower for the slower methods. Please note that this result is only valid for this particular case. Earlier studies have shown that the different iterative methods may give slightly different results.

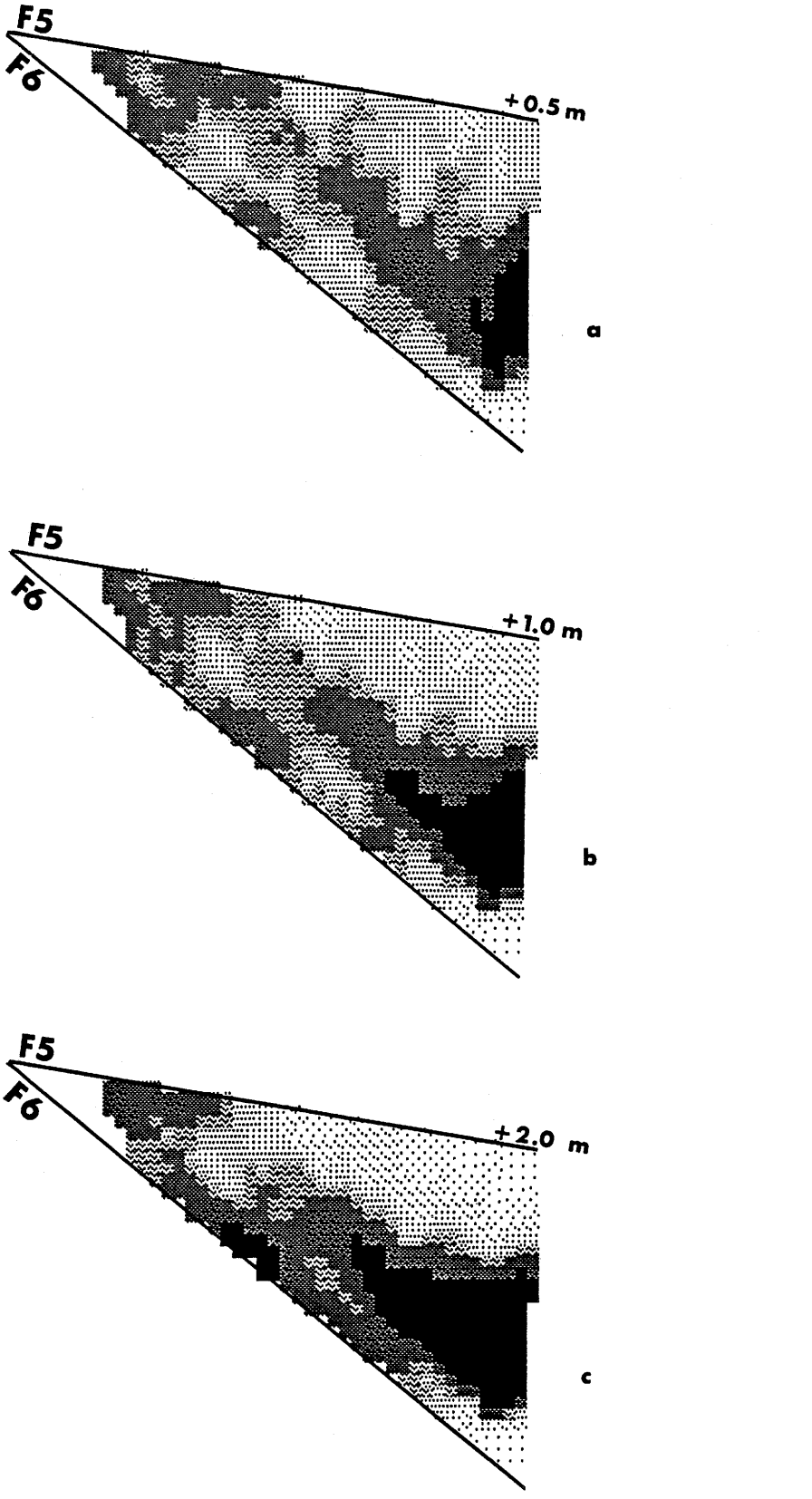

Figure 4-30. 0.5 m position error (a),
1.0 m position error (b),
2.0 m position error (c).

Figure 4-31. Solutions with SIRT (a), ART (b), and CG (c) after 10 iterations.

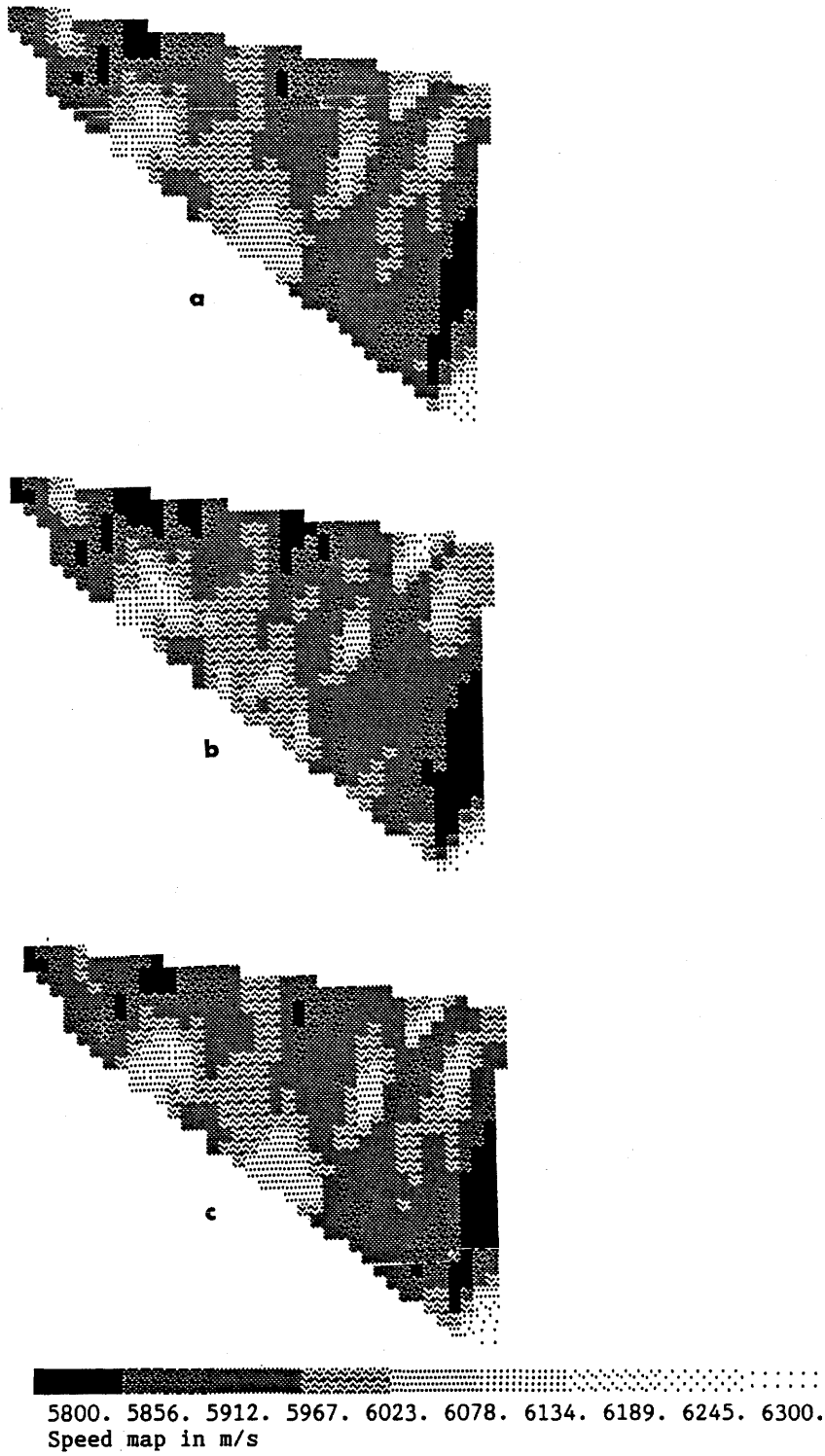

Figure 4-32. Solution with SIRT (a), ART (b) after 200 iterations and CG (c) after 74 iterations.

4.5.2 Confidence and resolution

Previously we have shown inversion results where the ray-path pattern and the damping level have been varied. The influence of such variations can be discussed in terms of confidence (stability of the solution in the presence of noise in the traveltime measurements) and resolution (possibility to map details in the structure in the noise-free case).

Figures 4-33 and 4-34 (a)-(c) show the expected relative errors in the velocity estimates at the typical velocity 5 km/s and an error of 0.5 ms (unrealistically high!) in the traveltime data. As is natural, the errors increase when a more sparse ray-pattern is used and they decrease when a higher level of damping is prescribed. It is important to choose an appropriate level of damping bearing considerations of this kind in mind.

Figures 4-35 and 4-36 (a)-(c) concern resolution. With a finite number of rays perfect resolution cannot be obtained: the velocity at each point can only be estimated as a certain average of the true velocities in a surrounding region. The figures show how well these averages are localized in the different parts of the crosshole area. As with the confidence figures, good results are obtained where the ray-path coverage is dense with crossing rays in many directions. The level of damping provides a means for trade-off between confidence and resolution: with high damping confidence is improved whereas resolution is impaired.
Figure 4-37, finally, shows the resolving power at two different locations in the crosshole area. What is shown is actually the values, put out at the appropriate places in the crosshole region, in two rows of the resolution matrix. In each case a normalization to the maximum value 1.0 was done. Note the comparatively sharp resolution that is obtained in (a). In (b) there is a smearing in the vertical direction, the main direction of the rays in this area.

4.6 TEST WITH HYDROPHONE RECEIVERS

A small test with hydrophone receivers was made between the holes F4 - F6. A comparison between signals from the borehole accelerometers and a hydrophone is depicted in Figure 4-38. The test was made at the top of the boreholes. The distance between source and receivers was 50 m. As can be seen in Figure 4-38 the registrations are quite similar. In the future it might be possible to replace the more expensive borehole receiver arrays with a chain of hydrophones. This would make it possible to do the measurements in a shorter time, as more receiving units could be used, resulting in a larger number of rays for each shot. On the other hand the hydrophones are not sensitive to the direction of the incoming wave.

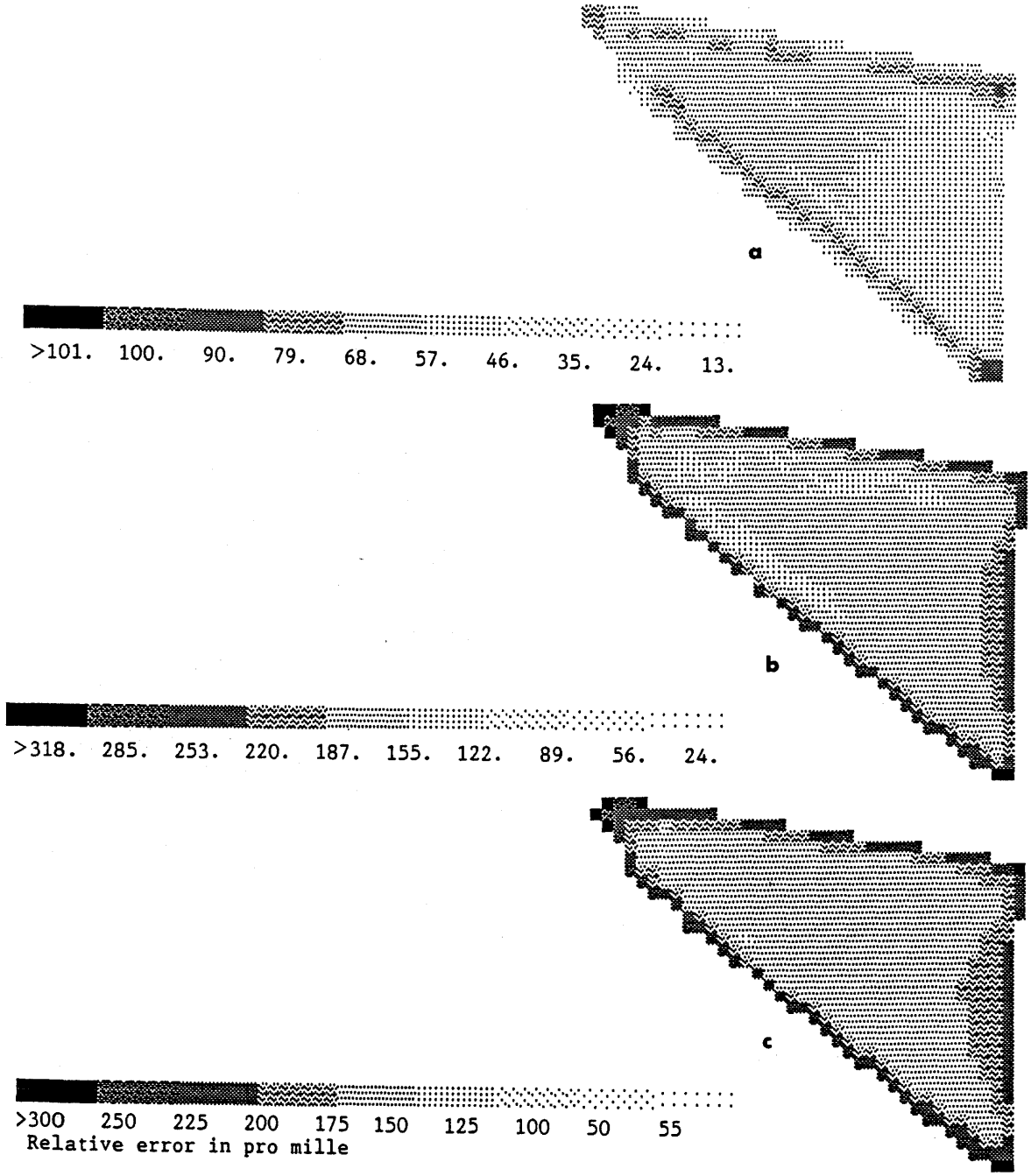

Figure 4-33. Expected relative errors, in % of the typical velocity 5 km/s, at assumed traveltime errors with a standard deviation of 0.5 ms. The number in brackets is the number of rays used in the inversion.

(a) All rays (493) damping 10
(b) A selection of rays (412) damping 10
(c) 50% of 412 rays damping 10

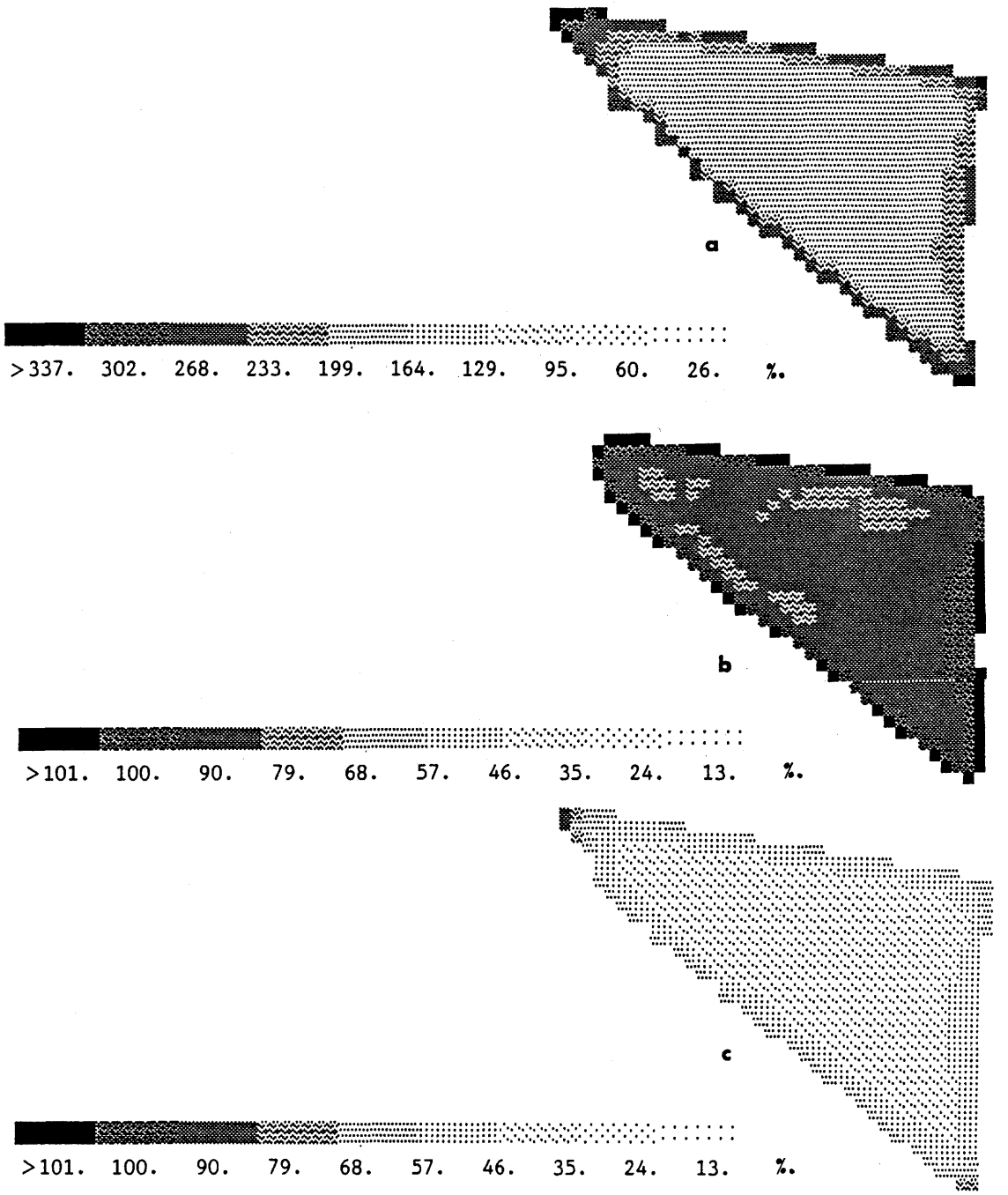

Figure 4-34. Expected relative errors, in % of the typical velocity 5km/s, at assumed traveltime errors with a standard deviation of 0.5 ms. The number in brackets is the number of rays used in the inversion.
(a) 25% of 412 rays damping 10
(b) A selection of rays (412) damping 20
(c) A selection of rays (412) damping 50

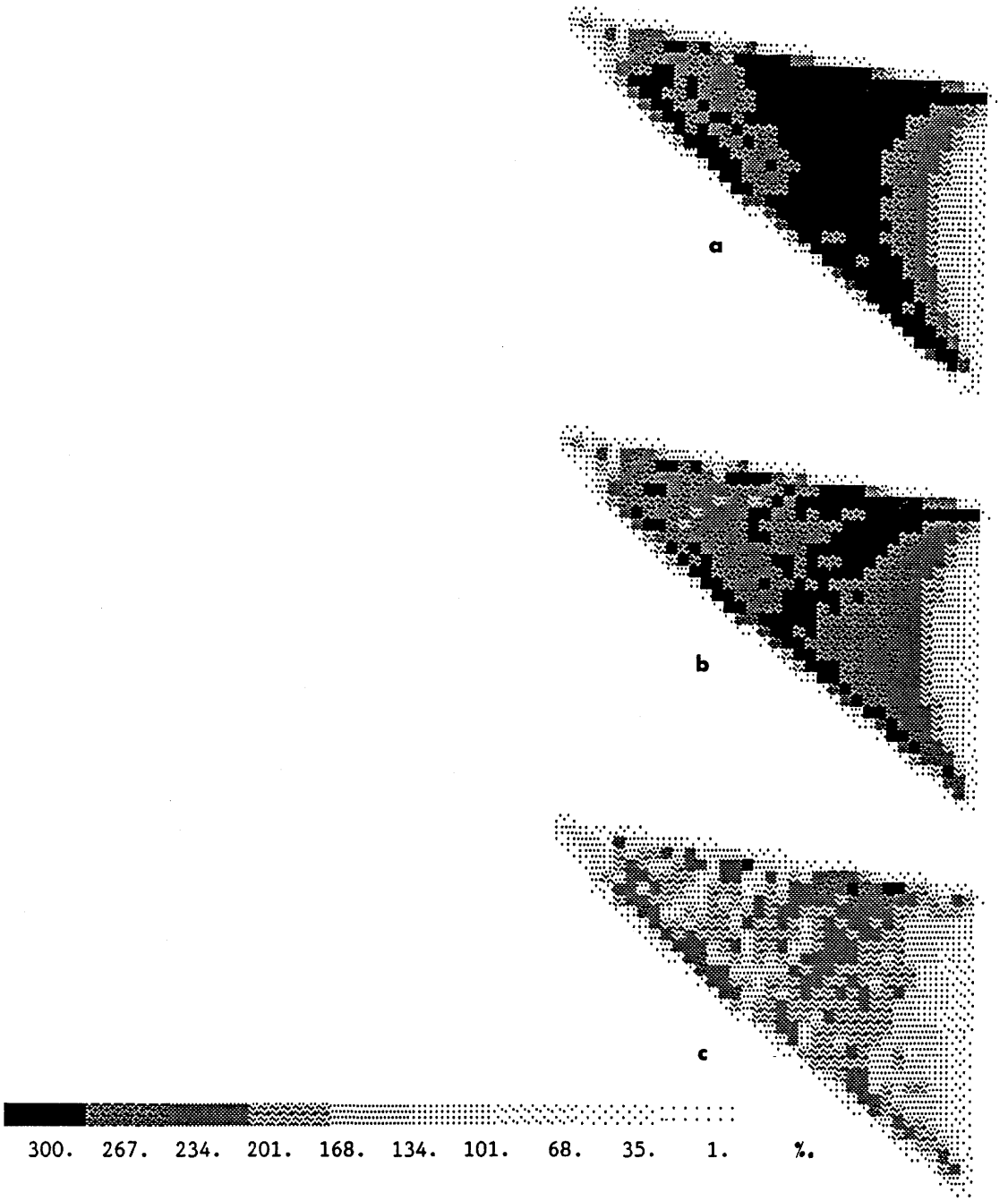

Figure 4-35. Sharpness of the obtainable resolution at different points in the crosshole area. The number in brackets is the number of rays used in the inversion.
(a) All rays (493) damping 10
(b) A selection of rays (412) damping 10
(c) 50% of 412 rays damping 10

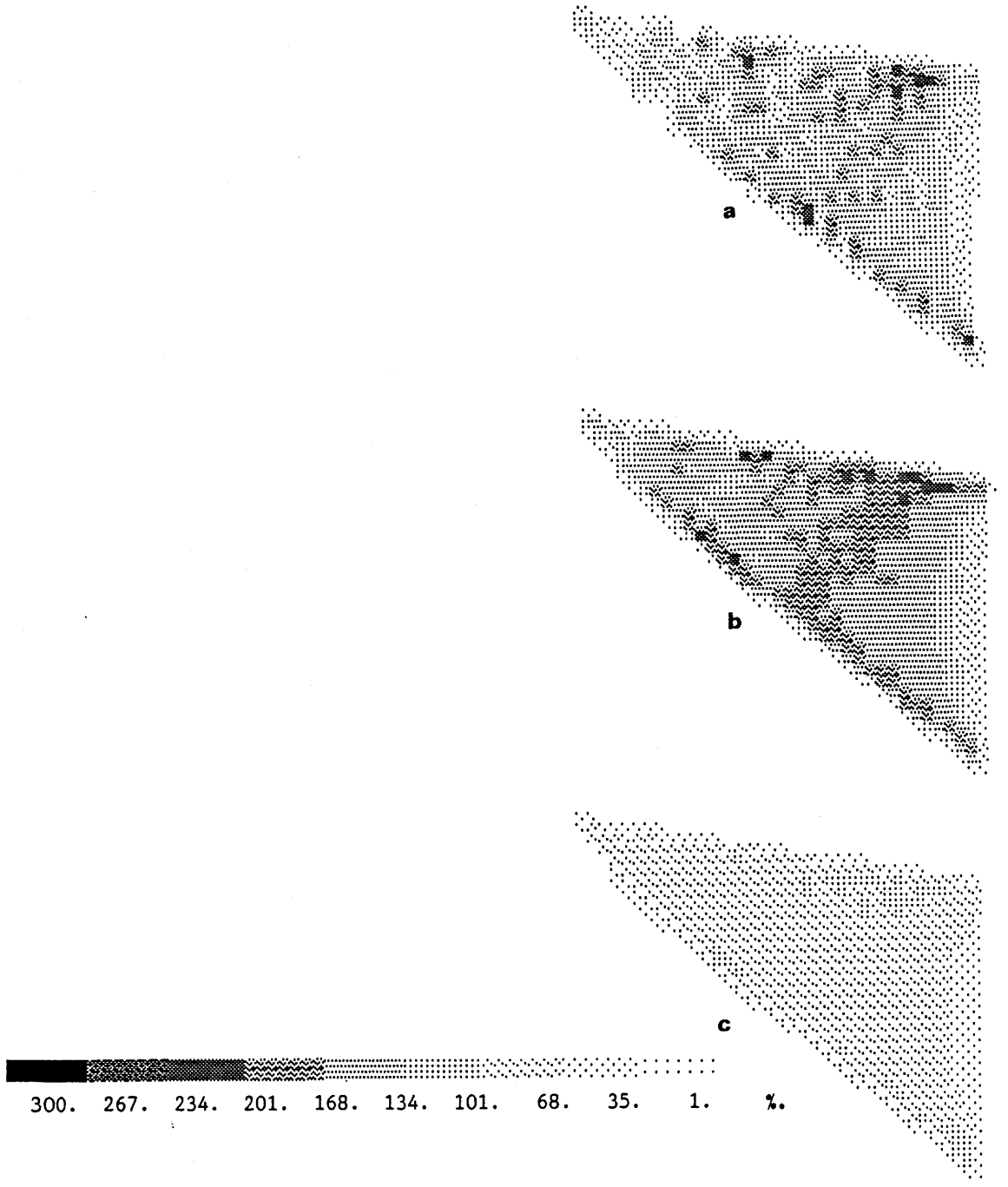

Figure 4-36. Sharpness of the obtainable resolution at different points in the crosshole area. The number in brackets is the number of rays used in the inversion.
(a) 25% of 412 rays damping 10
(b) A selection of rays (412) damping 20
(c) A selection of rays (412) damping 50

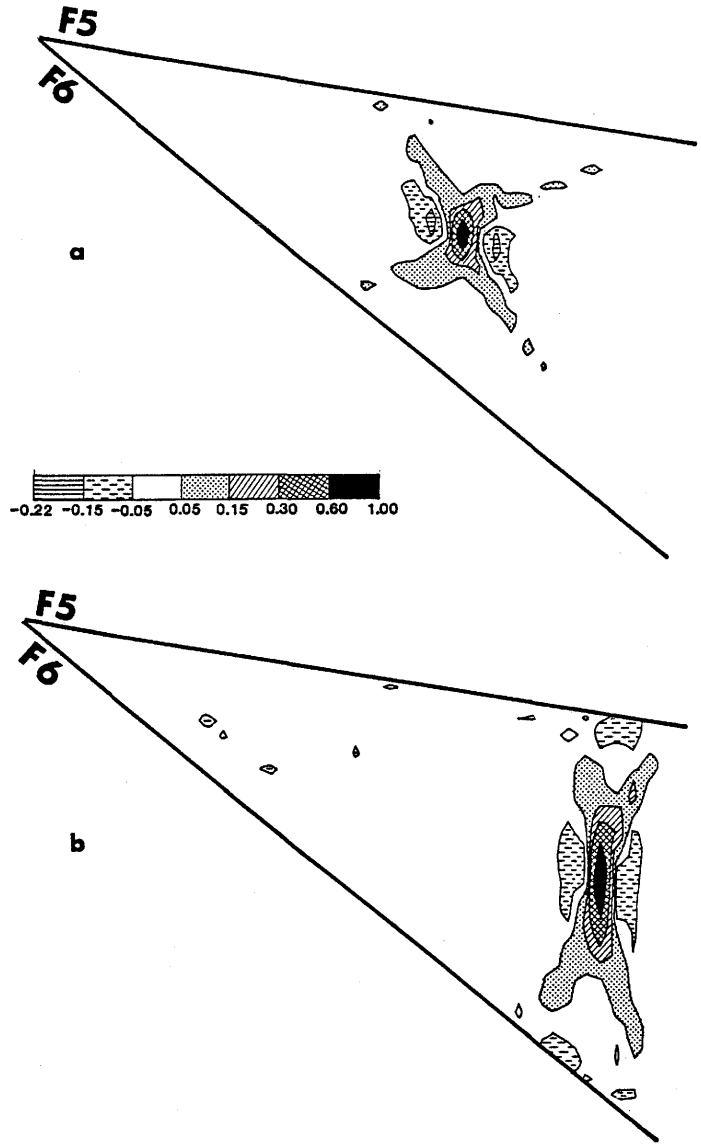

Figure 4-37. Obtainable resolution. Solution method: All rays (493) with damping 10.
(a) Resolving power at a point in the middle.
(b) Resolving power at a point in the bottom of the crosshole area.

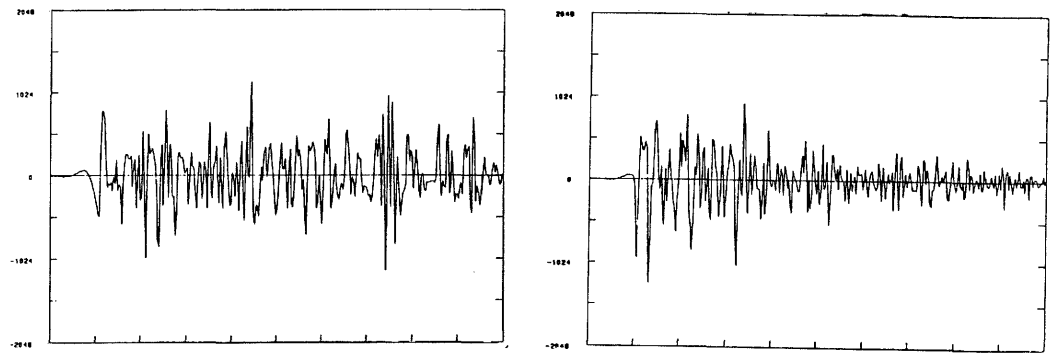

Figure 4-38. Comparison of a hydrophone (left) and an accelerometer (right) signal. Recording distances are 50 m.

4.7 CONCLUSIONS FROM THE SMALL-SCALE SEISMICS

The seismic field test at the small-scale site resulted in tomographic maps which show good agreement with other measurements.

The equipment, which was primarily developed for the large-scale experiment proved to be useful at short recording distances also.

The small-scale field test was focused on quite different aspects of tomographic analysis than were the large-scale tests. The test site had been specially designed for crosshole measurements. In particular there was no problem with curved boreholes. The short recording distances (below 200 m) and the isotropic rock made ray-bending corrections unnecessary.

Checks have shown that the Stripa granite is very homogeneous. This means that the analysis could be carried out in a straight-forward manner. The laborious parts of the analysis were data quality checks and elimination of systematic errors. The main cause of error was found to be the uncertainity in the borehole coordinates rather than the seismic measurements.

As was the case with the large scale tests, model calculations showed that artifacts can be present in the tomographic picture.

The successful test with hydrophones opens up new possibilities for measurements at short distances. A chain with many hydrophone receivers could shorten the time needed for a crosshole measurement considerably.

5 GENERAL CONCLUSIONS

The specially developed system for seismic tomography measurements has proved reliable and versatile in field work. The same equipment can be used for measurements from tens of metres up to a distance of 1000 m.

The explosive source has proven reliable, in use although time-consuming. It can be used over the full range of distances.

The quality of the tomographic analysis is strongly dependent on the area under study. In homogeneous rock, and at moderate (i.e. up to 200 m) distances, high-precision tomograms can be obtained. On the other hand, if the rock is heterogeneous, and/or the measuring distance large, the many possible solutions make the interpretation difficult. Information from other types of investigations are then usually needed in order to obtain a satisfactory result.

Three-dimensional measurements are possible, although time-consuming. It is our oppinion that the problems in large-scale seismics limits the use of 3-D measurements to rather small volumes.

The present Stripa Phase II programme demonstrates the usefulness of the seismic cross-hole method. With further development it should be possible to perform high-quality measurements at moderate costs. In order to achieve this, the following areas should be studied:

- Multi-component receivers (a hydrophone chain may be preferable at short distances)
- High precision bore-hole geometry logging
- Automated analysis on site
- Built-in data-quality controls

Today cross-hole seismic measurement and analysis is very much a craft which must be learnt by long and tedious experience. Hopefully, future work in this area will bring the method to such standards that it can be used as a normal tool in ground-rock investigations.

6 REFERENCES

1. K. Ahlbom, B. Albino, L. Carlsson, G. Nilsson, O. Olsson, L. Stenberg, H. Timje, "Evaluation of the geological, geophysical and hydrogeological conditions at Gideå", KBS TR 83-53, SKB, Stockholm, Sweden.

2. B. Albino, G. Nilsson, L. Stenberg, "Geological, tectonical and geophysical investigations at the Gideå study site", (in Swedish), KBS AR 83-19, SKB, Stockholm, Sweden.

3. H. Almström, S. Berglund, R. Hank, P. Morén, "Summary of test with a gas exploder", Stripa Project Quarterly Report January-March 1984, Appendix 3, SKB/KBS, Stockholm.

4. S. Bergh, U. Ekström, M. Gustavsson, H. Israelson, P. Morén and J. Pihl, "A vertical borehole geophone array", Geophys., vol. 48, pp. 1558-1559, 1983.

5. L. Carlsson, V. Stejskal, "Core-logs of the sub-horizontal boreholes N1 and E1, Stripa Project, IR 82-04.

6. S. Carlsten, K-Å. Magnusson, O.Olsson, "Crosshole Investigations-Description of the small scale site" Stripa Project, IR 85-05.

7. S. Carlsten, A. Stråhle, "Crosshole Investigations-Compilation of core log data from F1-F6, Stripa Project, IR 85-13.

8. C. Cosma, M. Ihalainen, R. Korhonen, "The crosshole seismic metod, report of phase II of development programme", Geotek OY, Helsinki, Finland, 1984.

9. M. Gustavsson, H. Israelson, S. Ivansson, P. Morén and J. Pihl, "A seismic crosshole experiment in crystalline rock", in Proc. Workshop on Geophysical Investigations in Connection with Geological Disposal of Radioactive Waste (Ottawa, Ont. Canada, sept. 1982), pp. 149-156.

10. M. Gustavsson, S. Ivansson, P. Morén and J. Pihl, "Seismic borehole tomography - measurement system and field studies", Proc. IEEE, vol. 74, no. 2, pp. 339-346, 1986.

11. S. Ivansson, "Remark on an earlier proposed iterative tomographic algorithm", Geophys. J. Roy. Astr. Soc., vol. 75, pp. 855-860, 1983

12. S. Ivansson, "Crosshole investigations - tomography and its applications to crosshole seismic measurements", Stripa Project, IR 84-08.

13. S. Ivansson, "A study of methods for tomographic velocity estimation in the presence of low velocity zones", Geophys., vol. 50, pp. 969-988, 1985.

14. S. Ivansson "Seismic borehole tomography - theory and computational methods", Proc. IEEE, vol. 74, no. 2, pp. 328-338, 1986.

15. A. Jämtlid, O. Olsson, "Hydrogeological and hydrogeochemical investigations - geophysical borehole measurements", Stripa Project, IR 84-03.

16. "LPA-11K laboratory peripheral accelerator users's guide." Maynard, MA: Digital Equipment Co., order no. EK-LPA11-UG-001, 1978.

17. P. Morén, "Microexplosions in boreholes - preliminary experiment in the Stripa mine", Stripa Project Quarterly Report January-March 1984, Appendix 2, SKB/KBS, Stockholm.

18. G. Nilsson, O. Olsson, "Crosshole investigations - description of the large scale site", Stripa Project, IR 86-01.

19. "RSX-11M/M-PLUS Executive Reference Manual", Maynard, MA: Digital Equipment Co., order no AA-L675A-TC, 1984.

20. "Special issue on computerized tomography", Proc. IEEE, vol. 71, no. 3, pp. 289-448, 1983.

21. L. Stenberg, O. Olsson, "The tube wave method for identifying permeable fracture zones intersecting a borehole", SKB AR 84-14, SKB, Stockholm, Sweden.

22. J. Wong, P. Hurley and G. West, "Crosshole seismology and seismic imaging in crystalline rocks", Geophys. Res. Lett., v. 10, pp. 686-689, 1983.

SEISMIC SYSTEM SPECIFICATION

A.1 EQUIPMENT

A.1.1 Seismic Source

The explosive paste Octol is used to avoid the colloidal carbon which is emitted from ordinary explosives.

The yield is typically 5 - 50 g for recording distances up to 1000 m in crystalline rock. For crosshole measurements over a few hundred metres a charge of 5 - 10 g is sufficient. The yield is chosen so that one shot will give sufficient energy for the largest recording distance, which means that no stacking is necessary. The source-hole must be water-filled. After each shot the ignition cable must be drawn up and a new charge adapted. The charge can be pushed into the holes with poles.

A.1.2 Seismic Receivers

Surface geophones:
Type: Vertical and horizontal
Sensor SM-4/7
Sensitivity: 0.29 V/cm/sec
Frequency response: 10-500 Hz.

Surface accelerometers:
Type: BBN 507 HS
Sensitivity: 200 mV/g
Frequency response: 2 - 8000 Hz (+- 3 dB)

Borehole accelerometers:
Type: BBN 507 HS
Sensitivity: 200 mV/g
Frequency response: 2 - 8000 Hz (+- 3 dB)

A.1.3 Recording And On-site Data-analysis System

Recording and analysis is done on the same system. It is based on a PDP-11/34 computer with the following peripherals:

- 26 Mbyte Winchester disc memory
- 2 magnetic tape drives, 800/1600 BPI, industry standard
- Analog-to-digital converter with 128 channels of 12-bit resolution
- Graphic terminals
- Colour printer/plotter

Specification of system:

- Maximum system sampling rate 150000 samples per second
- 60 analog inputs with band-pass filters and amplifiers
- Ultra low noise battery-powered preamplifiers
- Comprehensive signal-analysis package with all relevant functions for signal analysis (i.e. auto- and cross-correlation, 3D spectral analysis, signal filtering with adaptive parameters, etc)
- Data acquisition software developed by FOA permitting selection of any number of input channels and sampling frequencies up to system maximum

A.1.4 Data Processing System

The computer is a Digital Equipment VAX 11/750 with a floating point accelerator.
The working storage is 5.5 Mbytes
Word precision for floating point: 32, 64 or 128 bits.

Peripheral configuration:

- 5 discs, giving in total 1 Gbyte of storage
- 2 magnetic tape drives, 800/1600 BPI
- 1 line printer
- 2 printer/plotters (matrix type)
- 1 pen plotter
- 1 Tektronix 4114 graphic system with two-colour option
- 5 graphic terminals
- 20 alpha numeric terminals

The operating system is VMS, which supports real-time, time-sharing and multi-stream batch simultaneously. The theoretical maximum useful program size is 100 Mbytes, but in practice the useful size is in the order of 10 Mbytes.

Priorities can be varied for time-sharing users. Priviledged users can get higher priority for shorter response time.

System access is via directly connected terminals, via modem or via international packet-switch networks (X.25).

Data can be transferred by dial-up telephone lines at 300 or 1200 baud using SAFT or KERMIT protocols.

A.1.5 Field Data Analysis

During an experiment all data is normally stored on the disc memory for rapid access. The signals can be viewed on a graphic terminal or plotted on a colour printer/plotter. Spectral analysis can be made with standard FFT routines, auto-correlation techniques etc. Signal spectra can be displayed in 3D.

Traveltime determination is done at graphic terminals from signal plots with high resolution.

Tomographic calculations according to the SIRT method can be done on the field system. The Conjugate Gradients algorithm is also planned to be implemented there.

A.1.6 Data Presentation

The tomograms can be displayed in any form, ie colour plots, grey-scale plots and number matrices are all available.

A.1.7 Operation Mode Of Field Equipment

A.1.7.1 Environmental And Power Requirements

The shot-holes must be water-filled. If the water drains away we need water supply. The data-recording system needs power supply of 220 V, 50 Hz, 3.5 kW (16 A fusing) and an area of 5 - 6 m^2.